Integrated defensive states and their neuronal correlates in the Periaqueductal Gray

Integrierte Defensivzustände und ihre neuronalen Korrelate im Periaquäduktalen Grau

Doctoral thesis for a doctoral degree

at the Graduate School of Life Sciences,

Julius-Maximilians-Universität Würzburg,

Section Neuroscience

submitted by

Nina Schukraft, geb. Scheffler

from

Mannheim

Würzburg **2023**

Submitted on: ……..……..

Office stamp

Members of the Thesis Committee:

Chairperson:	**Prof. Dr. Carmen Villmann**
Primary Supervisor:	**Prof. Dr. Philip Tovote**
Supervisor (Second):	**Prof. Dr. Matthias Gamer**
Supervisor (Third):	**Prof. Dr. Charlotte Förster**

Affidavit

I hereby confirm that my thesis entitled "Integrated defensive states and their neuronal correlates in the Periaqueductal Gray" is the result of my own work. I did not receive any help or support from commercial consultants. All sources and / or materials applied are listed and specified in the thesis.

Furthermore, I confirm that this thesis has not yet been submitted as part of another examination process neither in identical nor in similar form.

Place, Date Signature

Eidesstattliche Erklärung

Hiermit erkläre ich an Eides statt, die Dissertation " Integrierte Defensivzustände und ihre neuronalen Korrelate im Periaquäduktalen Grau" eigenständig, d.h. insbesondere selbständig und ohne Hilfe eines kommerziellen Promotionsberaters, angefertigt und keine anderen als die von mir angegebenen Quellen und Hilfsmittel verwendet zu haben.

Ich erkläre außerdem, dass die Dissertation weder in gleicher noch in ähnlicher Form bereits in einem anderen Prüfungsverfahren vorgelegen hat.

Ort, Datum Unterschrift

Summary

In the face of threat, animals react with a defensive reaction to avoid or reduce harm. This defensive reaction encompasses apart from behavioral changes also physiological, analgetic, and endocrine adaptations. Nonetheless, most animal studies on fear and anxiety are based on behavioral observations only, disregarding other aspects of the defensive reaction, or integrating their inter-related dynamics only insufficiently. The first part of this thesis aimed in characterizing patterned associations of behavioral and physiological responses, termed integrated defensive states. Analyzing cardiac and behavioral responses in mice undergoing multiple fear and anxiety paradigms revealed a complex and dynamic interaction of those readouts on both, short and long timescales. Microstates, stereotypical combinations of i.e. freezing and decelerating heart rates, are short-lasting and were, in turn, shown to be influenced by slow acting macrostate changes. One of those higher order macrostates, called `rigidity`, was defined as a latent process that constrains the range of momentary displayed heart rate values. Furthermore, integrated defensive states were found to be highly dependent on the cue and the context the animals are confronted with. Importantly, same behavioral observations, i.e. freezing, were associated with distinct cardiac responses, highlighting the importance of multivariate analysis of integrated defensive states. Defensive states are orchestrated by the brain, which has evolved evolutionary conserved survival circuits. A central brain area of these circuits is the periaqueductal gray (PAG) in the midbrain. It plays a pivotal role in mediating defensive states, as it receives signals about external and internal information from multiple brain regions and sends information to both, higher order brain areas as well as to the brainstem ultimately causing the execution of threat responses. In the second part of this thesis, different neuronal circuit elements in the PAG were optically manipulated in order to gain mechanistic insight into the defense network in the brain underlying the previously delineated cardio-behavioral defensive states. Optical activation of glutamatergic PAG neurons evoked heterogeneous, light-intensity dependent responses. However, a further molecular restriction of the glutamatergic neuronal population targeting only Chx10+ neurons, led to a cardio-behavioral state that resembled spontaneous freezing-bradycardia bouts.

In summary, this thesis presents a multivariate description of defensive states, which includes the complex interaction of cardiac and behavioral responses on different timescales and, furthermore, functionally dissects different excitatory and inhibitory PAG circuit elements mediating these defensive states.

Zusammenfassung

Tiere reagieren mit einer Abwehrreaktion auf eine Bedrohung, um Schaden zu vermeiden oder zu verringern. Diese Abwehrreaktion umfasst neben Verhaltensänderungen auch physiologische, analgetische und endokrine Anpassungen. Dennoch stützen sich die meisten Tierstudien auf dem Gebiet von Furcht- und Angstforschung nur auf Verhaltensbeobachtungen und lassen dabei andere Aspekte der Abwehrreaktion außer Acht oder berücksichtigen ihre komplexen gegenseitigen Beziehungen nur unzureichend. Das Ziel des ersten Teils dieser Arbeit war, bestimmte Zusammenhänge von Verhalten und physiologischen Reaktionen zu charakterisieren, die hier als integrierte Defensivzustände bezeichnet werden. Um Defensivzustände bei Mäusen hervorzurufen, wurden diese mehreren Furcht- und Angstparadigmen unterzogen. Die Analyse der dabei hervorgerufenen Herzratenänderungen und Verhaltensanpassungen ergab eine komplexe und dynamische Interaktion dieser beiden Reaktionen, bei denen sowohl kurz- als auch auf längerfristige Änderungen eine Rolle spielen. Mikrozustände, stereotype Kombinationen von z. B. Freezing und Verlangsamung der Herzfrequenz, sind von kurzer Dauer und werden wiederum durch langsamer wirkende Makrozustände beeinflusst. Einer dieser auf einer übergeordneteren Ebene wirkenden Makrozustände, "rigidity" genannt, wurde als latenter Prozess definiert, der den Ausprägungsbereich der zu jedem Zeitpunkt möglichen Maximal- und Minimalherzfrequenz beschreibt. Darüber hinaus wurde festgestellt, dass integrierte Defensivzustände in hohem Maße von dem Auslösereiz und dem Kontext abhängen, mit dem die Tiere konfrontiert werden. Eine wichtige Erkenntnis hierbei war, dass dieselben Verhaltensbeobachtungen, z. B. Freezing, mit unterschiedlichen kardialen Antworten assoziiert sein kann. Dies unterstreicht die Bedeutsamkeit von multivariaten Analysen integrierter Defensivzustände. Defensivzustände werden vom Gehirn gesteuert, das evolutionär konservierte neuronale Überlebensschaltkreise entwickelt hat. Ein zentrales Hirnareal dieser Schaltkreise ist das Periaquäduktale Grau (PAG) im Mittelhirn. Diese Hirnstruktur spielt eine wichtige Rolle bei der Vermittlung von Defensivzuständen, da es diverse Signale über sowohl äußere als auch innere Zustände aus multiplen Hirnregionen empfängt und gleichzeitig Informationen an Hirnareale höherer Ordnung sowie an den Hirnstamm sendet, der letztendlich die Ausführung von Defensivreaktionen vermittelt. Im zweiten Teil dieser Arbeit wurden verschiedene neuronale Schaltkreiselemente im PAG optogenetisch manipuliert, um einen mechanistischen Einblick in das Defensivnetzwerk im Gehirn zu erhalten, das den zuvor beschriebenen kardio-verhaltensmäßigen Defensivzuständen zugrunde liegt. Die optische Aktivierung von

glutamatergen PAG-Neuronen war mit einer heterogenen, von der Lichtintensität abhängigen Reaktionen assoziiert. Eine weitere molekulare Restriktion der glutamatergen Neuronenpopulation, die nun ausschließlich auf Chx10+ Neuronen abzielte, führte hingegen zu einem kardio-verhaltensmäßigen Zustand, der vergleichbar mit zuvor beobachteten spontanen Freezing-Bradykardie-Zuständen war.

Zusammenfassend umfasst diese Arbeit eine multivariate Beschreibung von Defensivzuständen, die das komplexe Zusammenspiel von kardialen und verhaltensmäßigen Reaktionen auf verschiedenen Zeitachsen umfasst sowie - mittels Optogenetik - eine funktionelle Charakterisierung von verschiedenen exzitatorischen und inhibitorischen PAG-Schaltkreiselementen, die diese Defensivzustände vermitteln.

Table of Contents

1. Introduction

1.1. The defense reaction

Reacting adequately to threat is essential for survival and thus an evolutionary conserved, adaptive process. Depending on the nature of the threat, the defense reaction consist of a wide range of different defensive responses, which are aimed at coping with the respective danger (Anderson and Adolphs 2014). These defensive responses include behavioral, autonomic, and endocrine adjustments, such as flight reactions, heart rate (HR) changes or the release of glucocorticoids (Figure 1). Defensive reactions are distinguished in innate fear responses on the one hand and learned fear responses on the other. Innate fear responses are generated by inherently threatening stimuli and do not depend on any learning processes. During learned fear reactions, however, former neutral stimuli become associated with threatening stimuli. This can be experimentally modelled through classical pavlovian fear conditioning (Blanchard, Blanchard, and Hori 1989; Gross and Canteras 2012; LeDoux 2012). Stimuli triggering defensive reactions can be multivariate. External cues from the environment as well as internal, interoceptive modalities can contribute to the activation of brain networks resulting in a defensive reaction (Figure 1).

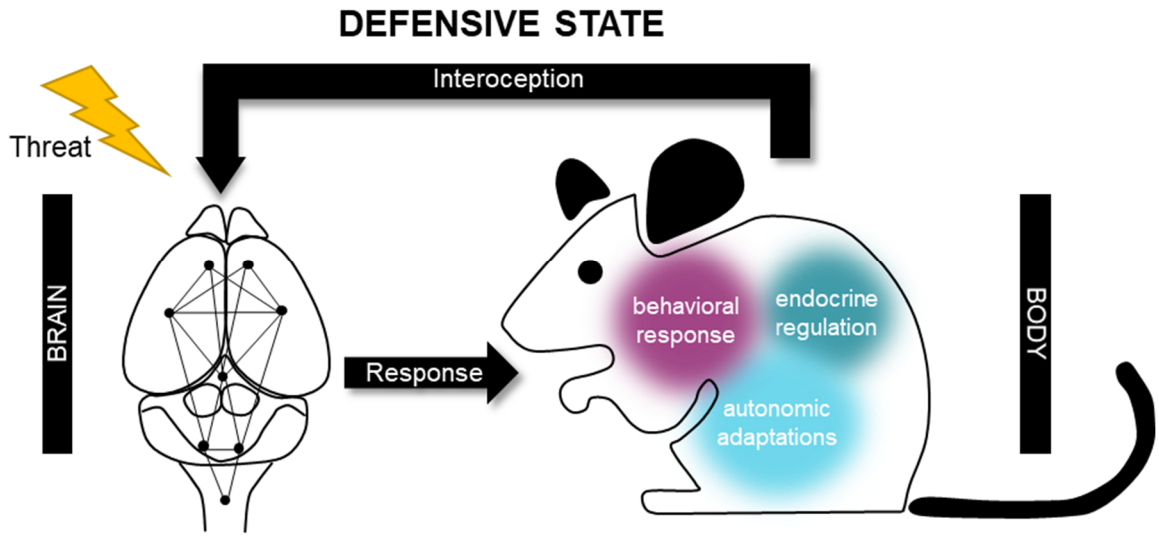

Figure 1 - The emergence of defensive states.
Upon exposure to threat, the mammalian brain generates emotional brain states such as fear and anxiety that trigger a defensive reaction. These bodily responses encompass behavioral, endocrine, and autonomic adaptations, which together constitute an integrated defensive state. The body, in turn, sends back interoceptive information to the brain. Icons adapted from BioRender.

Depending on the triggering stimuli, a rapid switching between distinct defensive reactions is key for the animals' survival (Silva, Gross, and Gräff 2016). The animals' reaction is also influenced by a constant weighing of internal needs (i.e. hunger) and risk of being detected by a predator. All these multifaceted defensive responses are orchestrated by brain-wide, neuronal fear networks, which change their activity patterns based on the integration of internal and external cues (Tovote, Fadok, and Luthi 2015).

1.1.1. Behavioral aspect of the defense reaction

Changing environments require organisms to rapidly weigh different options and switch between different defensive reactions. For instance, the spatial distance of a threat affects the type and expression intensity of a defensive reaction (Fanselow and Lester 1988). The 'threat imminence continuum' describes the expression of different defensive behaviors (e.g. freezing, flight) in dependence of the perceived threat level (Blanchard and Blanchard 1990; Fanselow and Lester 1988; Mobbs et al. 2020). According to this model, a relatively distant threat evokes freezing responses, classically defined as the complete absence of movement except respiration (Blanchard, Flannelly, and Blanchard 1986). The animals' lack of locomotion reduces the likelihood of being detected by the predator. Conversely, an imminent threat stimulus leads to an active coping style associated with a flight response, a form of locomotion that aims in the escape from a threat. Moreover, the availability of an escape route promotes flight over a freezing response (Blanchard and Blanchard 1989). Importantly, instead of defining freezing as a passive response, it can be also described as an active state during which appropriate responses are assessed and the body is prepared for action ('threat-anticipatory freezing', Roelofs and Dayan 2022). Risk assessment, on the other hand, poses a "pre-fear response" behavior, which serves to detect and analyze threat stimuli in order to choose the adequate defensive reaction (Blanchard et al. 2011). It is characterized by a lowered back and a stretched body position, sometimes a targeted approach towards the potential threat interrupted by immobility periods (Blanchard et al. 1990).

The vast majority of studies addressing fear and anxiety in rodents adduce behavioral responses to quantify these states (for example Fustiñana et al. 2021; Gründemann et al. 2019; F. M. Reis et al. 2021). Furthermore, fear is even equalized to behavior and defined solely on the basis of the same (Mobbs et al. 2019, "…emotions are states of an organism that are defined by what they do."). Consequently, in the recent years a substantial amount of tools to quantify behavior has emerged (Pereira, Shaevitz, and Murthy 2020). Machine-learning approaches improve the

precision and foster high-throughput, while reducing the need of time-consuming, manual annotations. A tool to track different body parts (DeepLab Cut, Mathis et al. 2018) facilitates subsequent annotations of behavioral events and by this can, for instance, allow for refined analysis of stimulus specific defensive behaviors (Storchi et al. 2020).

1.1.2. Autonomic aspect of the defense reaction

The defensive reaction includes multivariate changes of internal mechanisms that also encompass physiological processes activated by neural activity of the autonomous nervous system (ANS) as, for example, cardiovascular changes. A standard cardiac readout is the HR. While a slow resting HR is called bradycardia, an increased HR is termed tachycardia.

Cardiovascular changes associated with defensive reactions have been investigated in a multitude of studies (Koba, Hisatome, and Watanabe 2019; Koba, Inoue, and Watanabe 2016; Resstel et al. 2006; Swiercz et al. 2018; Walker and Carrive 2003). Beside the investigation of autonomic responses in innate fear reactions, classical fear conditioning is a commonly used paradigm when studying fear reactions. Here, an aversive stimulus (unconditioned stimulus, US), typically an electric foot shock, becomes associated with an initially neutral cue (conditioned stimulus, CS), so that the presentation of the CS alone elicits a fear reaction (Fanselow and Poulos 2005; Tovote et al. 2015). Presenting an aversively conditioned stimulus to an animal placed in its homecage was shown to be associated with a marked elevation of HR compared to controls (Stiedl and Spiess 1997; Zhang et al. 2019). In a similar experimental model, Swiercz et al. reported an increase in HR during CS presentation in an extinction session, while the mean arterial pressure did not differ between conditioned and non-conditioned subjects (Swiercz et al. 2018). On the contrary, others have reported decreases in HR after CS presentations in fear conditioned rats and rabbits (Gentile et al. 1986; De Toledo and Black 1966). Along these lines, re-exposing rats to a context, previously paired with foot shocks resulted – beside a general increase in HR - in net bradycardic responses when compared to sham conditioned control animals (Vianna and Carrive 2005). Not only both, accelerations as well as deceleration of HR values have been reported under threat conditions, but even when associated behavioral changes were taken into account, no clear picture of i.e. freezing associated HR changes arose from those studies (Stiedl and Spiess 1997; De Toledo and Black 1966; Walker and Carrive 2003). Moreover, innate behavioral responses were associated with cardiovascular changes, too. Exposing rats to a white noise sound was reported to cause a decrease in HR (Koba et al. 2019, 2016; Yoshimoto, Nagata, and Miki 2010). However, the

presentation of cat odour to rats, for instance, led to increased blood pressures although less pronounced when compared to conditioned cardiac fear responses, while no change in HR was observed (Dielenberg, Carrive, and McGregor 2001). These initially heterogeneous findings emphasize the influence of context and experimental set-up on the investigation of autonomic defensive responses.

Also in humans, changes in the ANS activity are intricately linked to the defensive reaction. A decelerating HR during threat encounter has been shown in a multitude of studies (Gladwin et al. 2016; Löw, Weymar, and Hamm 2015; Merscher et al. 2022; Roelofs, Hagenaars, and Stins 2010; Rösler and Gamer 2019). Furthermore, a tight correlation of this cardiac deceleration and freezing, measured as a reduced body sway in humans, after fear conditioning is evident (Gladwin et al. 2016; Szeska et al. 2021). This 'attentive freezing', a state that is defined by freezing and bradycardia, is hypothesized to rather reflect an active preparatory state in which perception is optimized by a slow beating heart and lack of movement rather than defenseless immobility (Gladwin et al. 2016; Roelofs et al. 2010; Rösler and Gamer 2019). Furthermore, as elaborated above for animal studies, again experimental set-ups between different reports have to be compared carefully. For instance, subjects displayed bradycardia if the threat was inevitably, however cardiac accelerations were measured when the threat became avoidable (Krause et al. 2018; Löw et al. 2015).

Changes in HR are mediated by the ANS. The ANS divides into the sympathetic (SNS) and the parasympathetic nervous system (PNS), whose respective activity is dynamically balanced. The PNS is predominantly active during rest and decreases the HR via the vagal nerves. The vagal nerves projects to the pacemaker nodes of the heart and act via acetylcholine release, which results in a decrease of the HR (Shaffer, McCraty, and Zerr 2014). However, a majority of the vagal fibers are afferent and signal information about the cardiac activity through the nodose ganglion to the brain (Dampney 2016; Silvani et al. 2016). Conversely, efferent sympathetic nerves accelerate the cardiac activity and release noradrenaline, which results in the activation of beta-adrenergic receptors in the myocytes of the sinoatrial node (Dampney 2016; Silvani et al. 2016). The brain can regulate the cardiovascular system either by direct commands ("central command center"), or by feedback reflex systems (Dampney 2016; Silvani et al. 2016). Neuroanatomically, the cardiovascular center is located in the brainstem. Main players are the rostral ventrolateral medulla (RVLM), the spinal cord, the hypothalamus and the nucleus of the solitary tract (NTS). Information are mediated by parasympathetic preganglionic neurons that are located in the nucleus ambiguous (NA), the dorsal motor nucleus of the vagal nerve (DMV), and the reticular formation as well as sympathetic nerve cell bodies located in the upper thoracic segments of the spinal cord (Silvani et al. 2016). The cardiovascular system integrates afferent,

sensory information from the heart with inputs from higher order brain regions and orchestrates the balance between SNS and ANS activity (Shaffer and Venner 2013). The intrinsic control of blood pressure and HR is achieved by the negative feedback loop of the baroreflex system (Wehrwein and Joyner 2013). Pressure-sensitive baroreceptors are located throughout the ventricles, the carotid sinus, and the aortic arch. Afferent information of these mechanosensors are relayed to the NTS, which in turn innervates the NA in the medulla by glutamatergic projections and modulates the activity of vagal outflow. Additionally, projections to the ventrolateral medulla are controlling the sympathetic nerve activity. Thus, an activation of the baroreceptors ultimately results in an inhibition of the SNS and an activation of the PNS, which leads to vasodilation and decrease of the HR (bradycardia). It is hypothesized that the baroreflex is adjusted in accordance to the momentary behavioral state (Dampney 2017). It is believed to be reset upon physical exercise or stress in order to continuously keep the arterial pressure around a certain level that is appropriate for a given condition (Dampney 2017).

Heart rate variability (HRV) is an intricate feature of the cardiac system. It reflects the interplay between autonomic neural activity adjusted via heart-brain interactions, blood pressure and respiration (Shaffer and Venner 2013). One way of analyzing HRV is the extraction of different frequency bands and their respective power/amplitude (see 2.7.1) (Shaffer and Venner 2013).

Another regulatory system controlled by the ANS that has also been shown to be implicated in defensive reactions is the regulation of body temperature (Vianna and Carrive 2005). For instance, rats that were re-exposed to a context which was previously associated with an aversive electric shock, displayed a drop in tail and paw temperature, which could not be observed in non-conditioned controls (Vianna and Carrive 2005).

In summary, adaptations of the ANS in threat situations highly depend on the nature of the threat (i.e. innate vs. learned, context vs. cue conditioning, familiar vs. unknown environment). Therefore, when comparing studies on the autonomic aspect of the defense reaction, a consideration of the concrete experimental set-up as well as the temporal dynamics is crucial.

1.2. The concept of defensive states

The report of subjective feelings poses a critical aspect in investigating emotional states in humans. In animals, however, only observational correlations between supposedly emotional stimuli and observed responses can be drawn, which makes studying ‘emotions’ in animals challenging (Anderson and Adolphs 2014). Consequently, it is argued that, rather than attributing experimental observations to the anthropological terms emotions and feelings, focus

should be put on survival circuits and adaptive functions (LeDoux 2012). A more general approach describes fear as a 'central state' that is induced by threatening stimuli and generates many parallel physiological and behavioral responses to the threat (Anderson and Adolphs 2014; Silva et al. 2016). However, as pointed out before, previous studies on defensive 'states' were predominantly based on behavioral responses, omitting physiological or endocrine aspects of the fear reaction (Fustiñana et al. 2021; Gründemann et al. 2019; Reis et al. 2021). Nonetheless, numerous studies have also addressed autonomic changes to threats, which sometimes led to seemingly paradoxical findings, as concomitant behavioral changes were integrated insufficiently (Resstel et al. 2006; Stiedl and Spiess 1997; Walker and Carrive 2003). Incorporating both, behavioral observations as well as autonomic responses, not only enriches the description of defensive states, but also allows a more comprehensive understanding of these states and the integration of their individual components.

1.3. Neuronal circuits underlying defensive states

Neuronal networks underlying defensive brain states encompass cortical as well as mid- and hindbrain structures (Adolphs 2013). A classical model for innate fear circuits suggests a division into three functionally different modules: a detection unit, an integration unit, and an output unit (Silva et al. 2016). On the detection level, internal as well as external information are perceived through sensory modalities, processed by primarily cortical regions, and conveyed to the amygdala and hypothalamus representing the integration circuit of the innate fear network (Silva et al. 2016).

A brain region intricately linked to the fear circuit is the medial prefrontal cortex (mPFC). It exerts an important role in integrating contextual information by relaying information about contextual fear discrimination to the vlPAG and basolateral amygdala (BLA) (McGarry and Carter 2017; Rozeske et al. 2018). The amygdala poses a central integration role as an 'emotion center' not only in innate, but also conditioned fear brain circuits (Janak and Tye 2015; Jimenez and Maren 2009; Krabbe, Gründemann, and Lüthi 2018; Tye et al. 2011; Wolff et al. 2014). Electrical stimulation of the amygdala evokes fear-associated responses like increases in HR or freezing (Iwata, Chida, and LeDoux 1987; Weingarten and White 1978). The amygdala is located in the temporal lobes and is anatomically divided into the central amygdala (CeA) and the BLA. The BLA further divides into the lateral (LA), basal (BA), and basal medial (BMA) amygdala. The LA is seen as the main input region, receiving information about sensory inputs (i.e. auditory tone or somatosensory inputs; Rogan, Stäubli, and LeDoux 1997). It poses an

important structure for associative learning as signals of the US (e.g. footshock) and the CS (e.g. auditory stimulus) converge here (Rogan et al. 1997). The CeA, consisting mostly of GABAergic (gamma-aminobutyric acid) neurons, provides the major output of the amygdala, projecting to hypothalamus, midbrain, and brainstem (Herry and Johansen 2014; LeDoux et al. 1988). Furthermore, growing evidence depicts the CeA as an essential site for plasticity and as an integrator (Ciocchi et al. 2010; Fadok et al. 2018; Krabbe et al. 2018). It is hypothesized that, depending on the nature of the threat (i.e. innate vs. learned), different regions of the amygdala are engaged, resulting in the activation of different output pathways (Gross and Canteras 2012). For instance, learned threats (e.g. conditioned stimuli) elicit output through the CeA to the ventrolateral (vl) part of the periaqueductal gray (PAG), whereas innate threats (e.g. predator cues) are processed in the BMA, and are relayed directly to the hypothalamus, which ultimately conveys the output to the dorsolateral (dl) division of the PAG (Gross and Canteras 2012).

The hypothalamus consists of many subnuclei and is located as part of the diencephalon ventrally to the thalamus. It controls basic vegetative body functions and, thus, plays an important role in metabolism, thermoregulation, sleep, and reproduction (Canteras 2002; Saper and Lowell 2014). It has a critical role in the expression of defensive behaviors as demonstrated by stimulation experiments of the medial hypothalamus (Lammers et al. 1988; Silva et al. 2013; Silveira and Graeff 1992). Specifically the paraventricular nucleus of the hypothalamus directly innervates autonomic output centers like the NA and the DMV and, thus, mediates cardiac parasympathetic activity, i.e. slowing of the HR (Silvani et al. 2016). In the context of brain circuits related to fear and anxiety, the hypothalamus is classically seen as a relay center between amygdala input and downstream targets such as the PAG, exerting the defensive response (LeDoux 2012; Martinez et al. 2008). Nonetheless, it was shown recently that the ventromedial hypothalamus exerts control functions over defensive states by itself (Kennedy et al. 2020; Kunwar et al. 2015). Furthermore, the ventromedial hypothalamus and the dorsal PAG (dPAG) together were reported to encode for both sensory and motor aspects of the defense reaction during rat exposure (Esteban Masferrer et al. 2020).

Hindbrain structures are assumed to have executive roles in the fear network. The magnocellular nucleus (Mc), an aggregation of three brainstem nuclei (i.e. lateral paragigantocellular nucleus, LPGi; gigantocellular reticular nucleus ventral and alpha part, GiA and GiV), is involved in motor control actions and was shown to receive direct excitatory inputs from the PAG promoting freezing responses (Esposito, Capelli, and Arber 2014; Tovote et al. 2016). As mentioned above, brainstem regions, such as the dorsal vagal complex (DVC), a structure which encompasses the NTS, the DMV, and the area postrema, as well as brain areas such as the NA, and the reticular formation, represent the main output structures of the central

command center regulating cardiovascular function (Silvani et al. 2016). Again, the PAG serves as an important relay center by receiving cortical and subcortical information and passing the processed output further on to the aforementioned output structures. However, extending the PAG's view as a sole relay center, accumulating evidence suggests a more far reaching role of the PAG and attributes also integrative tasks to this midbrain structure (Deng, Xiao, and Wang 2016; Evans et al. 2018; Reis et al. 2021; Walker et al. 2020; Wright et al. 2019; Wright and McDannald 2019).

1.3.1. The Periaqueductal Gray

The PAG is a central part of the fear network located in the midbrain surrounding the cerebral aqueduct. It is an evolutionary conserved structure and is present in different vertebrates sharing homologous functions, but differs in the distribution of cell populations (Kingsbury et al. 2011; Silva and McNaughton 2019). Electrical as well as pharmacological stimulation of the PAG were shown to be associated with the expression of defensive responses (Bandler 1982; Bittencourt et al. 2005; Hunsperger 1956). A first demonstration of the PAG's involvement in fear-associated responses came from Hunsperger and colleagues, who electrically stimulated the central gray matter in cats (Hunsperger 1956). Next to its central role in defensive responses, the PAG is linked to sexual and maternal behavior as well as vocalization (Jürgens 1994; Lonstein and Stern 1997). Furthermore, the PAG was also shown to be involved in pain processing, as lesions of the vlPAG attenuated pain perception (Behbehani et al. 1990).

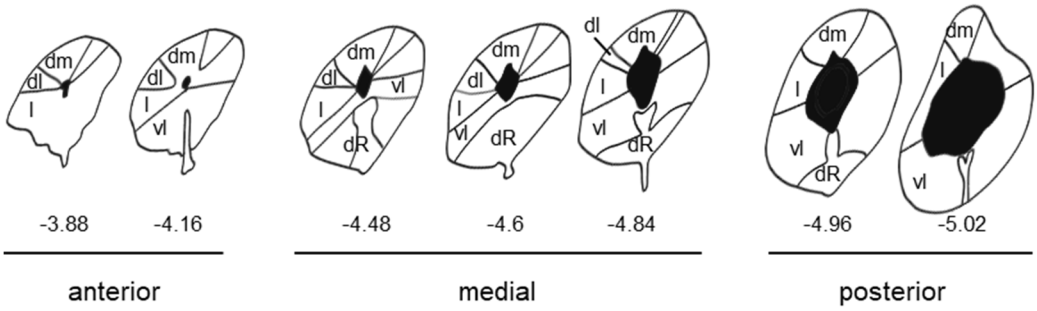

Figure 2 - Columnar organization of the PAG throughout the anteroposterior axis.
Numbers indicate bregma level. dm: dorsomedial, dl: dorsolateral, l: lateral, vl: ventrolateral, dR: dorsal raphe nucleus. Adapted from Allen Brain Atlas, Franklin & Paxinos.

In humans, fMRI studies and deep brain stimulation showed PAG activation in response to the anticipation of pain or aversive stimuli as well as modulation of the cardiovascular response (Green et al. 2010; Mobbs et al. 2007).

Classically, the PAG is anatomically divided into a columnar organization (Figure 2, Bandler et al. 2000; Depaulis, Keay, and Bandler 1992). Following the dorsoventral axis, it consists of

a dorsomedial (dm), dorsolateral (dl), lateral (l) and ventrolateral (vl) subregion. The dorsal raphe (dR) nucleus, a structure located most ventrally to the PAG, is argued to be considered as a component of the PAG complex as well (Silva and McNaughton 2019). Lesion studies as well as microinjections of excitatory and inhibitory agents into the different columns of the PAG built the basis for this topographic distinction. While an activation of the dorsal and lateral aspects of the PAG are associated with active coping strategies like a flight reaction and concomitant tachycardia, stimulation of the vlPAG was shown to result in hyporeactivity, bradycardia, and opioid mediated analgesia (Bandler 1982; Bandler et al. 2000; Bandler and Shipley 1994; Carrive 1993; Depaulis, Keay, and Bandler 1994; Fanselow 1991). These findings built the basis for the model of the columnar PAG function, however some reported results differ from this model. For instance, excitation of the caudal lPAG was shown to cause immobility, while electrical stimulation of the vlPAG have been reported to result in escape bouts (Depaulis et al. 1992; Vianna, Landeira-Fernandez, and Brandao 2001). These results were underpinned by optogenetic perturbations in the PAG. Unilateral optical activation by ubiqutinously expressed Channelrhodopsin (ChR2) of the vlPAG subregion in rats induced freezing at low light power intensities, while higher intensities evoked activity responses (Assareh et al. 2016). Furthermore, with increasing light powers, animals receiving lPAG stimulation displayed the full range of defensive strategies from freezing to flight (Assareh et al. 2016).

With the advent of optogenetics, a more specific dissection of fear circuits became feasible. Going beyond stimulation of entire brain regions, optogenetics allowed to optically activate molecularly defined subpopulations of neurons and thus contributed to mechanistically characterize the PAG neuronal circuitry further. Whereas the exclusive stimulation of glutamatergic neurons in the vlPAG were reported to evoke freezing responses, the inhibition of the same population was associated with decreased freezing levels and reduced innate fear reactions (Tovote et al. 2016). However, electrical recordings from the vlPAG of identified glutamatergic neurons showed a correlation with freezing only in half of the recorded neurons (Tovote et al. 2016). Recently, only a sparse subset of glutamatergic l/vlPAG cells was targeted in order to refine the manipulated cell population even further (La-vu et al. 2022). As opposed to the freezing response elicited by the broad activation of the vlPAG, selective activation of cholecystokinin-releasing l/vlPAG neurons resulted in flight to safer regions (La-Vu et al. 2022). The dlPAG, in turn, was considered to play a key role in mediating innate defensive behaviors (Bandler and Depaulis 1988; Vianna et al. 2001; Watson et al. 2016). In fact, activation of dorsal regions of the PAG was shown to be associated with flight responses, but, interestingly, also with increased freezing levels (Deng et al. 2016; Esteban Masferrer et al.

2020; Evans et al. 2018; Tovote et al. 2016). In addition, dPAG was shown to mediate also risk assessment behavior and avoidance of open spaces (Deng et al. 2016; Gomes et al. 2014; Sukikara et al. 2010).

The PAG can be seen as an functional interface between the forebrain and the brainstem, as it is densely connected to both structures (Benarroch 2012). Afferent projections from the forebrain to the PAG originate in the cingulate and medial prefrontal cortex and the CeA (Floyd et al. 2000; Rizvi et al. 1991). The PAG receives strong innervation from the hypothalamus as well (Roeling et al. 1994; Shimogawa, Sakuma, and Yamanouchi 2015). Functional investigations of projections from the ventromedial hypothalamus to the dPAG were shown to elicit immobility (Wang, Chen, and Lin 2015). Furthermore, dissecting the hypothalamus-midbrain circuit in a cell-type specific manner, lateral hypothalamus excitatory projections to the PAG were shown to control evasion from danger, while inhibitory projections drive predatory attack (Li et al. 2018). Focusing onto the brainstem, medullary afferents, like the caudal part of the NTS, the ventrolateral medulla, and even parts of the spinal cord connect to the PAG, while omitting the dlPAG as target (Blomqvist and Craig 1991; Herbert and Saper 1992). These projections provide bottom-up signaling and thus are important for delivering input about interoceptive processes. The intra-PAG connectivity is strong throughout the anteroposterior axis between all subregions, with the dorsolateral part building an exception to receive only afferents from the dmPAG (Jansen et al. 1998). Also in terms of efferent projections, the dPAG occupies an extraordinary role. Unlike vl/lPAG subregions, the dm and dlPAG project only sparsely to forebrain structures, like the hypothalamus (Meller and Dennis 1991). Furthermore, the dPAG shows prominent connections to the ventrolateral medulla and spinal cord (Carrive 1991; Henderson, Keay, and Bandler 1998; Silva and McNaughton 2019). The vlPAG and the dR, in turn, send mostly dopaminergic projections to the CeA (Reichling and Basbaum 1991). Moreover, the vlPAG sends projections to the hippocampus and hypothalamus (Meller and Dennis 1991; Shimogawa et al. 2015). Here, the dlPAG strongly projects to the anterior hypothalamic nucleus, thus providing an important ascending projection mediating aversive associative learning (Kincheski et al. 2012). In terms of downstream targets in the hindbrain, the pre-motor Mc represents another important target structure of the vlPAG (Esposito et al. 2014; Tovote et al. 2016). The suggested disinhibitory freezing pathway describes long range GABAergic neurons projecting from the amygdala to the vlPAG and inhibiting local GABAergic interneurons, leading to an activation of glutamatergic vlPAG-to-Mc neurons (Tovote et al. 2016). As previously mentioned, also in mediating cardiac function, neuroanatomically, the PAG constitutes an important integration center. The lateral and ventrolateral division of the PAG were shown to project to the NA in the RVLM and the

DMV/NTS, where cardiovascular responses are regulated (Bandler and Tork 1987; Chen and Aston-Jones 1996; Critchley and Harrison 2013; Farkas, Jansen, and Loewy 1997). Furthermore, mostly posterior lPAG divisions project to the caudal ventrolateral medulla (Chen and Aston-Jones 1996).

The groundwork of the PAG's role in cardiovascular responses was built by Bandler and colleagues, who dissected in a series of experiments the cardiac responses after activation or inhibition of the different subregions (Bandler and Carrive 1988; Bandler, Carrive, and Zhang 1991; Bandler and Shipley 1994; McDougall, Dampney, and Bandler 1985). While, injection of excitatory amino acids into the vlPAG of cats decreased HR (Carrive and Bandler 1991), electrical stimulation of the dPAG in anesthesized rats was reported to induce tachycardia (Lovick 1992). It is hypothesized that the PAG exerts these effects through the NTS, as its blockade resulted in an attenuation of the cardiac response after dlPAG stimulation (Huang et al. 2000). Looking at the PAG's role in mediating cardiovascular responses in the context of conditioned and innate fear responses, Walker and Carrive showed that pharmacological blockade of the vlPAG evoked next to decreased freezing levels, increased HR values in a contextual fear paradigm (Walker and Carrive 2003). Further investigating the role played by the PAG in the generation of bradycardia during fear reactions, pharmacological vlPAG activation was shown to mediate a suppression of bradycardic events during an innate fear response to white noise exposure (Koba et al. 2016).

Taken together, with its multiple input/output neuronal connections as well as the tight intra-PAG connectivity, this midbrain region, neuroanatomically, builds an optimal center for the coordination of different bottom-up and top-down information. Consequently, in recent years, evidence is accumulating that, rather than seeing the PAG as a mere 'effector' brain region for fear reactions, it might serve as an active integrator of relevant threat stimuli and threat probability estimator itself (Reis et al. 2021; Wright and McDannald 2019). Electrical recordings in the vlPAG revealed a correlation of threat probability with neuronal activity in this region, independent of the displayed fear output (Walker et al. 2020; Wright et al. 2019; Wright and McDannald 2019). Similarly, also the dPAG seems to have a broader function than a premotor center by acting as a risk estimator that represents approach-avoidance states (Deng et al. 2016; Reis et al. 2021). Making use of an aversive overhead looming stimulus, Evans et al. suggest the dPAG to compute escape decision by thresholding threat information (Evans et al. 2018). Moreover, two major, non-overlapping populations in the dPAG were found to be correlated either to avoidance behaviors and were active farther from threats or to risk assessment behaviors and near threats (Reis et al. 2021). Finally, the PAG's strong ascending

projections to forebrain structures like the hypothalamus suggests a more complex modulation of defensive responses than a mere downstream target of the defensive network in the brain (Motta, Carobrez, and Canteras 2017a).

1.4. Aim of thesis

The defense reaction includes multiple interacting behavioral, autonomic and endocrine adaptations that depend on external as well as internal cues. However, most studies so far investigated behavioral or autonomic measures only in isolation and, therefore, based fear and anxiety only on these individual entities (Gründemann et al. 2019; Koba et al. 2016). For instance, freezing is correlated to "fear" without considering potential varieties in the concomitant cardiac responses. In order to refrain from equating fear to single entities considered in isolation, this thesis aimed to investigate the integrated nature of defensive states consisting of stereotypical combinations of behavioral and autonomic read-outs. To this end, behavioral, cardiac as well as thermal read-outs were recorded simultaneously, while multifactorial experimental conditions (e.g. changes of the context) were considered in an integrated analysis on different time scales of the resulting multimodal datasets. In particular, the dynamics of cardiac responses during defensive reactions have been taken into account by building an analytical framework. This framework aimed in a more fine-grained description of cardio-behavioral defensive states by disentangling HR dynamics into global, slow acting macrostates as well as short-term, fast acting microstate switches.

Next, by using the suggested integrated framework to better describe defensive states in mice, perturbational methods were used in an attempt to identify neuronal correlates responsible for an individual defensive state. By optical manipulations, different circuit elements in the PAG were tested for their involvement in the generation of cardio-behavioral defensive states. In a first step, the entire glutamatergic cell population was optically activated and evoked cardio-behavioral responses were observed. Subsequently, in order to narrow down potential candidates involved in the defensive reaction, only a subpopulation of glutamatergic neurons, Chx10+ cells, were targeted and investigated by both, optical activation and inhibition. Lastly, optical manipulations on inhibitory GABAergic neurons were conducted. With the aim of identifying downstream targets of glutamatergic neurons, subsequently, anterograde tracing experiments were conducted. Having identified potential brainstem projection targets of those neurons located in the PAG that may convey information about the defensive state to the heart and muscles, an intersectional optogenetic approach was used to target cell population - and

projection-specific neurons. Cardio-behavioral state observations during projection-specific circuit manipulations were expected to give further insights into the brain defensive network. This experimental outline could answer if the activation of vlPAG neurons projecting to a brainstem target responsible for mediating freezing responses, also elicits bradycardic responses and vice versa.

By exploiting modern neuroscience techniques, it was aimed to resolve better anatomical-functional relationships in specific defensive circuit elements in the PAG, which are determined by their molecular identity and projection profile. A detailed description of evoked cardio-behavioral states during optical manipulation of distinct neuronal populations will reveal potential defensive microstate generators in the brain.

2. Material and Methods

2.1. Animals

Wildtype as well as mutant mice were bred in the animal facility of the Institute of Clinical Neurobiology at the University Hospital of Würzburg. All animal procedures were performed in accordance with institution guidelines and were approved by a license of animal testing (authorization 55.2.2-2532-2-509 and 55.2.2-2532-2-1067) and in accordance with the local veterinary authority (Veterinäramt Würzburg) and Committee on the Ethics of Animal Experiments, i.e., Regierung von Unterfranken, Würzburg. Mice were housed individually in a 12:12 hours light:dark cycle at constant temperature 22 ±1.5 °C and a humidity of min. 55 %. Food and water were available *ad libitum*. *VGlut2-IRES-Cre* knock-in mice (stock no. 208863) and *Gad2-IRES-Cre* knock-in mice (stock no. 028867) were obtained from Jackson Laboratory. *Chx10-Cre* animals were kindly provided by Ole Kiehn (University of Copenhagen). were used. For all experiments, mice that were heterozygous for the respective transgene were used. Transgenic mouse lines and the sequences of primers that were used for the respective genotyping are provided in
Table **2**. Genotyping was performed by Katrin Walter. While for behavioral experiments only male mice were used, tracing experiments were performed in female mice. All experiments were carried out in mice in the age of two to seven months.

2.2. Viral vectors

Adeno-associated viruses (AAVs) were used as vectors to transduce neurons *in vivo* and, by this, transfer genes encoding fluorescent molecules for tracing or opsins for optogenetic experiments, respectively. AAVs are non-pathogenic viruses, which excel long-term expression and minimum immune responses, making them an ideal tool to safely deliver transgenic material (Samulski and Muzyczka 2014). The AAV genome consists of two open reading frames, Rep and Cap. Rep genes are translated into proteins necessary for packaging, while Cap genes are translated into proteins required for the viral capsid. Additionally, a helper plasmid encoding adenovirus genes (*E4*, *E2A* and *VA*) is needed for replication into host cells (Samulski and Muzyczka 2014). The transfer plasmid itself delivers the genes of interest for the respective experiment (see 2.2.1).

AAVs were produced in house by Hildegard Troll. Briefly, human embryonic kidney cells (HEK-293) were transfected with all three plasmids (*Rep/Cap* plasmid, AAV helper plasmid, and transfer plasmid) with the transfer plasmid flanked by two inverted terminal repeats (ITR). After two to three days of incubation, HEK cells were harvested, lysed and viral particles were purified by an Iodixanol gradient with ultracentifugation. After harvesting the viral fraction, it was washed with phosphate buffered saline (PBS) and centrifuged in three rounds to remove iodixanol residues and to concentrate the virus.

2.2.1. Plasmids

To gain specificity of targeted neuronal subpopulations, it was made use of the Cre-Lox system (Haery et al. 2019) in all performed experiments. To this end, transgenic mice, expressing the Cre-enzyme in a specific neuronal population (see 2.1) were transduced with AAVs delivering genes flanked by Lox sites, short palindromic sequences that, in the presence of the Cre-enzyme and depending on their orientation, results in either deletion, inversion, or exchange of gene cassettes (www.addgene.org/guides/aav/).

For experiments presented in this thesis, several Cre-dependent plasmid constructs were used. In order to manipulate cell activity by light stimulation, it was made use of a plasmid encoding for a red-activatable Channelrhodopsin (*hSyn-FLEX-ReaChR-Citrine-WPRE*), an optical actuator (Lin et al. 2013). A corresponding control plasmid encoded solely for a red fluorescent protein (*hSyn-FLEX-mCherry-WPRE*). Furthermore, a plasmid delivering - in the presence of Cre - genetic information for an optical inhibitor, Archaerhodopsin (*CAG-FLEX-ArchT-tdTomato*) was used (Chow et al. 2010). Anterograde tracing experiments were performed with the help of a construct expressing cre-dependently a synaptophysin fused Myc-tag, labeling presynaptic terminals (*CAG-floxed-Synaptophysin-10xMyc-WPRE*) (kindly provided by Silvia Arber). For intersectional optogenetic experiments, it was made use of a double-conditional approach, using a combination of a *CAG-Floxed-FlpO-2A-H2BV5-WPRE* (kindly provided by Silvia Arber) and a *hSyn-Con/Fon-hChR2(H134R)-EYFP-WPRE* plasmid (kindly provided by Johannes Letzkus). A list of plasmid constructs used with respective AAV capsids and their titers is summarized in Table 3.

2.2.2. Viral vector testing

To control for sufficient titers of in house produced viruses, viral vectors were tested quantitatively (quantitative PCR) as well as qualitatively (*in vitro* HEK cell transduction). The latter was performed by using a HEK293 cell line, which stably expresses the Cre recombinase gene under a suCMV promoter and carries Blasticidine as a selection marker (GenTarget). HEK293-Cre cells were kept in complete medium supplemented with Basticidine (10 µg/ml). Cells were split two to three times a week by shortly washing them in HBSS, followed by dissociating cells with Trypsin-EX (diluted 1:5 in HBSS). Trypsinization was stopped by adding an excessive amount of complete medium followed by titration with a glass pipette. Cells were diluted 1:5 in medium and grown in T25 cell flasks at 37 °C and 5 % CO_2. 50.000 HEK293 cells were seeded on Poly-L-ornithine coated cover glasses and infected with 1µl AAV diluted in 500 µl complete medium. Cells were incubated for three days before they were fixed in 4 % paraformaldehyde (PFA) for 15 minutes at 37 °C. After washing with PBS, cells were submitted to an immunocytochemical staining to visualize expressed plasmid markers. Briefly, after incubating cells in blocking solution (Table 7) for one hour, primary antibodies diluted in blocking solution were added for two additional hours. Following a washing step, cells were incubated in the secondary antibody likewise diluted in blocking solution. Cell nuclei were counterstained with DAPI (4′,6-diamidino-2-phenylindole), washed and cover slips were mounted onto object slides for imaging. For qualitative *in vivo* tests of AAVs, Cre-dependent viruses were injected into brains of heterocygous *VGlut2-IRES-Cre* animals. To control for off-target expression, also wildtypic mice were injected intracranially with the respective viruses (protocol, see 2.3.1). Animals were sacrificed after four weeks and brains were sectioned and processed as described below (see 2.9 and 2.10).

2.3. Stereotaxic surgeries

For all stereotactic procedures, mice were prepared for surgery with an administration of Buprenorphin (Buprenorvet, Bayer) for systemic analgesia. Mice were deeply anesthetized for 2-3 minutes with 4-5 % isoflurane/O2 (Anesthetic vaporizer, Harvard Apparatus), head was shaved and all remaining hair were removed with a depilatory cream (Veet). Mice were then fixed in a stereotactic frame (Kopf, Model 1900) and anesthesia was maintained with 1.5-2 % isoflurane throughout the surgery. During procedures, animals were kept on a heating pad. A subcutaneous injection of Ropivacain (Naropin, Aspen) was used for local analgesia before opening the scalp. Following the respective procedure (stereotactical injection, implantation of optical fibers, or implantation of electrocardiogram (ECG) electrodes, see 2.3.1 - 2.4), for post-

surgery-analgesia, a subcutaneous injection of Metacam (Metacam, Boehringer Ingelheim) was applied. Mice were closely monitored and kept under infrared light until they displayed normal locomotive and grooming behavior. For at least seven days following the surgeries, mice were monitored daily by controlling their body weight, physical appearance and behavior. Additional doses of Metacam were applied, whenever necessary.

2.3.1. Intracranial injections

Mice were prepared like described above and skull was calibrated in the stereotactic frame with bregma and lambda as reference points. Craniotomies with a diameter of 0.4 mm were performed at bregma coordinates anterior-posterior (AP) -4.7 mm, mediolateral (ML) +/-0.55 mm for injections into the vlPAG and at AP -6.3 mm, ML +/-0.65 mm for injections into the Mc. A glass pipette (Drummond Scientific, USA) filled with the according viral vectors (Table 3) was slowly lowered to the target depth of -2.8 mm (dorsoventral, DV) for the vlPAG and -6.2 mm for the Mc from bregma. While inserting the pipette into the brain tissue, any bleeding was avoided. Depending on the experimental setup and the AAV used, a volume of 50-100 nl was injected with a pressure injector (NPI electronic, Germany) at an injection speed of 30-40 nl/min. After injection, the capillary was hold in place for additional eight minutes before retracting. The wound was closed and treated with antiseptics (Braunol, Braun).

2.3.2. Implantations of optical fibers

Optical fibers were either implanted in the same procedure as the injection or in a second surgery. After removing a skin patch of 1 cm in diameter from the scalp, the skull surface was cleaned and carefully dried. To increase the skull surface and guarantee proper attachment of the head cap, the bone was scratched with a scalpel blade.

For bilateral light delivery to the target region (vlPAG) during optogenetic experiments, two self-produced optical fibers (optical fiber: Thorlabs, 200 µm, 0.39 NA; ceramic ferrule: Thorlabs; exclusion of fibers with light loss > 25 %) were inserted bilaterally at an angle of 20°. Craniotomies were performed at bregma coordinates AP -4.7 mm, ML +/-1.6 mm. Fibers were calibrated to brain surface and lowered -2.1 mm in DV direction at a speed of 0.5 mm/min. Ferrules were fixed to the skull by multiple layers of cyanacylate glue. As a last layer, black, intransparent glue was applied on the head cap and ferrule bases in order to prevent visual irritation of the animal during light delivery during behavioral experiments.

2.4. Implantation of HR connectors

All animals were equipped with electrocardiogram electrodes for measuring HRs during behavioral experiments. For this purpose, three teflon-coated 7-strand stainless steel wires (Science Products, Germany) were soldered onto micro connectors (Omnetics MSA components, Germany). Two wires were used for HR derivation, and the third was used for grounding. Soldering joints were insulated by a layer of cyanacrylate glue.
Implantation of wires was performed in the same surgery as for implantation procedures. Two small incisions were made rostral to the right and caudal to the left foreleg (Figure 4A). With a blunt-ended feeding needle (Fine Science Tools), a subcutaneous tract was created carefully, starting from the chest incision towards the incision on the head. Three millimeters of the wire end were stripped and passed through the hollow cannula. The cannula was removed and the wire ends equipped with a small glue ball on the very distal wire end. Coils were sutured onto the exposed muscle (*Musculus pectoralis* and *abdominalis external oblique*) on the thorax. The skin was closed and disinfected, the connector was mounted onto the skull, and ultimately enclosed into the head cap.

2.5. Behavioral paradigms

In order to investigate defensive responses, mice were tested in a series of different anxiety and fear paradigms. Starting with exploratory and mild anxiogenic tests (Open Field, Elevated Plus Maze, Light Dark Box), mice ultimately underwent the Conditioned Flight Paradigm (CFP), a modified version of a classical fear conditioning paradigm (Figure 3). Mice were handled for at least three days before starting data acquisition to habituate them to the procedure of cable connection for the electrocardiogram recordings. During all paradigms, videos, HRs and thermal data were recorded.

2.5.1. Anxiety Tests

Open Field

The apparatus of the Open Field test (OF) consisted of a 50 cm x 50 cm x 50 cm white square box. At the center of the context a light intensity of 330 LUX was measured. Animals were placed inside the box for 15 minutes and freely explored the environment.

Elevated Plus Maze

The Elevated Plus Maze (EPM) consisted of two elevated (25 cm height) open and two wall-enclosed arms (8 cm width, 28 cm length). The four arms met in the middle at a platform from which the animal could enter all four arms. Animals were placed on the crossing point and et freely explore the context for 15 minutes.

Light Dark Box

The context of the Light-Dark Box (LDB) consisted of two equally shaped compartments (30 cm x 15 cm), where one is non-illuminated and built with black walls (50 Lux) and the other side is covered by white walls and enlightened by a LED strip (350 Lux). Mice were placed inside the dark compartment and recorded for 15 minutes while freely exploring the box.

2.5.2. Conditioned Flight Paradigm

The CFP is a modification of classical auditory Pavlovian Fear Conditioning (Fadok et al. 2017; Hersman et al. 2020; Totty et al. 2021). The auditory CS consists instead of a single cue of a serial compound stimulus (SCS) comprising ten seconds pure tone (7.5 kHz, 75 dB, 500 ms beeps, 1 Hz) followed by ten seconds white noise sound (1-20 kHz, 75 dB, 500 ms bursts, 1 Hz), the US is a foot shock (0.9 mA, 1 s, Model 2100 Isolated Pulse Stimulator, Figure 3). While mice respond to the pure tone with a high probability with freezing, the white noise evokes higher probabilities of flight (Figure 3).

Pre-exposure day

Mice were placed on the first day into a neutral context (cylindric white chamber with a diameter of 27 cm), in which the SCS was played four times with a randomized inter-stimulus interval (ISI).

Conditioning day 1 & 2

During Conditioning day 1 and 2 (CD1, CD2), the conditioning context consisted of a red transparent square box (30 x 30 cm) with a grid floor to deliver footshocks, which was wiped with 70 % ethanol. The conditioning was performed on two consecutive days with five tone shock pairings (pseudorandomized inter-stimulus interval of 170-230 s after a three minute baseline period) on each day. Total recording time per session was 20 minutes.

Retrieval

For the Retrieval day, animals were placed into a cylindric chamber (27 cm in diameter) which was cleaned with 1 % acetic acid. 16 pseudo-randomized presentations of the SCS (pseudorandomized ISI of 80-140 s) were presented during a 32 minute session. A second group of animals were placed in their homecage instead a new context while replaying the SCS cues. In a separate experiment, animals were likewise recorded in their homecage, but left unperturbed for 40 minutes. Then the pure tone component of SCS was presented for 2 minutes.

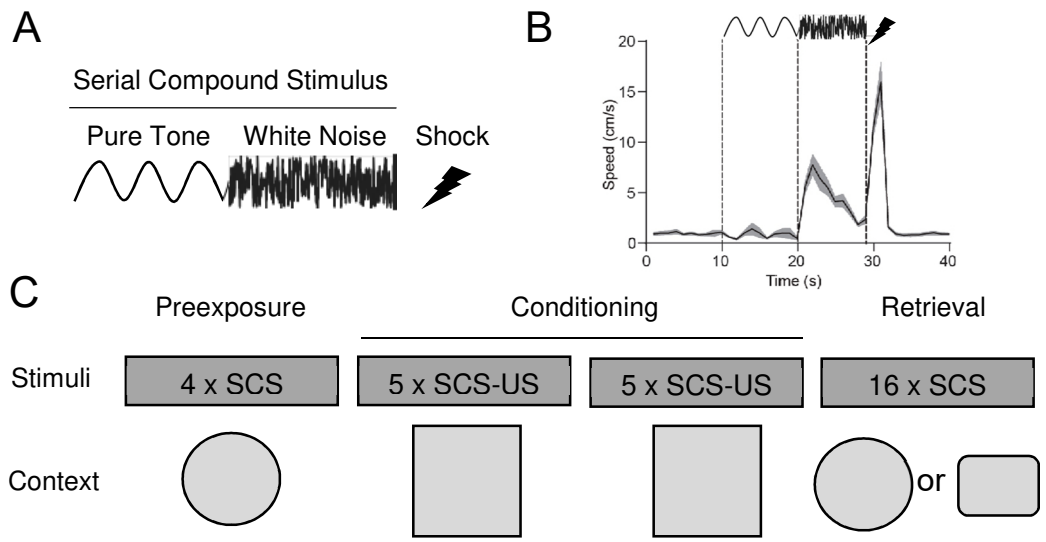

Figure 3 - The Conditioned Flight Paradigm allows for observation of two opposite coping mechanisms within the same paradigm.
(A) The acoustic serial compound stimulus (SCS) consists of 10 s pure tone beeps and a 10 s white noise sound, which is followed by a footshock. (B) Behavioral response to the SCS presentation and the footshock (adapted with permission from Fadok et al. 2017). (C) Overview of the paradigm. After the preexposure, where animals are presented with the SCS alone, on the second and third day, animals receive repeated pairings of SCS and footshocks in the same conditioning context. On the last day, animals are put into either a new context or their homecage and are presented again with the SCS alone.

2.6. Recording of behavior

Behavioral experiments were conducted in sound-attenuated chambers (100 cm x 80 cm x 116 cm), in which an adjustable LED ring lamp was mounted. Depending on the experiment, different contexts were placed into the chambers. One chamber served as low anxiogenic environment with dim light (130 Lux) and lined with dark foam and cleaned with 1 % acetic acid. A second chamber was used for the conditioning sessions, enlightened with 350 Lux, lined with white foam and cleaned with 70 % ethanol. During all sessions, animals were recorded with a RGB camera (Pike Camera F-032C, Allied Vision, Campden Instruments). The recording system consisted of an acquisition system (Plexon, Omniplex system), with which analog as well as digital signals were recorded. The software CinePlexStudio (Plexon, version

3.0) was used for video recording and online tracking whenever closed-loop optogenetic stimulation was necessary. The software Radiant (Plexon, version 2.2.0.19) was used for general triggering start and stop of the recordings as well as creating stimulation protocols for optogenetic experiments. A RZ6 Multi-I/O processor (Tucker-Davis Technologies) served as online processing machine, auditory signal processor to deliver acoustic stimulations via a multi-field magnetic speaker (MF1, Tucker-Davis Technologies) and to control shock delivery by the stimulus isolator (Model 2100 Isolated Pulse Stimulator, A-M Systems). In order to guarantee synchronization between RGB and thermal camera as well as ECG recordings, a MATLAB/RPvdsEx interplay was implemented (custom written code developed by Jérémy Signoret-Genest).

2.6.1. Motion tracking

Animals were tracked offline by processing RGB movies from the top view camera using a custom written MATLAB code (developed by Jérémy Signoret-Genest) with an interactive GUI. In principle, a calculated background was subtracted from each frame to determine the animals' position. The 80^{th} percentile of an evenly distributed set of frames across the recording was used to calculate the background. A threshold was set manually and refined by adjusting values for morphological opening and closing of the contour as well as removal of small objects interfering with a proper detection of the mouse body shape. Coordinates for contour and center of gravity were extracted for further analysis. Furthermore, the GUI allowed for distance calibration, such that normalization among different contexts and calculation of speed values were possible. Motion measure was computed as the percentage of pixel change of the mouse contour from one frame to the next (non-overlapping pixels / total pixel count).

2.6.2. Scoring of behavioral bouts

DeepLabCut (DLC, Mathis et al. 2018; Nath et al. 2019, version 2.1.8.1) was used to track specific body parts: snout, ears, paws and tail divided in five parts. Using the obtained coordinates, a custom written MATLAB GUI (developed by Jérémy Signoret-Genest) was used to annotate the time intervals in which the following behaviors occurred: immobility, rearing, grooming, stretch-attend posture, immobility, fast locomotion, and head dips (specific only for EPM recordings). The GUI provided a semi-automated threshold-based detection of the aforementioned behavioral bouts, which were visually inspected and, if necessary, refined by

the experimenter. A combination of specific values for body part positions, angles and distances were used as thresholds to determine the respective type of behavior. Thresholds could be adjusted manually to improve detection whereby rather conservative settings were aimed to reduce false positive behavioral bout detections. Frames with cable obstruction or periods in which the animal was entangled with cables and could not freely move were excluded within the same GUI.

2.7. Analysis of autonomic parameters

2.7.1. HR acquisition and extraction

Electrocardiogram data were differentially recorded from the two wires sutured subcutaneously to the animals' chest (compare 2.4, Figure 4A). Signals were acquired at 5 kHz and amplified and filtered by a differential amplifier (DPA 2FX/FS, npi electronics). Data were written and saved as .pl2 files (Plexon, version 2.2.0.19). R Peaks of the ECG signal were extracted with a custom-written MATLAB GUI (by Jérémy Signoret-Genest). Briefly, signal was bandpass filtered, enhanced and smoothed by a Gaussian filter. The resulting peaks were thresholded and each heart beat was compared to a template heart beat, which was created by averaging the waveforms with amplitudes between the 70^{th} and 90^{th} percentiles of all the waveforms' amplitudes. A selection process, which scores the similarity to the template and the distance from previous heart beats, was applied. The R peaks extracted by this procedure were subsequently visually inspected by the experimenter and ranges with high noise contamination were manually excluded. Following the manual post-processing, the HR was computed by using a sliding window of 0.6 seconds and resampled to a fixed sampling rate of 4 Hz.

To extract the low frequency (L.F.) band of the HR, which ranges between 0.4 and 0.8 Hz in mice (Thireau et al. 2008), continuous 1-D wavelet transform (MATLAB wavelets toolbox, The MathWorks, version 5.3) was used to extract this frequency band. Figure 4 visualizes a raw HR signal, the extracted signal of the L.F. range and its respective amplitude throughout the session. In order to account for the rising HR in general as well as for the decreasing minima of HR values throughout the sessions, a 'HR-to-ceiling' measure was introduced. HR values were subtracted from a local theoretical maximum HR curve (Figure 4C). This was calculated by extracting local maxima from a resampled and filtered HR and then smoothed with a sliding quadratic linear regression.

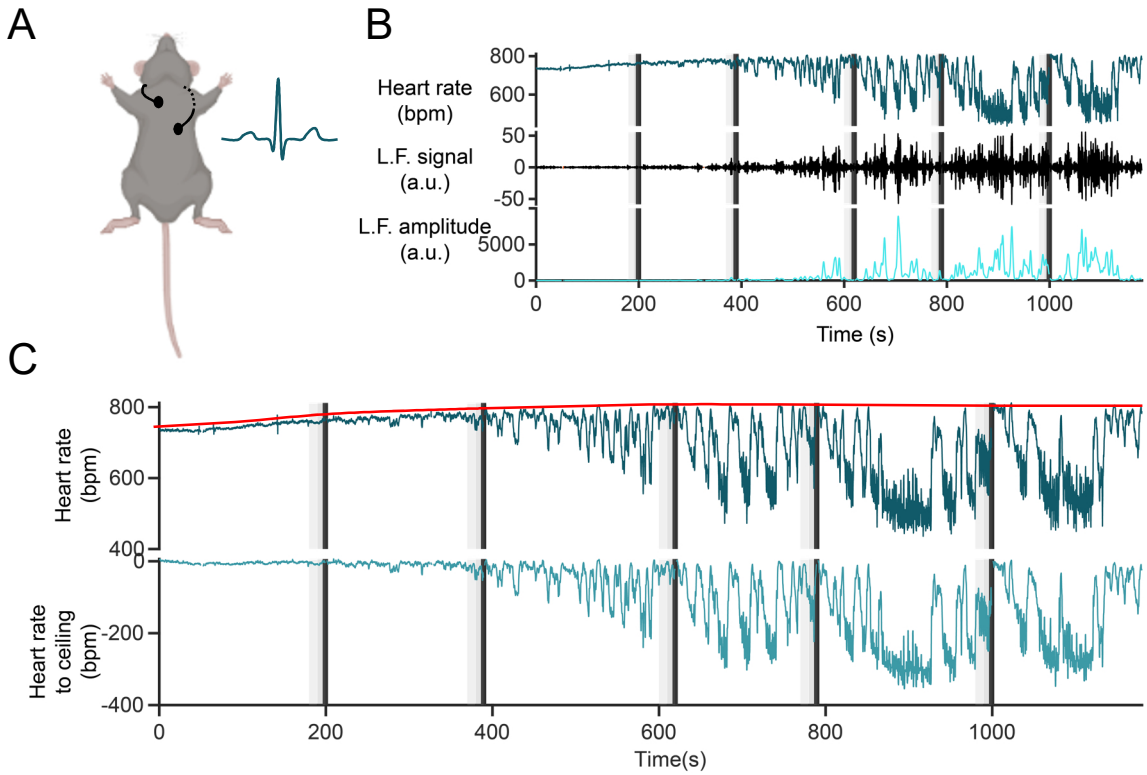

Figure 4 - HR measurements and extraction of cardiac derivates.
(A) Electrocardiogram recordings were derived from subcutaneously implanted ECG electrode wires sutured onto the chest. (B) Example HR trace with respective signal and amplitude of the extracted low frequency band (0.4-0.8 Hz). (C) Example HR trace and theoretical maximum HR curve (ceiling curve, red) obtained by extraction of local maxima and subsequent smoothing and visualization of resulting HR-to-ceiling curve (analysis done by Jérémy Signoret-Genest). Mouse image adapted from BioRender.

2.7.2. Thermal imaging

An infrared camera (A655sc, FLIR) was used to acquire temperature data. Data were displayed and written within a custom written MATLAB GUI (developed by Jérémy Signoret-Genest), which was also used for calibration and focusing prior to experiments. Recordings were triggered (start and stop) by PlexBright, which sent signal to the RZ6 and a MATLAB/RPvdsEx interplay (Tucker-Davis Technologies). TTL signals were broadcasted to all systems to allow

for later offline synchronization between cameras and ECG recordings. Thermal data were saved as .seq files and converted to .mj2 files (range limit 15-50 °C, 8 bits). Like described above for tracking of the RGB videos, mice were tracked also in the thermal video recording to obtain coordinates for mouse position, contour and motion. RGB and thermal camera data were synchronized temporally. After determination of the transformation between both cameras (Procrustes analysis), camera views were aligned spatially in order to transfer coordinates of body parts obtained by DLC derived from the RGB movie onto the thermal movies. The tail was subdivided in four segments with rectangular masks overlaid. The highest temperature from each mask was extracted. The thermal data presented in this thesis show temperatures of the second tail segment.

2.8. Optogenetics

Mice undergoing optogenetic experiments were admitted to a minimum of seven days of recovery after optical fiber implantation before starting to habituate them to the handling procedure on four consecutive days. Depending on the experimental set-up, chosen opsin and injected brain region, a series of recording days was performed. For optical stimulation, a LED fiber light source was used (Ce-YAG optical head, Doric). Depending on the opsin in use, different bandpass filters were applied (Table 1). Light intensities were adjusted using an optical power meter (Thorlabs). The software Radiant (Plexon, version 2.2.0.19) was used to create stimulation protocols.

Table 1 - Used opsins and respective bandpass filters.

Opsin	Bandpass filter/ wavelength
ChR2	473 nm
ArchT	549 nm
ReaChR	612 nm

Optical activation in naïve mice

Naïve mice were placed in a cylindric context and stimulated with increasing light intensities and frequencies during a first screening to determine stimulation settings of the laser. These settings were then used in a standardized protocol with repeating stimulations across a ten minutes recording on a second test day (five stimulations for 10 s with an ISI of 105-155 s). For this, animals were placed also into a cylindric chamber (30 cm in diameter) with the floor being covered with homecage bedding. Stimulation frequencies and intensity differed among the

mouse lines. *VGlut2-IRES-Cre* mice were stimulated with low (intensity 0.5 mW, 20 Hz, 10 ms) and high (intensity 3.5 mW; frequency 10 Hz, 20 Hz or constant, pulse width 10 ms) stimulation settings in two different sessions. *Chx10-Cre* mice received stimulations with an intensity of 7 mW (30 Hz, 10 ms). Naïve *Gad2-IRES-Cre* mice were stimulated for longer periods (5 times for 30 s, 12 mW, 30 Hz, 10 ms), while exposed to the OF context instead of a cylindric chamber.

Optical activation in the homecage

A subset of *VGlut2-IRES-Cre* mice underwent the same optogenetic protocol described above a second time on the following day, while being in their homecage instead of a neutral cylindric chamber.

Optical activation during CD2

VGlut2-IRES-Cre and *Chx10-Cre* mice were conditioned during CD1 without any optogenetic interference (see 2.5.2). On CD2, second, fourth, and fifth CSUS presentation was paired with an optical stimulation during either the pure tone (in *VGlut2-IRES-Cre* mice) or the white noise component (in *Chx10-Cre* mice), while the first and the third CSUS were presented in absence of optical stimulation. Here, same light settings were used as during optogenetic manipulations in naïve mice.

Comparison of optically induced and spontaneous freezing bouts in *Chx10-Cre* mice

Chx10-Cre animals were placed into an OF context without bedding and optically stimulated with short periods. The average length of spontaneous freezing bouts of another batch of naïve animals exploring the OF context were calculated with 1.1 seconds excluding the first three minutes of the session or 2 seconds, including the first three minutes of the session. Animals were optically induced 12 times with alternating stimulation lengths of either 1.1 or 2 seconds.

Optical inhibition in *Chx10-Cre* mice during context retrieval

Prior to the optogenetic experiments, mice were conditioned for two days in a conditioning box (see 2.5.2). On the third day, mice were placed into the same context and were optically stimulated for four times for 20 seconds during a 15 minutes recording (ISI of 190 – 210 s). Constant light with a wavelength of 549 nm and power of 7 mW was applied.

Intersectional optical activation

For optogenetic experiments targeting glutamatergic vlPAG-to-Mc projections, mice were screened during the first day by applying increasing light intensities (0.8 mW, 1.8 mW, 4.6

mW; 20 Hz, 20 ms), each parameter presented three times for five seconds across a 19 minutes long session. Blue light (473 nm) was applied to activate Channelrhodopsin. During a second session, mice were stimulated in a cylindric chamber five times for five seconds across 9 minutes with constant light (7 mW).

Real-Time Place Preference Test

During the Real-Time Place Preference Test (RTPP), mice were placed for 15 minutes into an apparatus consisting of two equally sized compartments, whereby one was paired with a fixed pattern of light stimulations. While the mouse was tracked online, light stimulations was applied whenever it entered the side paired with optical stimulation. Mouse line-specific stimulation parameters were used: *VGlut2-IRES-Cre* mice were divided into two groups, one being stimulated with low (0.3 - 0.4 mW, constant), the other with high intensities (3.5 – 4.2 mW, 20 Hz, 10 ms). *Chx10-Cre* mice received stimulations with 8 mW (20 Hz, 10 ms). *Chx10-Cre* mice were stimulated for 1 second followed by 3 seconds interruption of optical stimulation (1 s on, 3 s off). *Gad2-IRES-Cre* mice received constant light stimuli (8 mW) in a 1 second on, 1 second off fashion. The latency of the subject to escape from the light-paired compartment as well as the number of entries into this compartment was automatically extracted by using the Software CinePlexEditor (Plexon, version 3.6.0).

Tail Immersion

One to two cm of the subjects' tail tip was dipped repeatedly into 50°C hot water (KISS 104A, Huber). The inter-trial interval was 40 seconds. The first four trials served as baseline measurements, while the subsequent four trials were paired with light stimulations. For this, a five second light stimulation preceded the tail dip. The latency time of tail flicking was analyzed from side view video recordings by the experimenter, who was blinded to the experimental conditions.

2.9. Perfusion and brain sectioning

Mice were deeply anesthesized with a mixture of Ketamin (100 mg/kg) and Xylazine (10 mg/kg), injected intraperitoneally. After ensuring the absence of reflexes, mice were transcardially perfused with a perfusion pump (Reglo Analog, Ismatec). The blood was washed out with PBS for five minutes, followed by the perfusion of 4 % paraformaldehyde (PFA) for additional five minutes to fixate tissue. Brains were dissected and post-fixated over-night in 4

% PFA at 4 °C. Samples were washed in 1xPBS and embedded in 6 % agarose cubes. Coronal sections (60 µm thick) of respective brain regions were obtained using a vibratome (VT1200, Leica) and collected in PBS.

2.10. Immunhistochemistry

Immunhistochemical stainings were performed for visualization of Chx10-positive neurons and of traced neuronal compartments as well as for assessing the expression of the ArchT opsins and placement of optical fibers. Free-floating sections were incubated for two hours in 400 µl blocking solution (Table 7). Subsequently, tissue was incubated with primary antibodies diluted in 1:10 blocking solution over night at 4 °C (Table 4). After washing sections three times in 1xTBS-T for ten minutes, incubation with the secondary antibodies diluted in TBS-T (Table 4) followed for two additional hours at room temperature. Sections were washed again and incubated in DAPI (1:5000) for visualization of cell nuclei. A last washing step was followed by mounting the tissue on object slides and embedded with Mowiol (custom-made glycerol-based medium, Table 7). Brain samples of optogenetic experimental animals injected with either *AAV2/5-hSyn-Flex-ReaChR-Citrine-WPRE* or *AAV2/5-hSyn-Flex-mCherry-WPRE* were only counterstained with DAPI, and no immunhistochemistry was conducted because of sufficient endogenous fluorescent labeling (Citrine or mCherry).

2.11. Image acquisition and processing

An AxioImager2 fluorescent microscope (Zeiss) with an Apotome function was used for image acquisition. It was equipped with Plan-Apochromat 5x/0.16 and 20x/0.8 Objectives and 385, 475, 555, and 630 nm Colibri LED Modules.

For the verification of viral expression patterns and fiber placement of optogenetic experiments, single plane images (8 bit, 2320 x 1870 µm / tile, 851 x 687 pixels / tile, 3x3 binning) depicting whole brain sections with the 5x objective and 3 x 3 tiles were taken. For visualization of tracing experiments, the 20 x objective and Apotome function was used (8 bit, 585 x 472 µm / tile, 1292 x 1041 pixels / tile, Z-Stacks). The software Zeiss ZEN blue was used for post-processing of all images. Z-Stacks were merged and brightness and contrast were adjusted in the software.

2.12. Statistical analyses and figures

Graphs showing whole traces as well as peri-stimulus time histograms (PSTH) for HR, motion, and temperature depiction were plotted with custom written MATLAB codes (MATLAB v2019b).

Whole session traces are depicted as averaged data ± standard error of mean (SEM). Data for PSTHs were resampled around the synchronizing event to fixed timestamps to allow for averaging across animals and trials. The 3D plot illustrating HR developments concomitant with spontaneous freezing bouts was created by merging multiple PSTHs (60 s long for session plot, 1.5 s snippets for bout length plot) from overlapping time windows (30 s overlap for session plot, 1.4 s overlap for bout length plot) across the session.

All statistical analyses except the repeated measure two-way ANOVA test were performed using a custom written, python-based widget developed by Dennis Segebarth (dcl_stats_n_plots, v0.3.1, https://github.com/DSegebarth/dcl_stats_n_plots). The repeated measure two-way ANOVA test was performed with GraphPad Prism (version 9.5.1). Plots depicting statistical analysis were created with the same tool. Data sets were tested for normal distribution (Shapiro-Wilk test) and for equality of variances (Levene's test). Parametric or non-parametric tests were applied accordingly. N represents the number of animals. The box area in the boxplots was defined as the interquartile range (IQR, 1st to 3rd quartile) and the whiskers extend to the maximal or minimal values, but no longer than 150% of the IQR.

To analyze group effects of the HR compared between homecage and new context sessions, the HR of 50 second bins during the first ten minutes of the recording were averaged and a repeated measure two-way ANOVA test with post-hoc Šídák's multiple comparisons test for each time bin was conducted. For comparisons of defensive states between different contexts, HR values measured during immobility bouts with a duration of at least 2.5 s were extracted during 250 and 900 s of the session. For comparisons of HR values of different behaviors, data of CD2 starting from 250 s of the session were used. For both comparisons, a Kruskal-Wallis test (non-parametric) followed by a pairwise comparison with Mann-Whitney-U test with Bonferroni correction was used. For comparison of experimental and control mice in optogenetic experiments, HR and motion values during optogenetic stimulation were normalized by substracting the stimulation period by a baseline (time period of equal length right before stimulation start) and averaged for all stimulations in one session per animal. Data sets were compared with either a parametric unpaired t-test or a non-parametric Mann-Whitney-U test. For comparison of HR and motion of mice stimulated in homecage and new context on two

consecutive days, a parametric paired t-test or a non-parametric Wilcoxon signed-rank test for dependent samples was used. For statistical analysis of the RTPP, average time spent in stimulation side per visit was calculated per animal and compared between experimental and control mice. Unpaired t-test or Mann-Whitney-U tests were applied accordingly. Data points for the correlation plot depicting a comparison of spontaneous and optogenetically evoked freezing bouts were derived from the corresponding PSTHs. For each data point on the time axis HR-to-ceiling values of spontaneous and evoked curves were plotted against each other and the linear regression coefficient (R^2) was determined. For within subject analysis of projection-specific optogenetic experiments, mean normalized motion and HR values were compared to 0 (no change). Parametric one-sample t-test or non-paramteric one sample Wilcoxon rank-sum test were used.

Detailed statistical information are provided in the respective figure legends.

Figures were created with Adobe Illustrator CC 2018 (Version 22.1) and Microsoft PowerPoint 2016 (Version 16.0).

2.13. Material

Table 2 - Specification of used mouse lines, origin, and primers used for genotyping.

Mouse line	Origin	Stock nr	Primer
VGlut2-IRES-Cre	Jackson Laboratory	208863	ACA CCG GCC TTA TTC CAA G (Mutant Reverse) AAG AAG GTG CGC AAG ACG (Common) CTG CCA CAG ATT GCA CTT GA (Wild type Reverse)
Gad2-IRES-Cre	Jackson Laboratory	028867	CAC TGC ATT CTA GTT GTG GTT TG (Mutant Forward) TCG TTG CAC TGA CGT GTT CT (Wild type Forward) AAC AGT TTG ATG AGT GAG GTG A (Common)
Chx10-Cre	Ole Kiehn (University of Copenhagen)		CCACTTGGGCTGCCGCCTGGTTGGATA (Chx10 Forward) GTCGGGGACCCGTTGACTTTAGG (Chx10 Reverse) GTTGCATCGACCGGTAATGCAG (Cre Reverse)

Table 3 - Used AAV constructs with respective capsid and titer information.

Expression plasmid	AAV capsid	Titer	Origin
hSyn-FLEX-ReaChR-Citrine-WPRE	AAV 2/5	4×10^{12}	In house production
hSyn-FLEX-mCherry-WPRE	AAV 2/5	1×10^{13}	In house production
CAG-floxed-Synaptophysin-10xMyc-WPRE	AAV 2/5	1.5×10^{12}	In house production
CAG-Floxed-FlpO-2A-H2BV5.rev.WPRE	AAV (retro)	6×10^{11}	In house production
CAG-FLEX-ArchT-tdTomato	AAV5	7×10^{12}	Addgene (28305)
hSyn-Con/Fon-hChR2(H134R)-EYFP-WPRE	AAV 2/5	unknown	Johannes Letzkus

Table 4 - Used primary and secondary antibodies with order information and respective dilutions.

Antibody	Host	Company	Order number	Dilution
		Primary Antibodies		
Cre	mouse	Millipore	MAB3120	1:500
GFP	chicken	Abcam	ab13970	1:1500
Myc	goat	Abcam	ab9132	1:1000
NeuN	guinea-pig	Synaptic Systems	266004	1:400
RFP	rabbit	Rockland	600-401-379	1:1000
V5	rabbit	Novus	NB600-381	1:1000

Secondary Antibodies				
anti-chicken Alexa488	donkey	Jackson ImmunoResearch	703-545-155	1:800
anti-goat Cy3	donkey	Jackson ImmunoResearch	705-165-147	1:800
anti-rabbit Cy3	donkey	Jackson ImmunoResearch	711-165-152	1:800
anti-guinea pig Cy5	donkey	Jackson ImmunoResearch	706-175-148	1:800
anti-mouse Cy5	donkey	Jackson ImmunoResearch	715-175-150	1:800

Table 5 - Used materials with company information and product number.

Material	Company	Product number
Baseplates	Inscopix	1050-002192
Cage	Altromin	1264C00SU
Cage Grid	Tecniplast	1264C116
Circular Miniature Connector (ECG), female	MSA Components	A79109-001
Circular Miniature Connector (ECG), male	MSA Components	A79108-001
Cover glass, object slide	Hartenstein	DH50
Cover slips, round	Hartenstein	DKR0
ECG Wire	Phymep	793200
Ferrules, 6.4 mm long, 230 µm bore size, ceramic	Thorlabs	CFLC230-10
Glue black	Wekem	WK-2400
Glue transparent	Silisto	71024
GRIN lenses	Inscopix	1050-002179
HEK293-stable Cre cells	GenTarget	SC004-Bsd
Micropipettes, 1-5 µl	Drummond Scientific	2-000-001
Multimode Optical Fiber, 0.39 NA, 200 µm core	Thorlabs	FT200EMT
Object slides, superfrost	Langenbrinck	03-0060
Soldering Tin	Intos Electronics AG	43047D
Suture material ECG	Seralene	LO07340B
Suture material skin, silk	SMI	8101516

Table 6 - Used Chemicals with company information and product number.

Chemicals	Company	Product number
Acetic Acid	Sigma-Aldrich	33209
Acetone	Sigma	32201-1L
Agarose	Biozym	840004
Benzalkoniumchloride	Sigma	12060
Blasticidine	Invivogen	ant-bl-05
Braunol	Braun	190971

Buprenorphin	Bayer	PZN - 01498870
DAPI	Roth	6335.1
Depilatory cream	Veet	
Di-sodium hydrogen phosphate	Carl Roth	P030.2
DMEM-GlutaMAX	Thermo Fisher Scientific	61965026
Donkey serum	Merck	S30
Ethanol	Th. Geyer	GE/2299
Fetal Calf Serum	Linaris	SBF3119KYA
Glycerol	AppliChem	1513391211
HBSS	Thermo Fisher Scientific	14170-138
Isofluran	cp-pharma	AP/DRUGS/220/96
Isopropanol	Sigma-Aldrich	33539-2
Ketamin	Serumwerk	FI-11-16
Metacam	Boehringer Ingelheim	EMEA/V/C/000033
Mowiol	Sigma-Aldrich	324590
Naropin	Aspen Global	PZN - 02749854
Non-essential amino acids	Gibco	11140-035
Paladur	Kulzer	Pala
Paraformaldehyde	Merck	AP211511.1211
Penicilline-Streptomycine	Thermo Fisher Scientific	15070063
Poly-L-Ornithine Solution (0.01%)	Merck	A-004-C
potassium chloride	Merck Millipore	1049361000
Potassium di-hydrogen phosphate	Carl Roth	P018.1
Ringer	Braun	PZN 01471411
Sodium chloride, 0.9 %	Braun	3570410
Tris Base	Roth	4855.3
Triton X-100	Sigma-Aldrich	X100
Trypsin EDTA	Fisher Scientifica	25-200-056
Tween 20	Sigma-Aldrich	P1379
Vitagel	Bausch & Lomb	1318187
Xylavet	cp-pharma	1205

Table 7 - Used solutions and respective compositions.

Solution	**Composition**
10X PBS	81.8 g NaCl, 2g KCl, 14,4 g Na_2HPO_4, 2g KH_2PO_4, ad 1 l ddH_2O, pH 7.0
10X TBS-T	24.2 g Tris Base, 80 g NaCl, 10 ml Tween 20 %, ad 1 l ddH_2O, pH 7.6
Blocking solution	1x TBS-T, 10 % donkey serum, 0.3 % Triton X100

Complete Medium	D-MEM GlutaMAX, 10 % FCS, 1% non-essential amino acids, 1 % pen-strep
Cutasept	72 ml Isopropanol, 0.025 g Benzalkoniumchlorid, ad 100 ml ddH_2O
Mowiol	2.4 g Mowiol, 6 g Glycerol, 6 ml ddH2O, 12 ml 0.2 M Tris
Paraformaldehyde	4 % paraformaldehyde (PFA) pellets in 1X PBS, stir at 60°C for 1 hour, pass through paper filter, pH 7.4

Table 8 - Used equipment with company and model information.

Equipment	**Company**	**Model**
Acquisition system	Plexon	Omniplex system
Amplifier	npi electronic	DPA 2FX/FS
Anesthetic Vaporizer	Hugo Sachs Elektronik	34-1041
Cabinets Mouse Housing	Scanbur	Scantainer
CE:YAG Bandpass Filters	Doric Lenses	YBPF_549/015, YBPF_612/069
CE:YAG Optical Head	Doric Lenses	YLEDH_465
Drill bit, Stereotax	Union Tool	119-0033
Feeding needle cannula	Fine Science Tools	18061-75
LED lamp, circular	Proxistar	LED-240
Microscope	Zeiss	AxioImager 2 with Apotome
Motorised Manipulator	Scientifica	IVM Mini Triple
Multi-I/O Processor	Tucker Davis	RZ6
Optical Power Meter Console	Thorlabs	PM100D
Patch Fiber	Thorlabs	BFYL2LF01
Perfusion pump	Ismatec	Reglo Analog
Pressure Injector	NPI electronic	PDES-02DX
RGB camera	Campden Instruments	Pike Camera F-032C
Soldering station	Velleman	VTSSC40N
Speaker	Tucker Davis	MF1
Stereotax	Kopf	Model 1900
Stimulus isolator	A-M Systems	Model 2100 Isolated Pulse Stimulator
Thermal camera	FLIR	A655sc
Vibratome	Leica	VT-1000
Water bath	Huber	KISS104A

Table 9 - Used softwares for data acquition, processing and analysis with respective version..

Software	Company	Version
Adobe Illustrator	Adobe	22.1
CinePlexEditor	Plexon	3.6.0
CinePlexStudio	Plexon	3.0
Prism	GraphPad	9.5.1
MATLAB	MathWorks	R2019b
PowerPoint	Windows	16.0
Python		3.7
Radiant	Plexon	2.2.0.19
RPvDsx	TuckerDavis	95
ZEN blue	Zeiss	2.5

Table 10 - List of used custom written GUIs in Matlab provided by Jérémy Signoret-Genest.

GUI/ Script	Purpose
Behavior_Scorer	Semi-automated tool to score behavior bouts (Tail Rattling, Grooming, Rearing, head dips, stretch-attend posture, immobility)
ECG_Process	Extraction of heart beats (R Peaks)
HeartRate_Extract_General	Extraction of HR-to-ceiling curve data
MasterPlotter	Plotting tool that provides templates to plot behavioral, cardiac and temperature data
Prepare_Tracking	Extraction of mouse contour, center of gravity, motion measure values
Temperature_Extraction	Extraction of temperature of body parts based on tracking data obtained from RGB camera information

3. Results

3.1 Characterization of defensive states

By describing correlative changes in behavioral patterns and autonomic readouts as well as their respective dynamics, in a first step, this thesis aimed at identifying integrated defensive states on different timescales. In order to provoke different defensive states, mice were first subjected to a series of classical anxiety tests (OF, EPM, LDB, Figure 5A, top). These tests are established paradigms that allow for investigation of exploratory and anxiety behavior in rodents (Crawley and Goodwin 1980; Denenberg 1969; Pellow et al. 1985). Furthermore, the CFP, a modification of the classical auditory Pavlovian Fear Conditioning, which allows for examination of the moment-to-moment switching between two defensive states, has been conducted (Figure 5A, bottom and detailed Figure 3, Fadok et al. 2017). The SCS, which serves as an auditory CS, consists of a pure tone beep followed by a white noise sound (Figure 3). During the preexposure day the SCS was presented alone in order to control for unconditioned responses to the CS. This day was followed by two consecutive days of conditioning, where a foot shock (US) was paired five times with the SCS (CS, Figure 3). On the fourth day, animals underwent a retrieval session, where the CS is presented in a new, neutral context or in their homecage, respectively. Next to video tracking, autonomic measurements (HR, tail temperature) were acquired (Figure 5B), whereby the animals' free exploration was guaranteed.

Figure 5C and D show average traces of the respective readouts from 29 mice submitted to CD1 and CD2 (19.5 minutes long). Both, on the behavioral as well as on the autonomic level, global changes became apparent (Figure 5C, D). During CD1, the animals explored their environment actively during the first minutes of the trial, which is reflected by high motion values (Figure 5C, top). However, immobility responses accumulated with an increasing number of presented CSUS pairings (Figure 5C, heat plot). Strong behavioral responses to the CS in terms of high locomotion, flight responses and jumps could be observed from the third pairing on.

During CD1, the absolute HR ranged for the whole session on average between 650 and 750 bpm (Figure 5C, middle). At the beginning of the recording, the HR increased rapidly to a value of ~730 bpm during the first 200 seconds (Figure 5C, middle), before an only slowly rising plateau phase was reached. A striking cardiac feature visible on a coarse level is the HR's global variability, which shows a development from low to increasingly higher variabilities over the course of the recording and over a growing number of CSUS presentations.

A more nuanced analysis of the HRV in the 0.4 - 0.8 Hz range, a frequency band that equates the low frequency component of the human HRV, the so called Mayer waves, revealed increasing values during the inter-stimulus interval towards the second half of the conditioning session (Figure 5C, middle, Schwerdtfeger et al. 2020). In contrast, cardiac responses to the US (foot shock) arose to be expressed with low variabilities and maximum HR values (~ 770 bpm), which exceeded the highest HR values in the initial cardiac rising phase (Figure 5C). All together, a phase with low HR variability was observed predominantly during the first ~ 7 minutes after placing the animal into the context. In a later phase of the recording, HR responses were dominated by increasingly strong immobility-associated bradycardia events, which appeared during inter-stimulus intervals, which were interrupted by US-associated fast rising HRs. These observations can be conceptualized as an overriding slow changing cardiac macrostate framing the maximum manifestation of moment-to-moment changing defensive responses. This characteristic will be called the *rigidity macrostate*, as the rigidity of the HR decreases over time, allowing for increasing bradycardia amplitudes throughout the recording. At the same time, maximum HR values were increasing throughout the recording, a feature that will be termed the *ceiling macrostate*. Taken together, the rigidity and the ceiling macrostates define the upper and lower boundaries of the HR, respectively.

As the baseline HR level slowly changes throughout the recording (ceiling macrostate) comparisons of HR values from different time points of the recording could be confounded. Consequently, in order to account for the rising HR throughout the session, a 'HR to ceiling' measure (HR-to-ceiling) was introduced (Figure 4 & Figure 5C and D). This detrended form of HR, which is calculated as the distance of the absolute HR from a modeled ceiling value (red curve in Figure 4C) that reflects the latent maximum HR, will prevent confounds of comparisons between individuals and different contexts. In this thesis, the HR-to-ceiling will be used primarily as the measure for cardiac readouts.

The mice's tail temperature could extend the description of the slow changing macrostate. After an initial comparable small decrease in temperature, an increase of up to 3.5 °C on average could be observed during CD1.

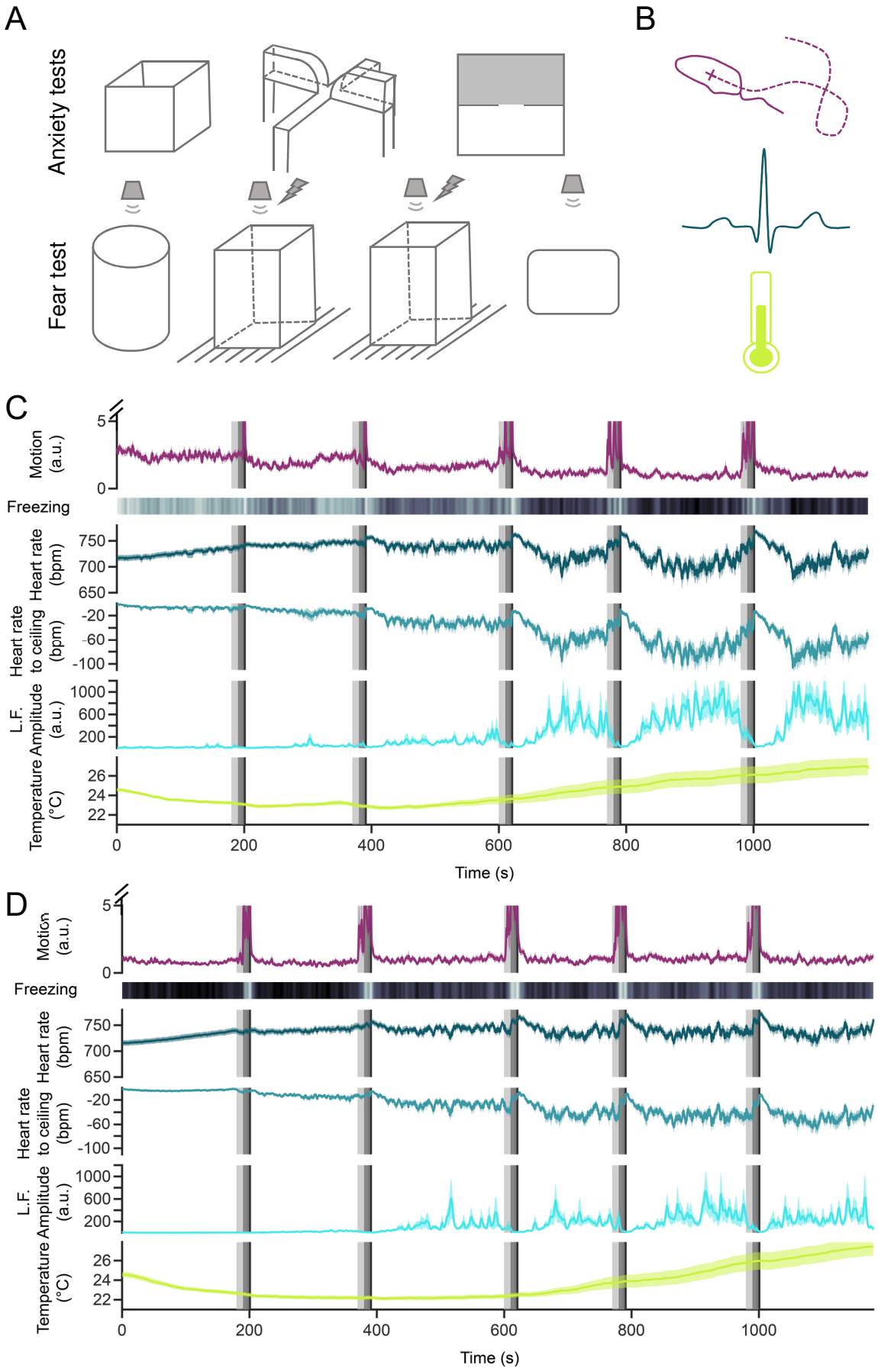

Figure 5 - Defensive States are accompanied by behavioral and autonomic reactions.
(A) *Overview of conducted anxiety and fear tests, top: Open Field Test, Elevated Plus Maze, Light-Dark Box Test,*
(continued on next page)

Figure 5 continued
bottom: Conditioned Flight Paradigm, Preexposure, Conditioning Day 1 and 2, Retrieval Test in new context or homecage. (B) Responses measured during behavioral tests. Top: Animals were recorded with a RGB camera, from which motion values were derived. Middle: Electrocardiogram recordings were derived from subcutaneously implanted wires picking voltage across the chest of the animal. Bottom: An infrared camera was used to record the animals tail temperature. (C, D) Average traces (± SEM) from 29 animals show different defensive responses along the recording during CD1 (C) and CD2 (D) of the Conditioned Flight Paradigm. Depicted is the motion measure, the freezing probability (heat plot; white: no freezing, black: high freezing), the absolute HR in bpm, the detrended HR-to-ceiling in bpm, the amplitude of the extracted L.F. band, and tail temperature. Grey vertical bars indicate 5 CSUS pairings (light grey: pure tone, dark grey: white noise, black: shock). N=29

On the second conditioning day (CD2), animals were exposed to the same context and again five CSUS pairings were presented. In contrast to the behavioral response during CD1, animals displayed constant levels of low motion measures and increased freezing probabilities during the whole session (Figure 5D, top). Furthermore, high motion measures during the white noise component were observed from the first CSUS pairing on (Figure 5D, top). Interestingly, a global similarity of the HR response compared to CD1 became apparent. Cyclic phases of increasing HRs during the white noise component of the CS and the shock and subsequent gradual decreases of HRs and higher amplitudes of bradycardic responses, reflecting the cardiac rigidity macrostate, did only start with the third CSUS pairing (Figure 5D). Nonetheless, global decreases of the HR during the ISIs were less pronounced compared to HR levels during CD1 (Figure 5C and D). Furthermore, when considering the freezing bout duration, further differences between CD1 and CD2 became apparent (Figure S1). While average immobility durations increased throughout the session in CD1, reaching maximum bout durations of 10 seconds, during CD2, animals displayed long freezing bouts from the start of the recording dropping to shorter bout lengths in the second half of the recording session (Figure S1). Similarly as in CD1, the tail temperature increased on average to 26 °C by the end of the recording (Figure 5D).

A closer inspection onto the SCS phases during the CD2 session revealed, as opposed to the slow changing cardiac macrostates, fast dynamics and state switches on a second-to-second time scale (Figure 6A). PSTHs are depicting average response traces of motion and HR-to-ceiling measures centered around the 5 CSUS pairing of 33 animals (Figure 6A). Behaviorally, freezing episodes appeared with high probabilities during the pure tone component, while the white noise component was correlated with high motion values interspersed with short immobility bouts (Figure 6A, compare Fadok et al. 2017). This switch from passive to active behavioral responses on a time scale of seconds occurred uniformly throughout the session (Figure 6A, top). Strikingly, as pointed out before, HR responses appeared heterogeneous when comparing early and late phases of the recording (Figure 6A, middle). While HR values displayed only minor changes, irrespective of the motion component of the defensive response in the early recording phase, towards the end of the session decreasing HR values became

apparent during the pure tone component (Figure 6A). These bradycardic events are followed by fast rises of the HR during the white noise component, again much more pronounced in later phases of the recording (Figure 6A).

Next, cardiac dynamics of spontaneous freezing episodes outside the CSUS pairings occurring during the inter-stimulus intervals were analyzed. Merging multiple PSTHs, each representing 60 seconds time bins along the recording (overlapping time windows, 30 s), with the start of freezing bouts as synchronizing event, into one plot, reveals a 3D landscape, which reflects freezing associated HR development throughout recording time (Figure 6B). Non-CS induced freezing events were similarly associated with stronger bradycardia in later recording phases compared to HR courses in the early phase (Figure 6B). As described above, immobility bout durations vary during CD1 and CD2 recordings (Figure S1). It was hypothesized that the bout duration affects the bradycardia's amplitude and thus this effect could explain the difference in the HRV between CD1 and CD2 (Figure 5C and D). Consequently, the influence of the immobility bout duration on the bradycardia amplitude was analyzed (Figure 6C). Again a 3D plot consisting of multiple overlapping individual PSTHs (1.5 seconds time bins, 1.4 seconds overlap) sorted by their bout duration was created (Figure 6C). Indeed, a marked correlation between the amplitude of the bradycardia and immobility bout duration became apparent, the longer the immobility bout duration, the higher the bradycardia's amplitude was (Figure 6C).

Taken together, these observations indicate that the HR does not simply follow changes in the behavioral responses, but instead is reflecting integrated defensive states, depending on the session time as well as bout durations. As opposed to the longer lasting macrostates, these transient switches reflecting behavioral and cardiac changes, will be termed microstates from here on.

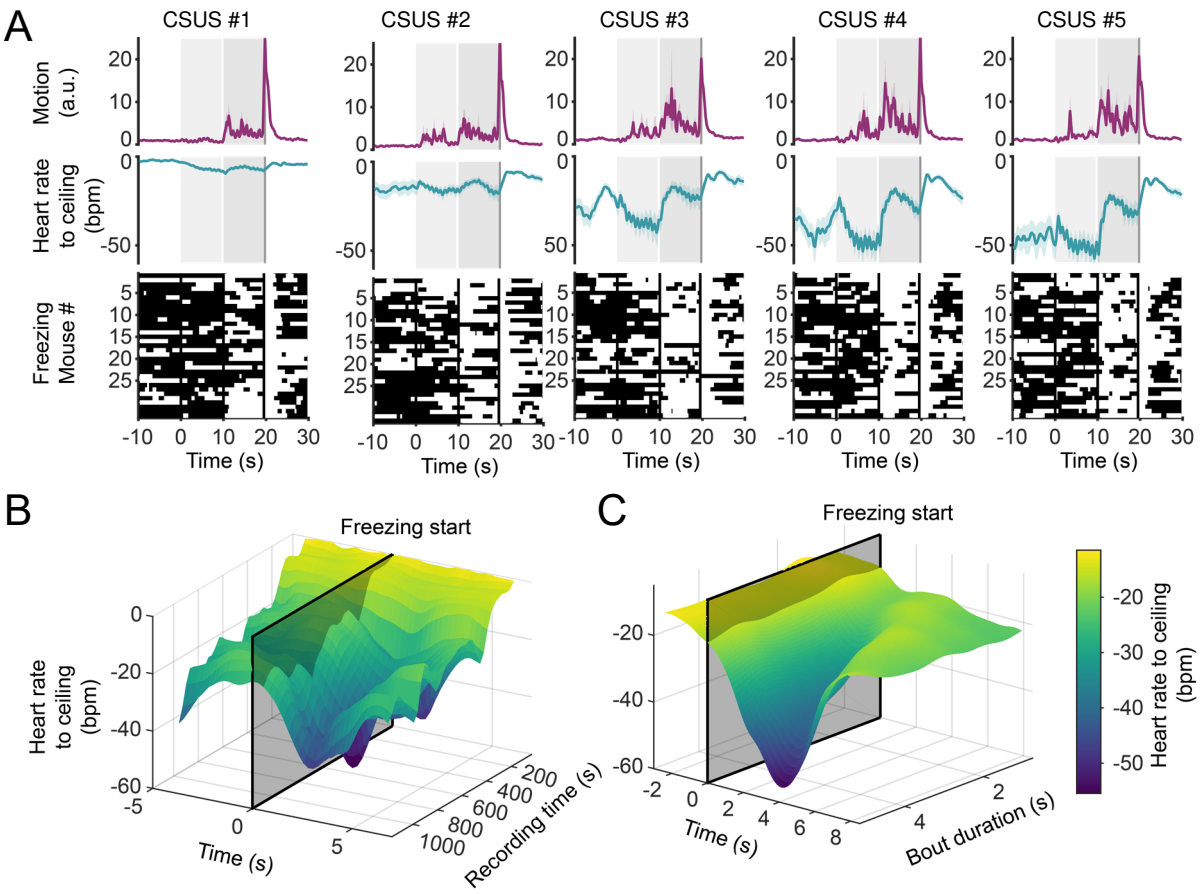

Figure 6 – Time-dependent changes of behavioral and cardiac responses during CD2.
(A) PSTHs (± SEM) of motion (top), HR-to-ceiling (middle) and individual freezing episodes per animal (bottom, black indicates freezing period) centered around CS-US pairings during CD2 from beginning (CSUS #1 left) to the end (CSUS #5 right) of the session. Grey bars indicate CSUS pairings (light grey: pure tone, dark grey: white noise, black: shock). (B) HR responses during spontaneous freezing episodes outside CSUS pairings during CD2. Depicted is a 3D plot representing consecutive PSTH windows (60 s, 30 s overlap) centered around freezing episodes with the respective HR development throughout the recording. (C) HR responses in dependence of the immobility bout length during CD2. The 3D plot represents consecutive PSTH windows (1.5 s, 1.4 s overlap) of the HR responses sorted by their bout lengths. N= 33

3.1.1 HR effects of handling in the homecage and an unfamiliar context

A dominant feature of the HR in all observed paradigms is the development from low to high variabilities throughout the recordings. Next, a potential cause for this cardiac development, termed previously rigidity macrostate, was investigated. It was hypothesized that either the handling procedure on the animal or the confrontation with an unknown, new context or a mixture of both factors could account for the cardiac effects. The HR of animals sitting in their homecage or in an unfamiliar, new context was recorded for 30 minutes, while taken out twice (after 15 and 20 minutes) during the recording to mimic handling effects (Figure 7). The handling period, which was approximately 20 seconds long, consisted of picking up the animal,

restraining it in the hand and replugging the HR connector. HR-to-ceiling average traces of 5 animals tested in their homecage and in an unknown, new context are shown (Figure 7A). Black bars on top of the graphs indicate timepoints of handling periods. In line with previous observations, the HRV increased over time. However, HR-to-ceiling values decreased faster during the homecage session compared to that of the animals measured in the unfamiliar context (Figure 7A and B). Average HR-to-ceiling values of 50 seconds bins were compared between homecage and new context sessions during the first ten minutes and revealed a significant difference between the groups (Figure 7B). A marked increase of the HR reaching maximal levels with low variabilities was apparent during all handling procedures in both contexts (Figure 7A). A comparison of the HR during the first 30 seconds after start of the handling procedure between test sessions in the homecage and the new context revealed on average a lower rise of HR-to-ceiling values in the new context animals (Figure 7C). It was hypothesized that this effect is due to a temporal shift of peak HR values in the new context group. However, comparing the time to reach the maximum HR initiated by the handling turned out to not be significant (Figure 7D). Importantly, pre-handling HRVs established fast after the handling when compared to the HRV development during the initial phase of the recording (not quantified).

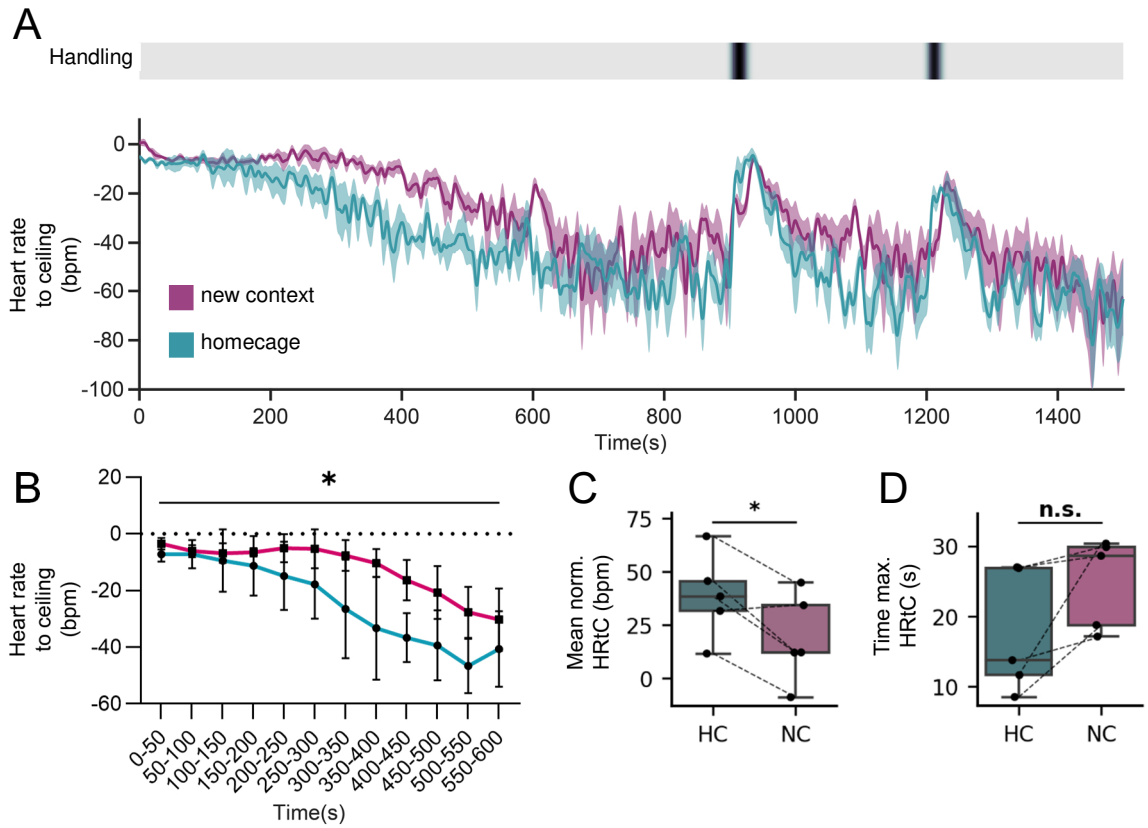

Figure 7 - Cardiac responses during handling procedures of mice in a new context vs. their homecage.
(A) Average HR-to-ceiling traces (± SEM) of 5 animals recorded in their homecage (blue) and in a new context (purple) while handled twice (after 900 and 1200 seconds, indicated by black bars on top) during the session. The handling periods evoke an immediate rise in HR-to-ceiling in both contexts, N = 5. (B) Initial rigidity decreases faster in the homecage session.
(continued on next page)

Figure 7 continued
Average HR-to-ceiling values of 50 seconds segments during the first 10 minutes of the recording. RM Two-way ANOVA, group (HC vs. NC) factor F (1, 8) = 6.811, $p < 0.05$ with post-hoc Šídák's multiple comparisons test for each time bin, all n.s. (C) Quantifications of HR-to-ceiling shown as mean normalized values per animal in a time window of 30 seconds after start handling (handling period subtracted by baseline period, mean of both handlings). Paired two sample t-test with Welch-correction, $t(4) = 3.27$, $p < 0.05$. (D) Quantifications of the durations to reach the HR-to-ceiling$_{max}$ in a time window of 30 seconds after start handling per animal (mean of both handlings). Paired two sample t-test with Welch-correction, $t(4) = -2.31$, $p = 0.08$.

In summary, during the first 10 minutes of the recording, the mice's HR developed differently when tested in their homecage or a new context. The handling of the mice led in general to a sudden and pronounced elevation of HR and interrupted the low rigidity, which established in later recording phases. However, during the handling procedure the HR increased less in the new context than in the homecage.

3.1.2 Cardio-behavioral state during cue retrieval in the homecage and a new context

The results presented so far suggest that not only the displayed behavior but also the context, in which the animals are tested, constitute important factors influencing the defensive state. To test this further, cardio-behavioral microstates of animals undergoing the retrieval session of the CFP, during which the CS was presented in either a new, unfamiliar context or in their homecage were compared. In contrast to their homecage, the new context is expected to be perceived as a higher contextual threat to the animals. While the locomotion of the animals in homecage and new context were hypothesized to be similar after the first CS presentation, the cardiac aspect of the microstate in the homecage group were expected to show higher immobility associated bradycardic amplitudes influenced by a higher rigidity reflecting a lower fear level. The animals were either placed into an cylindric transparent chamber or into their homecage and were presented the CS 16 times (pseudorandomized ISI of 80-140 s, Figure 8). HR-to-ceiling as well as behavioral responses were pooled in PSTHs for CS presentations 1-4, 5-8, 9-12 and 13-16, respectively (Figure 8). During the first four presentations, the mice showed freezing responses with high probabilities during the pure tone component (light gray), while the white noise component (dark gray) was associated with high probabilities of flight bouts and increased motion in both contexts (Figure 8). However, this effect mitigated throughout the retrieval session similarly in the new context and the homecage. In general, mice moved more in the homecage during the ISI's. Furthermore, in both contexts, strong freezing responses dominated post-CS sequences (Figure 8). At the end of the recording, motion measure values during the SCS showed only slight changes in the new context (Figure 8A, fourth column) or even decreasing values during the white noise component in the homecage

(Figure 8B, fourth column). However, post-CS freezing responses remained pronounced until the end of the session (Figure 8). A decrease in HR concomitant with the higher freezing probabilities during the pure tone and an increased HR during increased flight bouts during the white noise component was apparent (Figure 8).

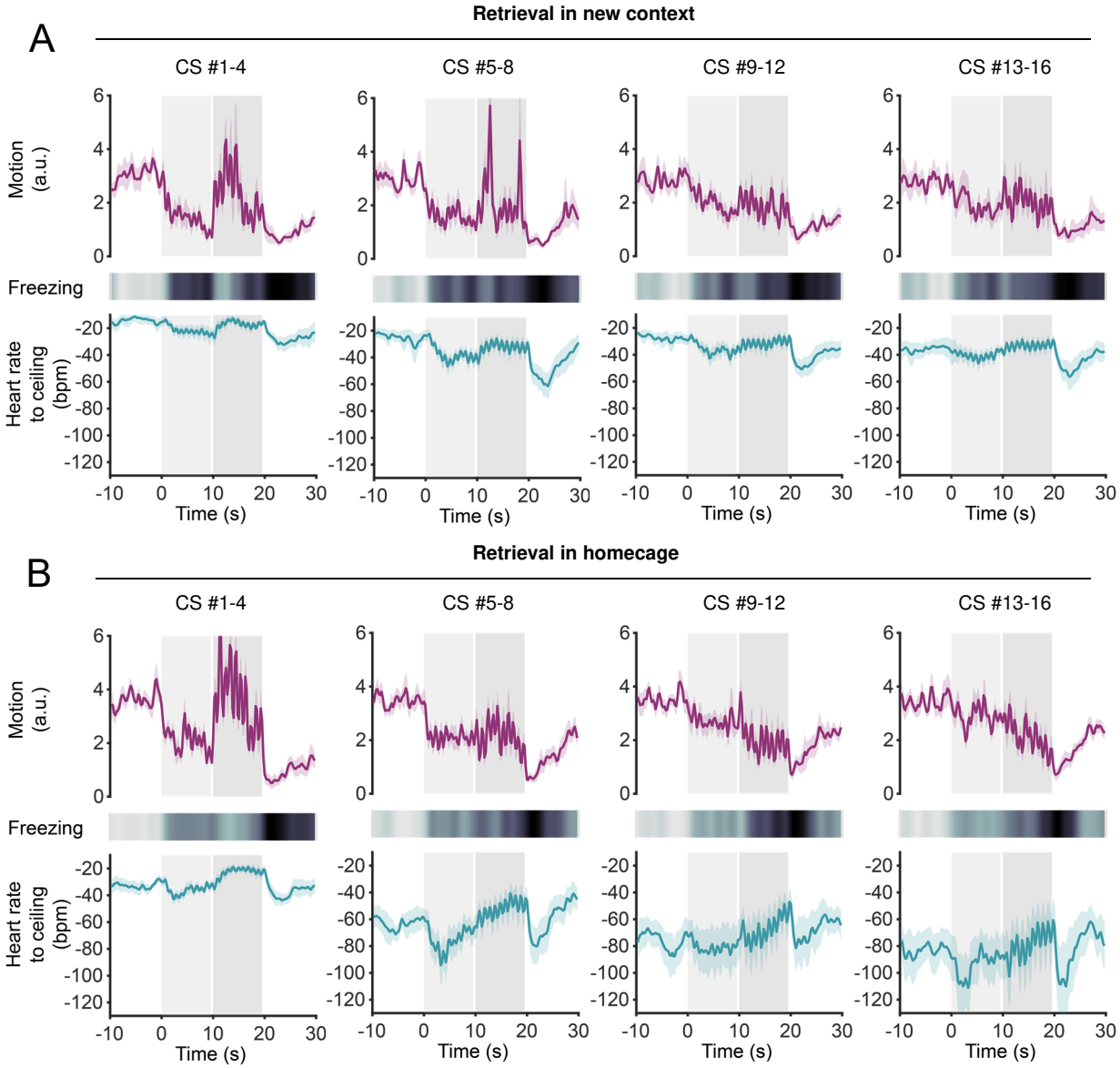

Figure 8 - Comparison of the cardio-behavioral state during retrieval sessions performed in a new context or the homecage. *PSTHs (± SEM) showing motion (top), freezing probabilities (middle), and HR-to-ceiling (bottom) centered around CS presentations of mice undergoing a retrieval session of the conditioned flight paradigm in a new context (A) or their homecage (B). 16 CS presentations are pooled into four time ranges to show the time-dependent development of the cardio-behavioral responses. Grey bars indicate CSUS pairings (light grey: pure tone, dark grey: white noise).* $N_{new\ context} = 10$, $N_{Homecage} = 8$

In the homecage, HR values during the white noise component increased to levels exceeding pre-CS values (Figure 8). HRs in both contexts are characterized by increasing variabilities over time reflecting the rigidity macrostate, which decreased over time. However, this effect was more pronounced in the homecage compared to the retrieval session in the new context (Figure 8). During the retrieval session, mice showed similar behaviors during the CS presentations when receiving the CS in a new context or the homecage. However, mice undergoing retrieval

in the homecage showed in general higher motion measure values and sharply defined post-CS freezing responses. While bradycardia was dominant during the pure tone component, tachycardia dominated the white noise component.

3.1.3 Context- and behavior-dependent cardiac responses

From the results presented so far, it can be summarized that the context, the animal is confronted with, plays a critical role in shaping the defensive responses. One possible explanation for this could be the varying threat levels that are associated with the contexts tested so far. Consequently, HR values of animals confronted with additional paradigms, which vary in their threat levels, were compared. To this end, HR values during immobility bouts, a behavior displayed throughout all paradigms, were analyzed. Mice were tested in classical anxiety paradigms (OF, EPM, LDB), the conditioned flight paradigm (CD1, CD2, Retrieval in new context, Retrieval in homecage) as well as in their homecage while left unperturbed (Figure 5A). HR-to-ceiling values during immobility bouts (≥ 2.5 s) were averaged across animals and compared across contexts (Figure 9A). A gradient of immobility-associated high HR values in high fear contexts like the conditioning and retrieval sessions in unfamiliar, new contexts towards decreasing HR values in low fear paradigms as OF, EPM and LDB as well as the unperturbed homecage sessions was observed (Figure 9A). Furthermore, compared to the high fear contexts, HR responses measured in animals recorded in their homecage showed much higher variabilities (Figure 9A). In a second approach, cardiac responses during multiple other behaviors (stretch-attend posture, rearing, locomotion, grooming, area-bound, freezing) occuring during CD2 were compared (Figure 9B). Indeed, various behaviors were associated with significantly different levels of HR-to-ceiling values (Figure 9B). Interestingly, highest HR values were found during stretch-attend postures, a behavior displayed for risk assessment (Figure 9B). While locomotion-associated HR changes were intermediate, immobility bouts were concomitant with decelerated HR responses (Figure 9B).

In a separate experimental setting, conditioned mice (CFP) were placed for 40 minutes into their homecage after connecting them to the acquisition system until HR values reached approximately 650 bpm (Figure 9C). Interestingly, on average, the HRV, influenced by the rigidity macrostate as described above, stabilizes and reaches a constant level after approximately 20 minutes of the recording (Figure 9C, bottom). After 40 minutes, the pure tone component of the SCS was presented for 2 minutes. Mice displayed strong freezing responses that were, however, not associated with bradycardia, as would be expected from previously

observed freezing-bradycardia states (Figure 9C). Instead, these behaviorally indistinguishable periods of immobility were associated with a sudden increase of HR values of about 150 bpm (Figure 9C). This result suggests a strong dependency of the cardiac responses on the momentary spatial and temporal context. In summary, cardiac responses are highly dependent on the context, the animals are confronted with as well as on the momentary displayed defensive behavior. Having described defensive states on the basis of behavioral as well as autonomic characteristics, in a next step it was aimed to identify neuronal mechanisms underlying those states.

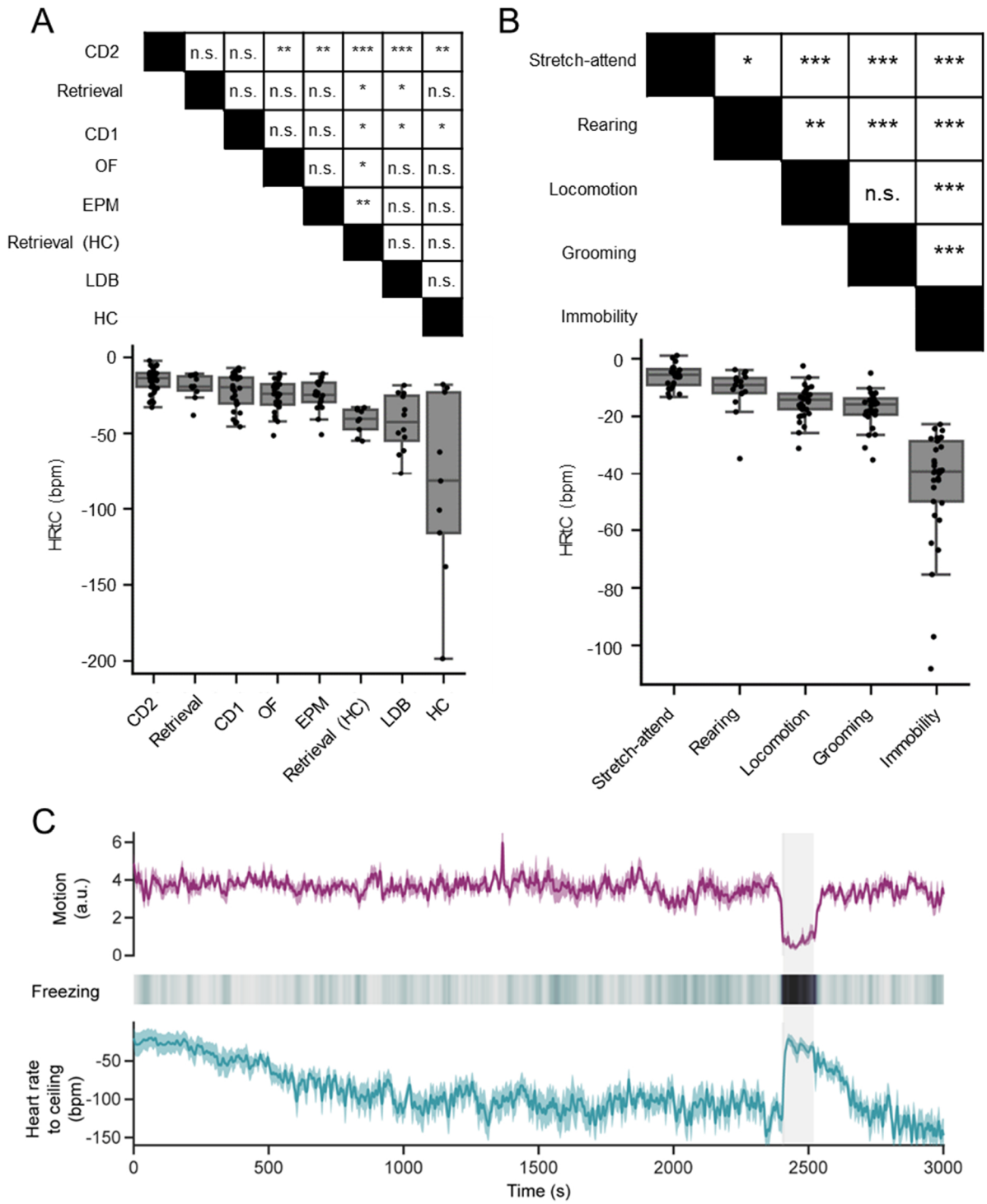

Figure 9 – Dependencies of HR responses on the context and the behavior.
*(A) Comparison of immobility-associated average HR-to-ceiling values in different paradigms varying in their threat level (bottom) and respective statistical analysis (top). Immobility bout length is restricted to ≥ 2.5 seconds and only bouts occuring after 250 seconds of the session are taken into account. Kruskal-Wallis test (non-parametric) followed by a pairwise comparison with Mann-Whitney-U test with Bonferroni correction. N_{CD2} = 33, $N_{retrieval}$ = 10, N_{CD1} = 30, N_{OF} = 25, N_{EPM} = 20, $N_{retrieval(HC)}$ = 9, N_{LDB} = 12, N_{HC} = 9. (B) Comparison of average HR-to-ceiling responses of different behaviors displayed during a CD2 session (bottom) and respective statistical analysis (top). Only behavioral bouts occurring after 250 seconds of the session are taken into account. Kruskal-Wallis test (non-parametric) followed by a pairwise comparison with Mann-Whitney-U test with Bonferroni correction. N = 33. * p < 0.05, ** p < 0.01, *** p < 0.001, n.s. p > 0.05. (C) Average motion (top) and HR-to-ceiling responses (bottom, ± SEM) of animals during a cue retrieval after a long baseline (40 minutes) in their homecage. The pure tone component of the SCS (grey bar) was presented for two minutes. Heat plot represents average freezing probability (middle). N = 8.*

3.2 Optical manipulation of different midbrain circuit elements

The PAG located in the midbrain is known to be a key region for defensive reactions in the brain (Assareh et al. 2016; Bandler 1982; Bandler et al. 2000; Bittencourt et al. 2005; Carrive 1993; Silva and McNaughton 2019; Tovote et al. 2016). Targeted optogenetic manipulations reveal causal relationships between observed behavioral – and autonomic – responses with neuronal activity. Thus, in a next step, it was aimed to investigate the aforementioned defensive states (see 3.1), i.e. combinations of different behavioral and autonomic responses and their temporal dynamics during optical manipulation of different neuronal populations of the vlPAG and by this make mechanistic assumptions about brain states. By taking advantage of the Cre-Lox-system, three different neuronal subtypes were targeted and optically manipulated. First, glutamatergic neurons, characterized by the expression of *vesicular glutamate transporter 2* (*VGlut2*) in this region were addressed. Glutamate is the most abundant excitatory neurotransmitter in the brain and glutamatergic somata are present in all divisions of the PAG (Clements et al. 1987). The role of the glutamate PAG system in behavioral defensive responses has been shown previously (Evans et al. 2018; Tovote et al. 2016). Optical activation of glutamatergic vlPAG neurons resulted in enhanced freezing responses in naïve animals, while inhibition of the same population evoked reduced freezing responses in fear conditioned animals, thus representing a promising target to investigate its role in mediating integrated defensive states including - next to behavioral - also autonomic aspects (Tovote et al. 2016). Second, only a subpopulation of this rather heterogeneous glutamatergic neuronal pool, Chx10+ neurons (Bouvier et al. 2015; Vaaga, Brown, and Raman 2020), was addressed and stimulated. This allowed approaching a distinct group of excitatory cells and investigating their contribution in mediating behavioral and autonomic aspects of different defensive states. Moreover, loss-of-function experiments were conducted in *Chx10-Cre* mice in order to gain information about the necessity of this neuronal population in mediating a certain defensive state. To this end, Chx10+ neurons were optically inhibited. Third, inhibitory GABAergic neurons in the PAG were transduced. The amount of GABAergic neurons in the PAG show a rostro-caudal as well as a dorso-ventral gradient (Silva and McNaughton 2019). While at rostral levels, the dorsolateral subdivision of the PAG show much higher numbers of GABAergic neurons, in more ventral regions, the amount of GABA+ cells is lower. On the contrary, at caudal levels, the distribution of GABAergic neurons reverses with more positive cell bodies

in ventral divisions (Barbaresi 2006). As for the other neuronal subtypes, also here rather caudal regions were targeted in optogentic experiments.

Mice of all three genotypes were stereotactically injected with an AAV construct encoding for a Cre-dependent, red-shifted Channelrhodopsin (*AAV2/5-hSyn-Flex-ReaChR-Citrine-WPRE*, Lin et al. 2013, Figure 10). Channelrhodopsins are light-gated ion channels that allow for depolarization of the neuron by conducting cations upon light exposure (Schneider, Grimm, and Hegemann 2015). A Cre-dependent red fluorescent protein (*AAV2/5-hSyn-Flex-mCherry-WPRE*) was used as control construct. Furthermore, a construct encoding for Archaerhodopsin (*AAV5-CAG-Flex-ArchT-tdTomato*) was used for loss-of-function experiments in Chx10-Cre mice (Han et al. 2011). Archaerhodopsins are light sensitive outward proton pumps that hyperpolarize cells upon light exposure (Chow et al. 2010).

In a second optogenetic approach, it was made use of an intersectional, viral strategy to gain also projection-specificity. Here, only those glutamatergic neurons, which project to the Mc, were optogenetically targeted. To this end, a retrogradely transported transgene delivering a FlpO enzyme (*AAV(retro)-CAG-Floxed-FlpO-2A-H2BV5.rev.WPRE*) was virally injected into the Mc, while at the same time an AAV delivering a Channelrhodopsin, which is expressed Cre- and FlpO-dependently (*AAV2/5- hSyn-Con/Fon-hChR2(H134R)-EYFP-WPRE*), was injected into the vlPAG. All mice were equipped with glass fibers to deliver light (473 nm, 550 nm or 612 nm wavelength) to the targeted region. The animals were recorded with a RGB as well as with an infrared camera in order to observe the animals' behavior and potential changes in tail temperature, i.e. vasoconstrictive processes, respectively. Concurrently, implanted electrodes allowed HR measurements.

Location of optical fibers and expression of respective constructs were verified by histological analysis of the brain tissue (Figure S2 - Figure S4).

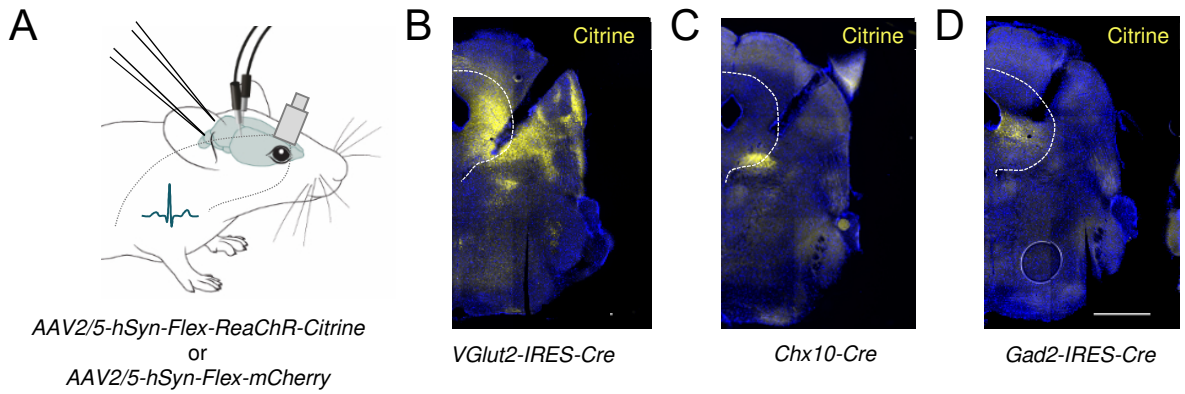

Figure 10 - Optical activation of glutamatergic, Chx10-positive, and GABAergic neurons with concomitantly recorded cardiac responses.
(A) Animals were bilaterally injected into the vlPAG with either AAV2/5-hSyn-Flex-ReaChR-Citrine *or* AAV2/5-hSyn-Flex-mCherry *and equipped with optical fibers as well as wires soldered onto a connector mounted on the head for HR derivation. (B, C, D) Brain sections of Cre-mouse lines representing the expression pattern of ReaChR and optic fiber placement. Yellow: Citrine-tag, blue: DAPI. Scale bar: 1 mm. Mouse image adapted from SciDraw.*

3.2.1 Qualitative testing of viral vectors

In order to test for sufficient expression of the used genetic constructs, qualitative *in vivo* tests of AAVs were conducted. Fluorescent tags allowed post-experimental verification of the expressed construct in the targeted brain area. Expression patterns of two viruses (*AAV2/5-hSyn-Flex-ReaChR-Citrine-WPRE* and *AAV2/5-hSyn-Flex-mCherry-WPRE*) injected into the PAG of *VGlut2-IRES-Cre* animals are shown in Figure 11. Sufficient expression levels were demonstrated by immunhistochemically enhancing the fluorescent tag signal (Figure 11 B, D). To control for off-target expression, Cre-dependent vectors were additionally injected into brains of wildtypic animals and incubated likewise for four weeks (Figure 11 A, C). The virus was mixed with blue fluorescent beads to detect the injection site. Wildtype animals injected with *AAV2/5-hSyn-FLEX-ReaChR-Citrine-WPRE* do not show any Citrine+ cells (Figure 11 C). However minor leaky expression was detected for *AAV2/5-hSyn-FLEX-mCherry-WPRE* (Figure 11A, arrow heads).

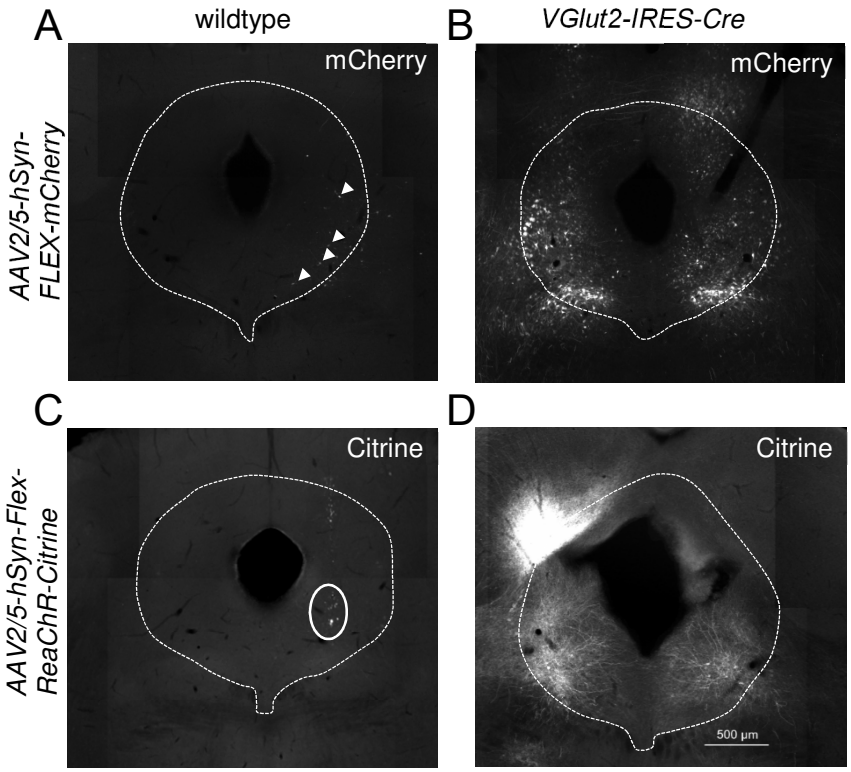

Figure 11 - Qualitative analysis of cre-dependent expression of AAV-mediated vectors by* in vivo *test injections into the PAG.
AAV2/5-hSyn-FLEX-mCherry (A, B) and AAV2/5-hSyn-Flex-ReaChR-Citrine (C, D) were injected into a wildtypic animals (A, C) to screen for off-target expression. White arrows in A indicate mCherry+ cells. Fluorescent beads mixed with AAV2/5-hSyn-Flex-ReaChR-Citrine are encircled in C. Brain sections of VGlut2-IRES-Cre *animals (C, D) show sufficient expression of respective constructs. Scale bar: 500 µm*

3.2.2 Optical activation of glutamatergic neurons in the PAG

Naïve *VGlut2-IRES-Cre* mice injected with *AAV2/5-hSyn-Flex-ReaChR-Citrine-WPRE* or *AAV2/5-hSyn-Flex-mCherry-WPRE* were placed into a neutral recording chamber and stimulated five times for a 10 seconds period with two different stimulation settings (Figure 12). As reported previously, vlPAG stimulation evoked a decrease in locomotion and freezing responses, although less pronounced than expected (Figure 12A (top and bottom) and D for quantification; compare Tovote et al. 2016). Concomitant with this behavioral response, a decrease in HR was observed (Figure 12A (middle) and D for quantification). However, this effect could only be evoked by using very low stimulation intensities (0.5 mW, 20 Hz, 10 ms). Strikingly, an increase in the stimulation intensity (3.5 mW, 10 Hz, 20 Hz or constant light) was clearly associated with an immediate switch to a behavioral activation, running and jumping, as illustrated in the motion measure curve (Figure 12B and E). However, flight responses were interrupted by short immobility bouts in some animals (Figure 12B, bottom). Furthermore, higher stimulation settings evoked likewise bradycardia, but more pronounced

compared to the low intensity stimulations (Figure 12B). The application of high intensity stimulations led on average to HR drops of 100 bpm compared to baseline (Figure 12B). The association of strong behavioral activation together with pronounced deceleration of the HR was unexpected as this combination was never observed in unperturbed, naturally behaving animals. Control animals of the same genotype injected with an AAV vector expressing a floxed fluorescent red protein (*AAV2/5-hSyn-Flex-mCherry-WPRE*) showed neither specific cardiac, nor behavioral responses (Figure 12C), excluding potential effects due to light irritations from evading light on the head cap. Since a recording-time dependent effect of cardiac responses to the conditioning stimulus during the conditioning of naïve, unperturbed mice was observed (Figure 5), also here, a potential time course effect was investigated. Figure 12F and G show the same data set as in Figure 12A and B respectively and depict average traces of motion, HR and temperature of animals stimulated five times with either low (Figure 12F) or high (Figure 12G) intensities across the session. Behaviorally, no change in the motion measure between beginning and end of the session were seen neither for low nor for high intensity stimulations (Figure 12F and G). Nonetheless, important to note are the post-stimulation freezing episodes after high intensity stimulations (Figure 12G, heat plot freezing). Strikingly, stimulation-evoked bradycardic responses linearly increased over time from the first to the last stimulation (Figure 12F and G). Additionally, the tail temperature was recorded. An initial decrease (3 °C) of the tail temperature was followed by a five minute stable course and an increase (5 °C) towards the end of the recording (Figure 12F and G, bottom panel).

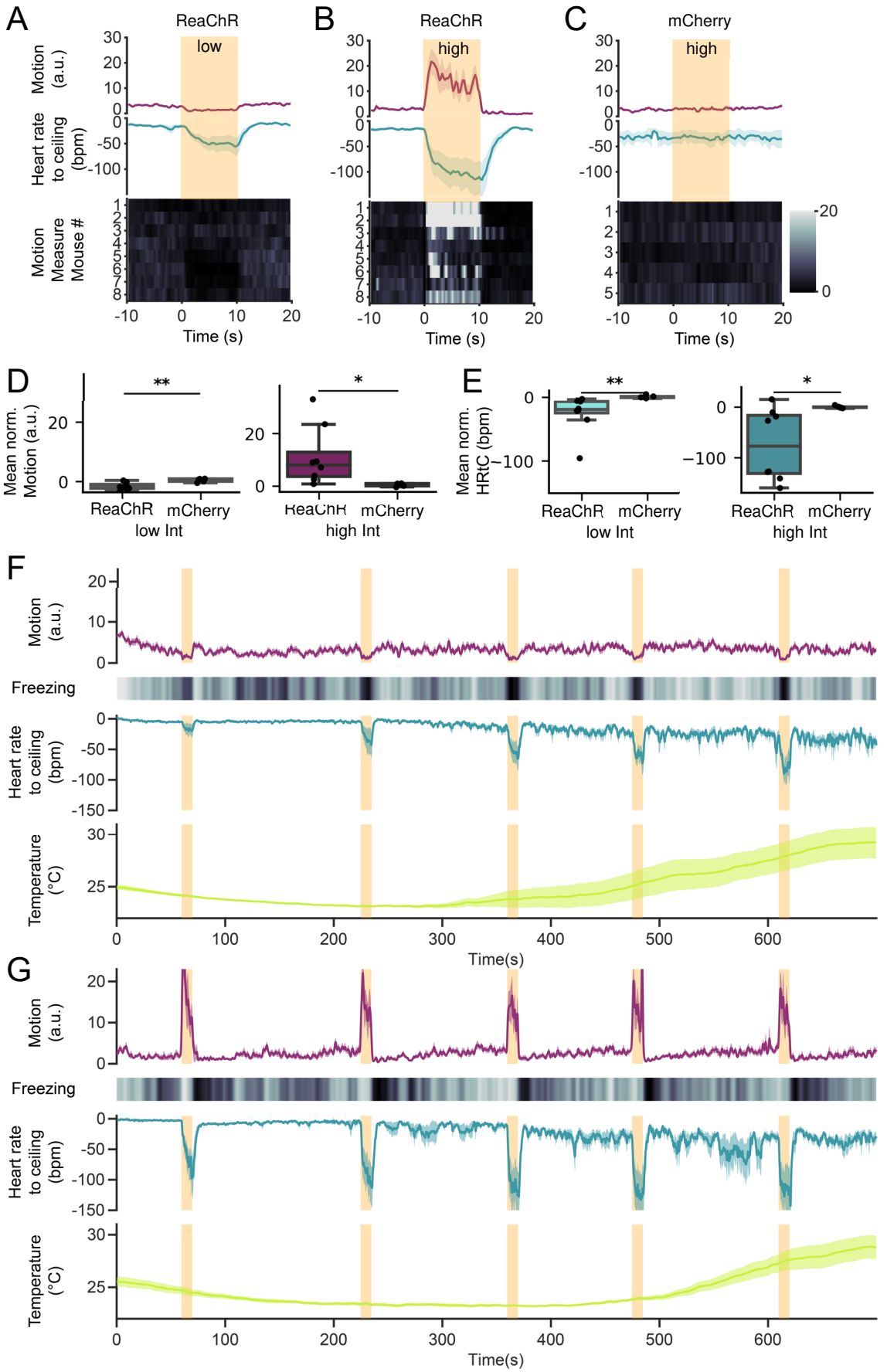

Figure 12 - Optical activation of glutamatergic vlPAG neurons with different stimulation intensities.
(continued on next page)

Figure 12 continued
(A, B) Effect of low (A) and high (B) intensity optical stimulation of glutamatergic vlPAG neurons on motion (top and bottom, heat plot with average motion measure per mouse) and HR-to-ceiling (middle). PSTH shows average (± SEM) of 5 stimulation trials (in one session) from 8 VGlut2-IRES-Cre *mice injected with a Cre-dependent ReaChR construct. Mice show decreased motion concomitant with a deceleration of the HR during low (A) and increased motion concomitant with a decrease in the HR during high (B) intensity stimulation. Stimulation parameters: low, 0.5 mW, 20 Hz, 10 ms, high. 3.5 mW, 10 Hz, 20 Hz or constant. (C) Control mice injected with a Cre-dependent mCherry construct do not show behavioral or cardiac effects during stimulations. Stimulation parameters: 3.5 mW, 10 Hz, 20 Hz or constant. (D, E) Quantifications of motion (D) and HR-to-ceiling (E) shown in A, B and C as mean normalized values per animal (stimulation subtracted by baseline). (D) Unpaired two-sided t-test with Welch-correction, $Motion_{low}$: $t(10.71) = -3.97$, $p < 0.01$; $Motion_{high}$: $t(7.06) = 2.67$, $p < 0.05$ (E) Mann-Whitney U test, $HRtC_{low}$: $U = 0$, $p < 0.01$; $HRtC_{high}$: $U = 5$, $p < 0.05$. (F, G) Behavioral effects upon optical stimulation remained constant, while stimulation evoked bradycardia increased throughout the session. Same data set as shown in A – C depicted as average traces (± SEM) along the recording for low (F) and high (G) intensity stimulation. Note post-stimulation freezing periods. Heat plot shows average freezing probability of all animals. Temperature (bottom) curve shows thermal profile of the second tail segment. Orange bars indicate light stimulations.* $N_{ReaChR} = 8$, $N_{mCherry} = 5$.

Next, mice were tested on two consecutive days with the same light protocol once in a neutral, new environment and afterwards in their familiar homecage, in order to examine potential context-dependent differences during glutamatergic vlPAG stimulations (Figure 13A-D). Low intensity stimulations were applied (0.5 mW, 20 Hz, 10 ms). Interestingly, course and magnitude of the bradycardia revealed no difference between the two environments (Figure 13D). In general, mice tended to move more in their homecage, even immobility responses during the stimulation periods were interspersed by short activity bouts (Figure 13A, top and bottom). Nonetheless, no significant change in the motion measure during the stimulation compared to baseline was detected between the two contexts (Figure 13C). Subsequently, it was hypothesized that the CS-induced responses in the conditioned flight paradigm (higher freezing probabilities during pure tone, higher probability of increased motion during white noise, compare Figure 3A and (Fadok et al. 2017)) during the CD2 could be overwritten by optic activation of glutamatergic vlPAG neurons. It was hypothesized that the expected flight response elicited by the presentation of the white noise component is reduced by optic illumination. Animals were conditioned in the first conditioning day without any optogenetic interference. On the second conditioning day, experimental and control mice were optically stimulated during the second, fourth and fifth white noise component of the SCS (Figure 13E-I). However, optical stimulation with low intensity during the white noise component of the SCS did not overwrite behavioral or cardiac responses in experimental mice as tested by comparison to animals expressing mCherry (Figure 13F-I).

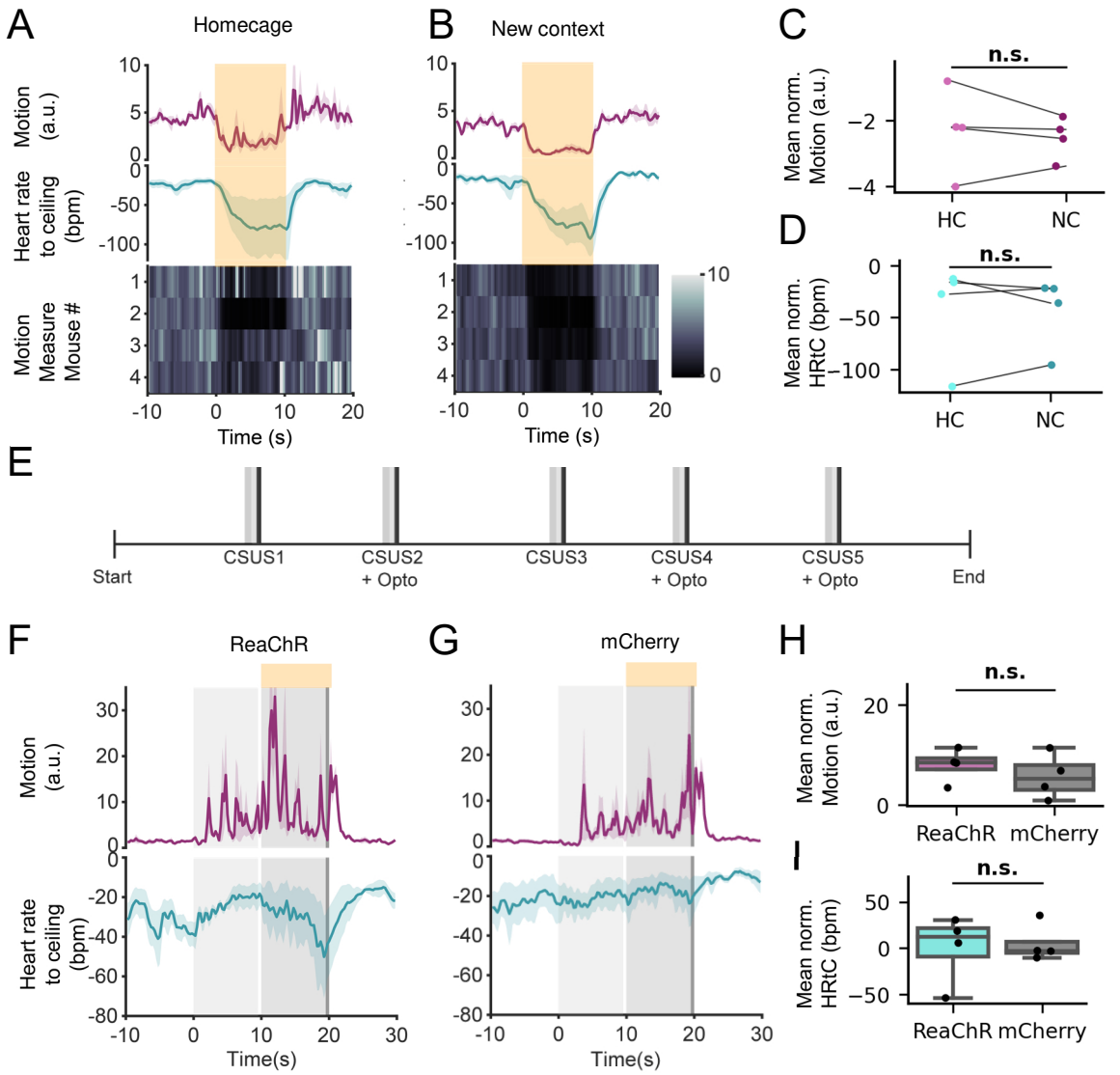

Figure 13 - Optical activation of glutamatergic vlPAG neurons compared between different contexts and effects of CS-concurrent stimulation during CD2.
(A, B) PSTHs show behavioral (top and bottom, heat plot) and cardiac (middle) responses upon optical stimulation of VGlut2-IRES-Cre *animals expressing ReaChR recorded in their homecage (A) and a new context (B). Animals received 5 stimulations (0.5 mW, 20 Hz, 10 ms) during one session, averages are shown. Motion measure (top, purple and bottom, heat plot with average motion measure ± SEM of 5 stimulations per mouse) and HR-to-ceiling (middle, blue, ± SEM) are depicted. (C, D) Mean normalized motion (C) and HR-to-ceiling (D) during optical stimulation in a new context vs. homecage. (C) Paired two sample t-test with Welch-correction, t(3) = 0.62, p = 0.06. (D) Wilcoxon signed-rank test, W =4, p = 0.88, N = 4. (E) Protocol showing a CD2 session with optical stimulation (+Opto) paired during the white noise component of CS 2, 4 and 5. (F, G) PSTHs of behavioral (top) and cardiac (bottom) responses are centered around CSUS pairings during CD2 of the conditioned flight paradigm, where the white noise component was coupled with optical stimulation (low intensity stimulation, indicated by orange rectangles) in VGlut2-IRES-Cre animals expressing ReaChR (F) or mCherry (G). (H, I) Quantifications of motion (H) and HR-to-ceiling (I) shown in (F) and (G) as mean normalized values per animal (stimulation during White Noise subtracted by baseline). Unpaired two-sided t-test, Motion: t(6) = 0.81, p = 0.45 (H); HRtC: t(6) = -0.21, p = 0.84 (I).* N_{ReaChR} *= 4,* $N_{mCherry}$ *= 4.*

Next, it was tested, if the modulation of glutamatergic vlPAG neurons is associated with an emotional valence. The post-stimulation freezing responses in *VGlut2-IRES-Cre* animals that received high intensity stimulations suggests an aversive reaction (Figure 12G). A RTPP was conducted, in which a chamber is divided into two equal compartments with one side being paired with light stimulations (1 s ON, 3 s OFF, Figure 14A). All *VGlut2-IRES-Cre* mice were

tested with high and low intensities in separate sessions (low intensity: 0.3 mW, constant; high intensity: 3.5 mW, individual frequency settings per animal). The average time that the subject spent per visit on the side paired with light stimulation was compared. Interestingly, low and high stimulations had different effects on the aversiveness to the stimulations in *VGlut2-IRES-Cre* mice (Figure 14B, top). Experimental animals induced with low intensities spent on average 37.5 seconds (SEM ±7.49 s) at the chamber paired with stimulation, while stimulation with high intensities tend to be aversive, which is reflected by an average visit time of 8.84 seconds (SEM ±3.01 s, Figure 14B, top). These animals showed directed flight bouts out of the stimulated side.

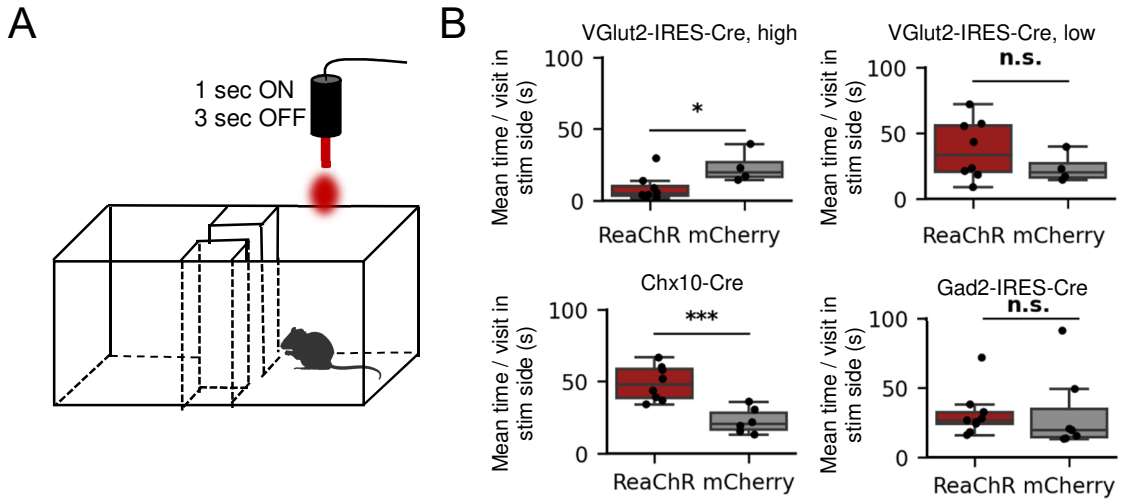

Figure 14 – Optical stimulation paired real-time place preference test.
(A) Experimental set-up composed of two equal chambers with one being paired with optical stimulations (right side). (B) Mean time per visit in stimulation side of VGlut2-IRES-Cre *(high and low intensity stimulation),* Chx10-Cre *and* Gad2-IRES-Cre *mice. VGlut2, high: Mann-Whitney U test, U = 3, p < 0.05; VGlut2, low: Unpaired two-sided t-test with Welch-correction, t(9.95) = 1.43, p > 0.05; Chx10: Unpaired two-sided t-test with Welch-correction, t(11.99) = 4.66, p < 0.001; Gad2: Mann-Whitney U test, U = 42, p > 0.05.* $N_{VGlut2,\ ReaChR} = 8$, $N_{VGlut2,\ mCherry} = 5$; $N_{Chx10,\ ReaChR} = 8$, $N_{Chx10,\ mCherry} = 6$; $N_{Gad2,\ ReaChR} = 10$, $N_{Gad2,\ mCherry} = 7$

Another important role of the PAG in the context of defensive responses is the mediation of analgesia. Stimulating PAG neurons electrically or optogenetically, evokes antinociceptive effects (Fardin, Oliveras, and Besson 1984; Tovote et al. 2016). Especially the ventral parts of the PAG were shown to mediate robust analgesia. The tail immersion test investigates nociception of animals by dipping the tail repeatedly into hot water and scoring the latency time of a tail flick or withdrawal of the tail (Ramabadran et al. 1989). Here, potential analgetic effects after PAG stimulation were tested. While low intensity stimulations of glutamatergic vlPAG neurons had no analgetic effects, high intensity stimulations led to an increase in the withdrawal latency (Figure S5).

In summary, activation of the same glutamatergic population in the PAG with either low or high light intensities evoked similar cardiac, but opposing behavioral effects. Low intensity stimulations led to moderate decreases in HR and freezing, high stimulations to pronounced

bradycardic events concomitant with high motion measures. Stimulated animals showed robust responses independent of contexts and CS-induced reactions could not be overwritten by light-induced PAG stimulations. The combination of defenisve responses during high intensity stimulation was unexpected and might represent an artificial concurrent exhibition of cardiac and behavioral responses. This might be a consequence of simultaneously addressing several neuronal subpopulations of the rather heterogenous group of glutamatergic cells, which would not be active together naturally. Therefore, we made use of a mouse line, which expresses the Cre enzyme under the Chx10 promotor, present solely in a subgroup of glutamatergic neurons in the vlPAG.

3.2.3 Optical manipulation of Chx10-positive neurons in the PAG

In order to gain more accuracy of the optically targeted neurons, in a next step, only a subgroup of glutamatergic neurons was activated. *Chx10* is a homeodomain transcription factor and defines a neuronal group in the brainstem that is involved in arresting locomotion by inhibiting locomotor networks in the spinal cord (Bouvier et al. 2015; Clovis et al. 2016; Cregg et al. 2020; Hayashi et al. 2018). Previously, optical activation of *Chx10-ChR2* expressing neurons in the vlPAG was shown to evoke robust freezing responses (Vaaga et al. 2020).

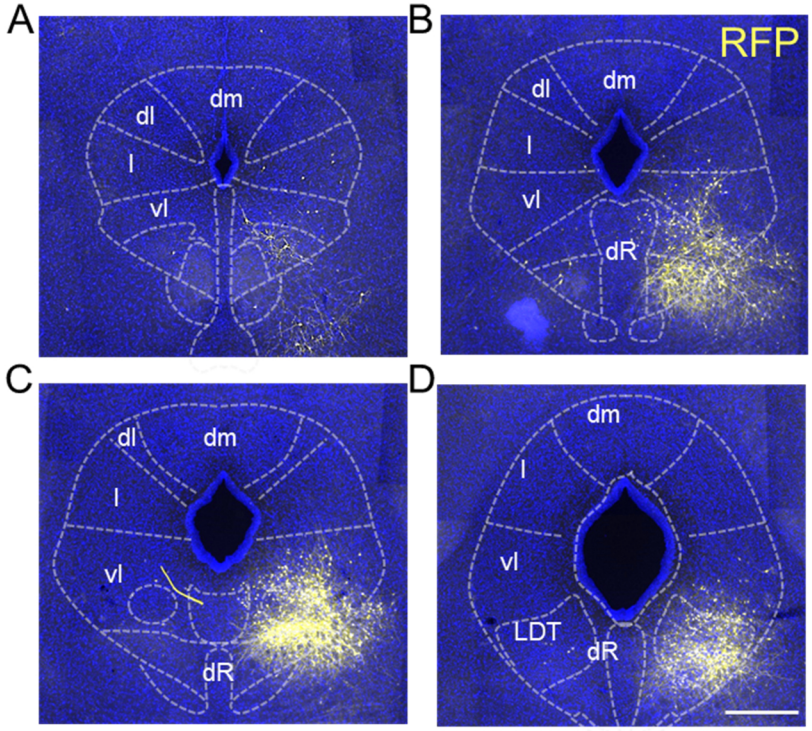

Figure 15 - Chx10 neuronal population in the antero-posterior axis of the vlPAG.
Representative images of immunhistochemical staining of brain sections from a Chx10-Cre animal injected with AAV2/5-hSyn-Flex-mCherry. *Bregma coordinates: -4.36 (A) -4.72 (B) -4.84 (C) -4.96 (D) mm. Abbrevations - dm: dorsomedial, dl: dorsolateral, l: lateral, vl: ventrolateral, dR: dorsal raphe nucleus, LDT: laterodorsal tegmental nucleus. Scale bar: 0.5 mm.*

Figure 15 illustrates the distribution of the Chx10 population in the PAG along the anteroposterior axis. *Chx10-Cre* mice were injected with an *AAV2/5-hSyn-Flex-mCherry* construct into the vlPAG and brain sections were immunhistochemically stained to enhance the fluorescent mCherry signal. While in the anterior parts of the PAG relatively low amounts of Chx10+ neurons are present, rather posterior parts show a defined cluster of Chx10+ cells in the vlPAG (Figure 15).

In the following set of experiments, the contribution of this cell population to the animals' defensive state was investigated. To this end, *Chx10-Cre* animals were, similar to the previous optogenetic experiment shown, injected with an AAV delivering ReaChR, which was expressed in a Cre-dependent manner in the vlPAG. Stimulation with high intensities of naïve animals resulted in pronounced freezing responses as expected (Figure 16, 7 mW, 30 Hz, 20 m, 10 s). The animals' ongoing behavior, for instance rearing, grooming, and walking, could be arrested instantly by light delivery (data not shown). Concomitantly, a marked decrease in HR was observed (Figure 16A, middle). A closer look at the stimulation periods revealed an almost immediate freezing response (Figure 16A, top). Additionally, stimulations with increasing intensities and frequencies revealed a motion effect in an "all-or-nothing" fashion (Figure S6). Mice were stimulated nine times with increasing intensities and varying frequencies and pulse lengths of the delivered light. Mice reacted only after a certain light power with a freezing response or a HR deceleration, which remained similar during all subsequent stimulations with higher intensities or frequencies (Figure S6). Similar to the low intensity stimulation of the *VGlut2-IRES-Cre* cohort, the magnitude of bradycardia increased with recording time, displaying the strongest HR-to-ceiling decreases towards the end of the session (Figure 16E, middle). The course of the tail temperature was comparable to unperturbed animals and showed no stimulation-specific changes (Figure 16E, bottom). Control animals of the same transgenetic line expressing only a fluorescent protein (*AAV2/5-hSyn-Flex-mCherry-WPRE*) showed neither a stimulation-specific cardiac nor a behavioral response (Figure 16B).

Next, the cardiac response dynamics of spontaneously occuring and stimulation-evoked freezing bouts was compared. Spontaneous freezing bouts of animals being exposed to an open field test were on average 2.1 seconds long. *Chx10-Cre* animals were optically excited with the same length. A comparison of HR responses displayed during spontaneous freezing bouts with optically evoked bradycardia revealed similar dynamics and amplitudes (Figure 17A, B). HR-to-ceiling values of spontaneous freezing bouts correlated well with those of optically evoked bouts along time (Figure 17B).

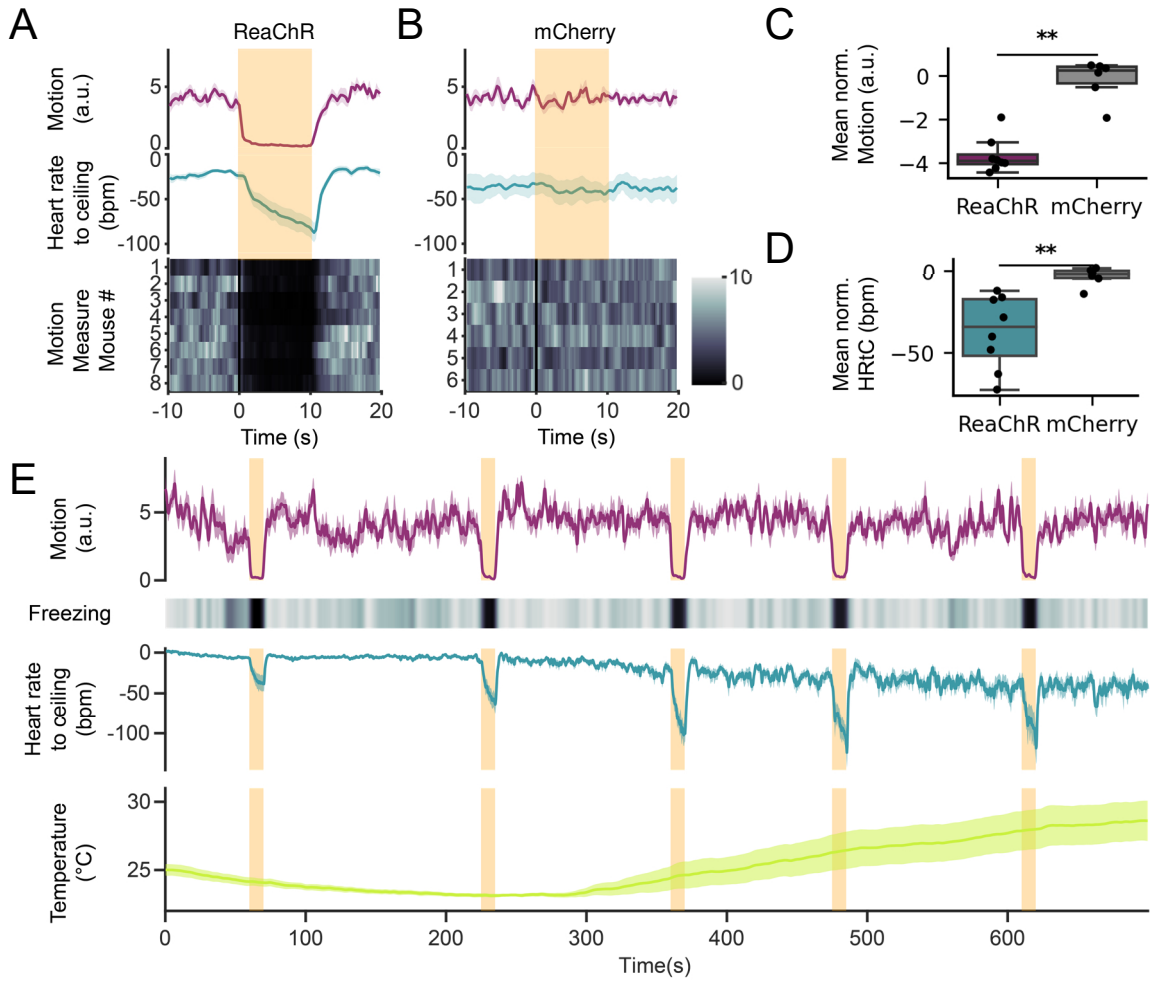

Figure 16 – Cardio-behavioral responses during optical activation of Chx10+ vlPAG neurons.
(A, B) PSTHs centered around optical stimulation (5 times with 7 mW, 30 Hz, 20 ms) of Chx10-Cre *animals injected with a Cre-dependent ReaChR (A) or mCherry construct (B). Plots show motion (top and bottom, heat plot with average motion measure ± SEM of 5 stimulations per mouse) and HR-to-ceiling (middle, ± SEM) curves. (C, D) Quantifications of Motion (C) and HR-to-ceiling (D) shown in (A) and (B) as mean normalized values per animal (stimulation subtracted by baseline). Mann-Whitney U test, (C) Motion U = 1, $p < 0.01$; (D) HRtC U = 1, $p < 0.01$. (E) Average trace (± SEM) of 8 mice shown in (A) with motion measure (top), freezing probability (heat plot), HR-to-ceiling (middle) and tail temperature (bottom). Orange rectangles indicate light stimulations.* $N_{ReaChR} = 8$, $N_{mCherry} = 6$.

In a next step, similarly as described above for *VGlut2-IRES-Cre* animals, it was tested, if an overwriting of the active response component during conditioning in the conditioned flight paradigm could be achieved by optical manipulation of these cells (compare Figure 13C). On CD2, a parallel optical stimulation of Chx10+ cells during the white noise compound of the CS as well as the US (foot shock) was applied (CSUS + Opto), with every second CS presented without optical stimulation (Figure 17C-F). Interestingly, a marked freezing response concomitant with strong bradycardia was observed during optic activation during the white noise component of the SCS in mice injected with *AAV2/5-hSyn-Flex-ReaChR-Citrine-WPRE* (Figure 17C). However, an increased motion and a slight increase in HR was observed during the white noise component of the CS in mice injected with *AAV2/5-hSyn-Flex-mCherry-WPRE*, which is comparable to the expected response combination of non-optogenetically manipulated animals (Figure 17D, compare Figure 5A). Since light stimulation was extended until the end

of the foot shock delivery, stimulated animals even showed reduced jumping during the unconditioned aversive stimulus compared to control animals (Figure 17C and D).

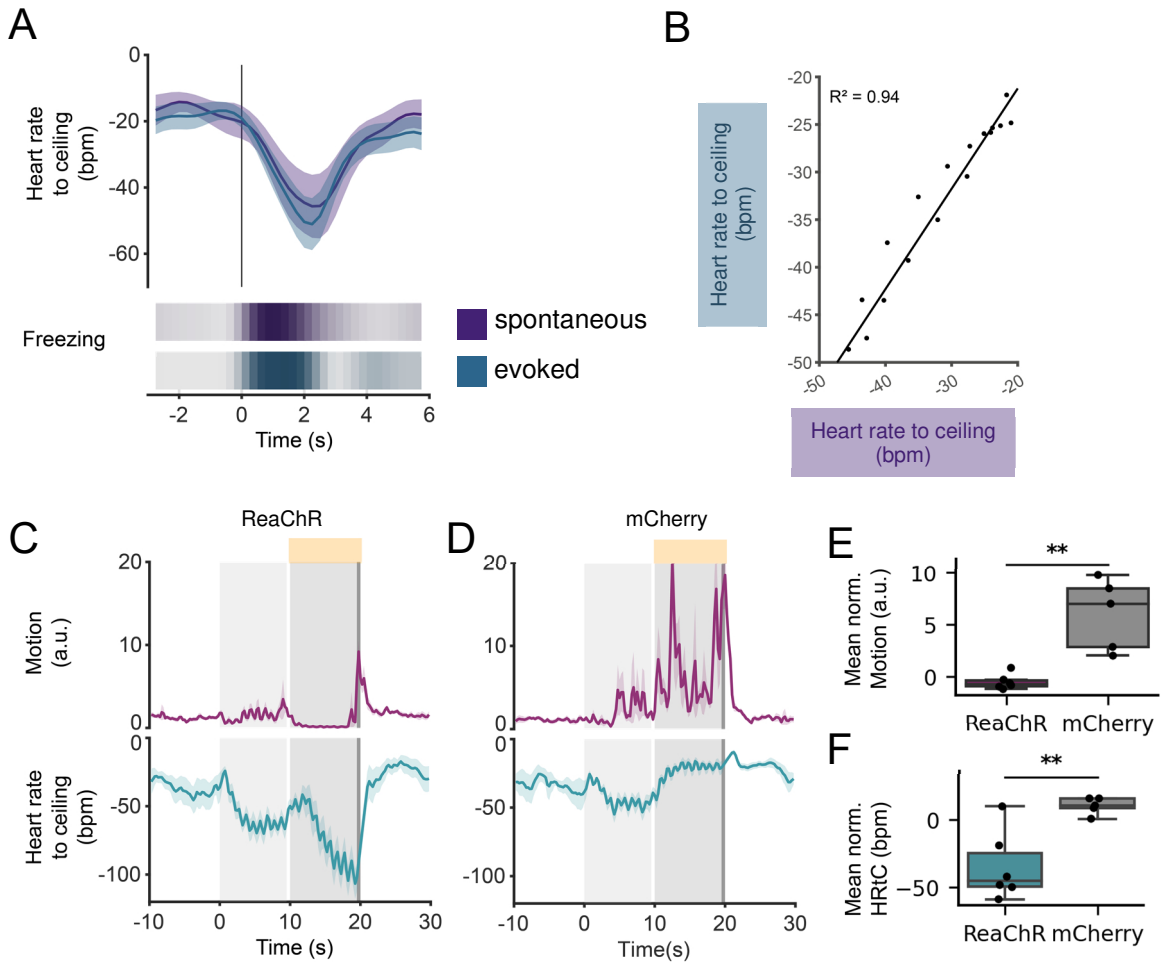

Figure 17 – Comparison of spontaneous and light-evoked freezing bouts in Chx10-Cre animals.
(A) Comparison of HR dynamics of spontaneous and evoked freezing responses. Average freezing lengths of animals displaying spontaneous freezing bouts in an OF test were used to optically activate Chx10+ vlPAG neurons with the same length. N_{evoked} *= 8,* $N_{spontaneous}$ *= 23. (B) Correlation plot of HR-to-ceiling values of time-matched immobility bouts compared between spontaneous (x-axis) and optically evoked (y-axis) episodes. Plot shows for each time point of the corresponding PSTH the average value of spontaneous against evoked HR-to-ceiling. Coefficient of determination* R^2 *= 0.94. (C, D) Averaged behavioral (top) and cardiac (bottom) responses of* Chx10-Cre *animals expressing ReaChR (C) or mCherry (D) are centered around CSUS pairings during the conditioned flight paradigm, with the 2nd, 4th and 5th presentation of the white noise component coupled with optical stimulation (7 mW, 30 Hz, 20 ms; indicated by orange rectangles). (E, F) Quantifications of motion (E) and HR-to-ceiling (F) shown in (C) and (D) as mean normalized values per animal (stimulation during White Noise subtracted by baseline). Mann.Whitney U test, U = 0,* $p < 0.01$ *(E), Unpaired two-sided t-test, t(5.7) = -4.16 (F),* $p < 0.01$. N_{ReaChR} *= 6,* $N_{mCherry}$ *= 5.*

The real-time place preference test revealed a putative appetitive effect upon optical activation, as the mice spent per visit significantly longer time in the stimulation side (Figure 14B). As described before, potential analgetic effects were measured in the tail immersion test. It yielded no pain reduction upon stimulation of Chx10+ neurons (Figure S5).

Having described effects of optic activation of Chx10+ neurons, next, in a loss-of-function approach, this neuronal population was tested in an inhibitory optogenetic experiment. An *AAV5-CAG-Flex-ArchT-tdTomato* construct was used to deliver a cre-dependent, inhibitory

opsin (ArchT) to the vlPAG. In order to test the effect of inhibiting a neuronal population, which is presumably responsible for generating a freezing-bradycardia microstate, first, a global fear state was induced by conditioning the mice for two days in the CFP, as described above (see 2.5.2). On the third day, mice were placed back into the context, they were conditioned in, and four light stimulations (7 mW, constant, 20 s, 550 nm) were applied during a 15 minutes recording (Figure 18). Mice showed globally a high probability of freezing that were interrupted by increased motion during light stimulations (Figure 18A, C). The HR was slightly increased during optic inhibition, albeit not significantly (Figure 18A, D). Importantly, these effects could not be observed in control mice, excluding potential irritating effects of the light stimulus on the head cap (Figure 18B-D).

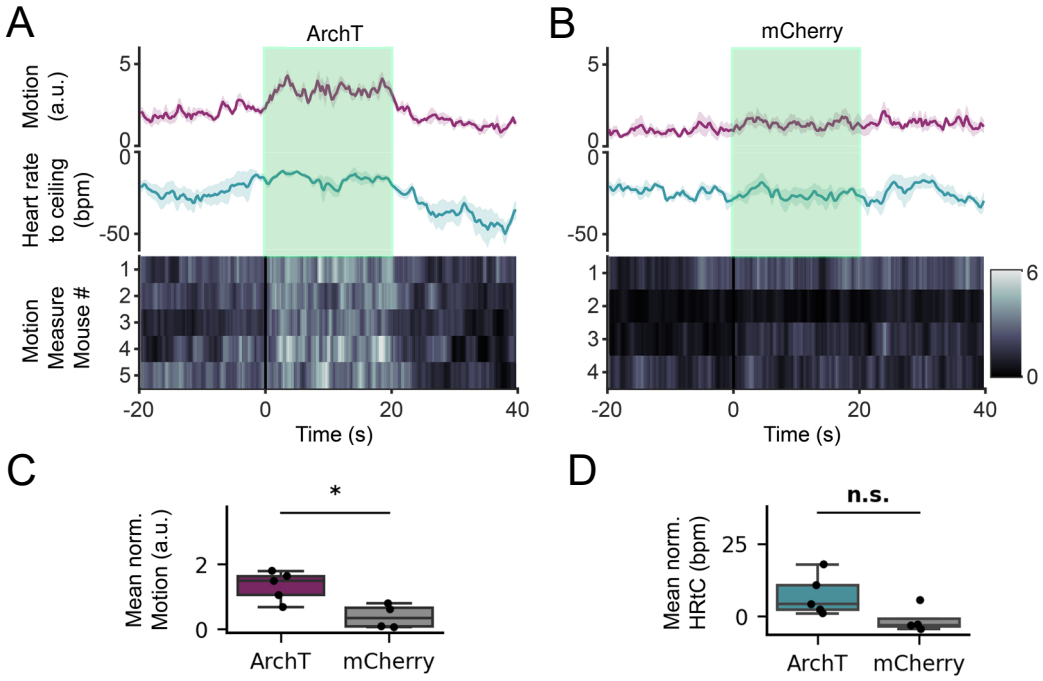

Figure 18 – Cardio-behavioral responses during optical inhibition of Chx10+ vlPAG neurons.
(A, B) PSTHs (± SEM) centered around optical inhibition events (4 times for 20 s with 7 mW, constant light) of Chx10-Cre *animals injected with a Cre-dependent ArchT (A) or mCherry construct (B). Optical stimulations were applied during reexposure to the conditioning context. Plots show motion (top) and HR-to-ceiling (middle) curves. Heatplot illustrates average freezing probability of 4 trials for each tested mouse. (C, D) Quantifications of Motion (C) and HR-to-ceiling (D) shown in (A) and (B) as mean normalized values per animal (stimulation subtracted by baseline). Unpaired two-sided t-test, Motion: $t(6.99) = 3.40$, $p < 0.05$; HRtC: $t(6.81) = 2.17$, $p = 0.07$. $N_{ArchT} = 5$, $N_{mCherry} = 4$*

In summary, activation of Chx10+ neurons in the vlPAG evoked a highly reproducible and robust freezing-bradycardia microstate during light stimulation. Behavioral and autonomic defensive responses were comparable to spontaneous freezing events of naïve animals tested in an OF context. Optical activation of Chx10+ neurons was sufficient to overwrite the naturally evoked flight-tachycardia response and instead resulted in freezing and a marked bradycardia during the white noise component and the shock of the conditioned flight paradigm. Optic inhibition of the same neuronal population resulted in a disruption of ongoing freezing behavior and a slight, non-significant increase of the HR.

3.2.4 Optical activation of GABAergic neurons in the PAG

Another neuronal population in the vlPAG, which plays a crucial role in modulating the behavioral aspect of the defensive response, are the inhibitory GABAergic interneurons in the vlPAG (Tovote et al. 2016). This population showed low firing rates during immobility bouts as well as impaired freezing response to aversively conditioned stimuli upon light stimulation (Tovote et al. 2016). Here, optical activation of GABAergic vlPAG neurons was tested in naïve animals in order to refine the picture of this populations' role in generating defensive states.

Naïve animals were tested in an OF context. The mice received five 30 seconds long stimulations (12 mW, 30 Hz, 10 ms) with an ISI of minimum 90 seconds. Figure 19A (top and bottom) illustrates an increase of locomotion during the stimulation, but no change in the HR. In general, optical activation evoked a rather diffuse, compared to Chx10-Cre animals, less time-locked general behavioral activation, which was characterized by higher motion measure values that were interspersed by flight bouts (Figure 19A, C). No such effects were observed in control animals (Figure 19B). Optical stimulation of inhibitory neurons in the vlPAG had no aversive or appetitive effects nor were analgetic impacts observed during the tail immersion test (Figure 14 and Figure S5).

Long-lasting optical activation of vlPAG Gad2+ neurons evoked a general behavioral activation characterized by increased locomotion, reduction of freezing events and accumulation of exploratory rearing events. Furthermore, HR values remained steady during stimulation periods.

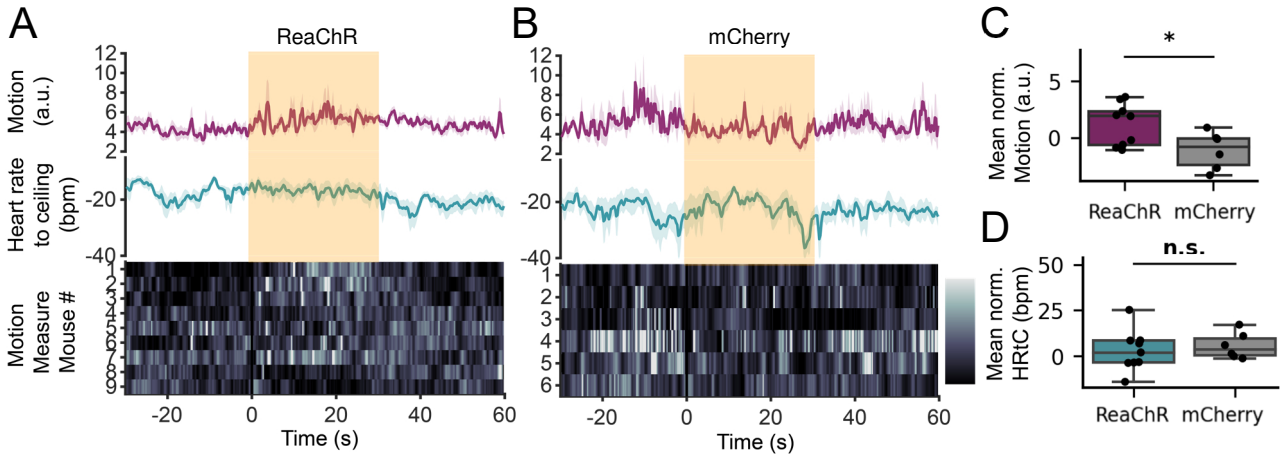

Figure 19 - Cardio-behavioral responses during optical activation of GABAergic vlPAG neurons.
(A) PSTH with events centered around optical stimulations (5 times for 30 s with 12 mW, 30 Hz, 10 ms) of Gad2-IRES-Cre *animals injected with a Cre-dependent ReaChR (A) or mCherry construct (B) tested in an open field context. Plots show motion (top, ± SEM) and HR-to-ceiling (middle, ± SEM) curves. Heat plot illustrates average freezing probability of 5 trials for each tested mouse. Quantifications of Motion (C) and HR-to-ceiling (D) shown in (A) and (B) as mean normalized values per animal (stimulation subtracted by baseline). Unpaired two-sided t-test with Welch-correction, Motion: $t(11.80) = 2.49$, $p < 0.05$; HRtC: $t(13.00) = -0.57$, $p = 0.58$. $N_{Gad2,\ ReaChR} = 9$, $N_{Gad2,\ mCherry} = 6$*

3.3 Anterograde projections of glutamatergic vlPAG neurons to brainstem targets

Different neuronal subpopulations in the vlPAG were shown to exert diverse effects on the defensive state of the animal, partially evoking opposite behavioral reactions in an intensity-dependent manner. The PAG's role in the defensive brain network was described as an output structure mediating defensive responses in a labelled-line like mechanism (Tovote et al. 2016; Vaaga et al. 2020). This mechanism assumes direct projections with each neuron(al population) targeting specific regions to fulfill a separate function. In a next step, potential projection targets of the vlPAG in the brainstem that could be involved in mediating the observed cardiac and behavioral responses were investigated by anterograde tracing experiments. Projection targets of glutamatergic vlPAG neurons were labelled by an AAV-based expression of synaptophysin fused to a Myc-tag (*AAV2/5-CAG-floxed-Synaptophysin-10xMyc-rev.WPRE*). At first, a qualitative *in vitro* testing of the AAV was performed in HEK293-Cre cells. These were infected with the virus (1 µl in 500 µl complete medium, Titer 10^{12} gc/ml), incubated for three days, fixated, and stained for the Cre enzyme as well as for the Myc-tag to identify infected cells (Figure S7). Cre-dependent expression could be verified by double-positive labelled cells (Cre and Myc, Figure S7A). Control cells, which are non-infected do not present positive Myc-Staining (Figure S7B).

Having confirmed sufficient Cre-dependent expression levels, *AAV2/5-CAG-floxed-Synaptophysin-10xMyc-WPRE* was injected into the vlPAG of *VGlut2-IRES-Cre* animals. After an expression time of four weeks, the brain tissue was processed and brainstem sections were screened for Myc-positive synapses. Figure 20 shows an overview of brainstem targets recruited by glutamatergic neurons of the vlPAG in a qualitative manner. The Mc, a conglomeration of LPGi, GiV and GiA, was shown to receive strong glutamatergic input from the vlPAG (Esposito et al. 2014; Tovote et al. 2016). As the Mc is implicated in motor control, this projection is suggested to promote freezing behavior (Esposito et al. 2014; Orlovsky, Deliagina, and Grillner 1999; Tovote et al. 2016). A strong innervation of the Mc by glutamatergic neurons originating in the vlPAG could be confirmed (Figure 20B, C, D). The GiA and LPGi of the Mc were identified as main targets, while ipsilateral projections were more pronounced (Figure 20B, C, D). Additionally, presynaptic terminals of glutamatergic neurons originating in the vlPAG were found in the dorsal vagal complex (DVC), a structure which encompasses the NTS, the DMV, and the area postrema. More precisely, the DMV where parasympathetic, preganglionic neurons are located (Silvani et al. 2016) and the posterior, but

not anterior parts of the solitary nucleus are targeted, however more sparsely compared to other brainstem targets (Figure 20D, E). Moreover, glutamatergic projections to the ipsilateral caudal ventrolateral medulla could be observed (Figure 20D, E). Additionally, the NA, a site that also contains parasympathetic cardiac preganglionic neurons, showed Myc+ terminals (Figure 20 E).

In summary, multiple brainstem targets related to motor control as well as cardiac function were shown to be targeted by glutamatergic vlPAG neurons.

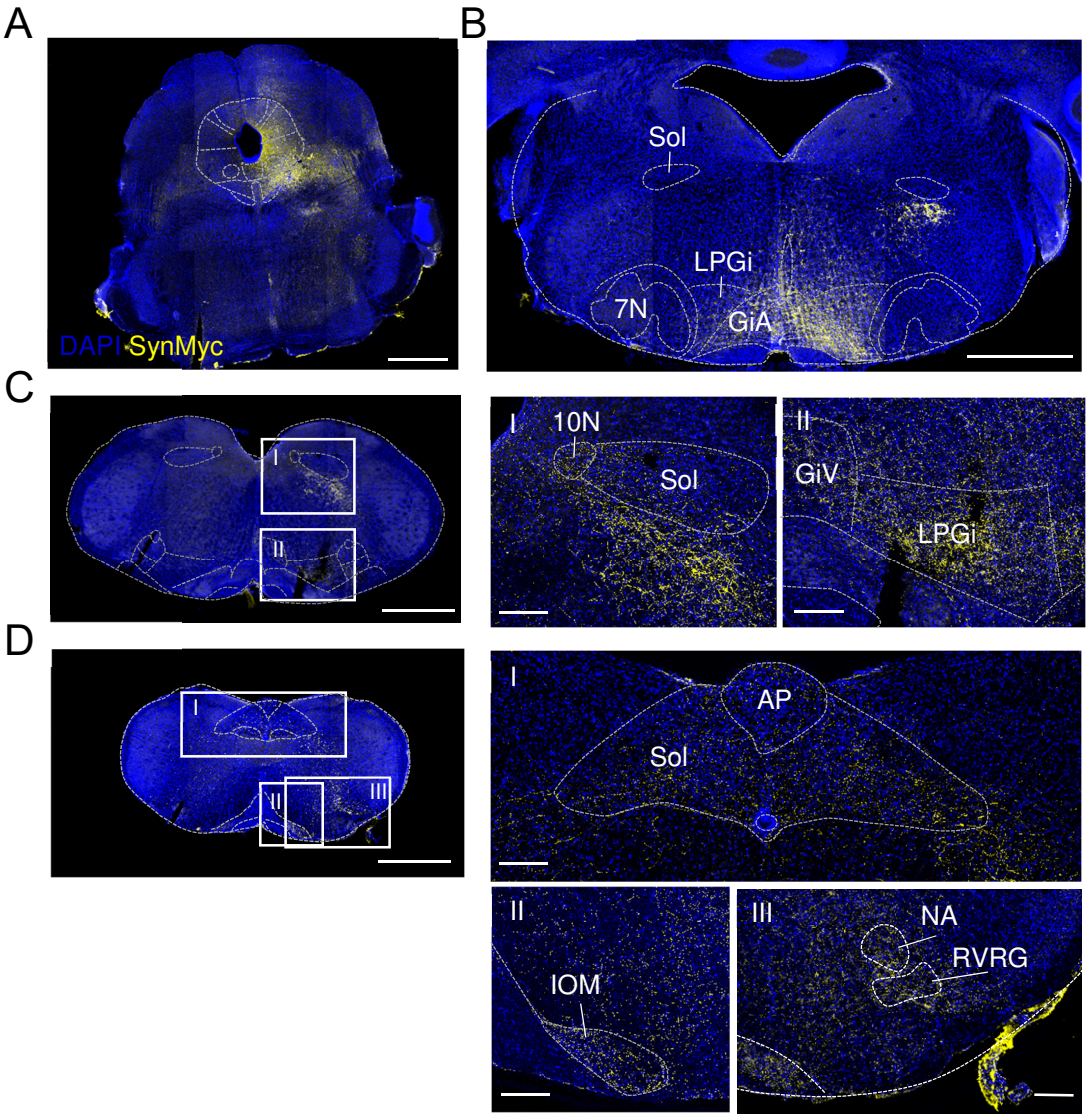

Figure 20 - Projection pattern of glutamatergic vlPAG neurons in the brainstem.
Projection targets were labelled by AAV-based expression of synaptophysin fused to a Myc-tag. (A) Injection site in the right vlPAG (scale bar: 1 mm). (B) and left panel of (C, D) shows overview images of brainstem sections (scale bar 500 µm), magnifications are depicted in the right panel of (C and D; scale bar 200 µm). Presynaptic terminals are located in the GiA and LPGi forming the Mc (B, C), the DMV (C I), posterior parts of the solitary nucleus (D I), the medial nucleus of the inferior olive (D II) and the NA (D III). Bregma levels: (A) -4.84 mm, (B) -6.36 mm, (C) -6.96 mm, (D) -7.64 mm. Abbrevations: 7N: facial nucleus, 10N: dorsal motor nucelus of vagus (DMV), AP: area postrema, GiA: gigantocellular reticular nucleus, alpha part, GiV: gigantocellular reticular nucleus, ventral part, IOM: inferior olive, medial nucleus, LPGi: lateral paragigantocellular nucleus, NA: Nucleus ambiguous, RVRG: rostral ventral respiratory group, Sol: solitary nucleus.

3.4 Projection-specific optical activation of glutamatergic PAG-to-Mc neurons

Having demonstrated the direct projection of glutamatergic neurons from the vlPAG to the Mc, in a next step, specifically those cells were targeted and optically activated. It has been shown that glutamatergic as well as Chx10+ vlPAG neurons projecting to the Mc are inducing freezing behavior upon optical activation (Tovote et al. 2016; Vaaga et al. 2020). Here, next to the behavior, cardiac reactions were investigated to understand better the neural circuit underlying the previously described defensive states between the midbrain PAG and an executive hindbrain region (Mc). To this end, it was made use of an intersectional strategy. Projection specificity was achieved by a retrogradely (from terminals to cell bodies) transported, Cre-dependent AAV injected into the Mc of *VGlut2-IRES-Cre* animals (*AAV(retro)-CAG-Floxed-FlpO-2A-H2BV5.rev.WPRE*). By the expression of a Flippase recombinase (FlpO), it endows neurons in the PAG projecting to the Mc to express a second AAV-delivered plasmid, which is FlpO-dependent and expresses a Channelrhodopsin variant (*AAV2/5-hSyn-Con/Fon-hChR2(H134R)-EYFP-WPRE,* Figure 21A). While retrogradely labeled cells projecting to the Mc can be identified by the immunohistochemically stained V5 molecule, neurons expressing the double conditional plasmid were tracked by EYFP (Figure 21B, C). Surprisingly, optical activation of glutamatergic vlPAG neurons projecting to the Mc resulted in a strong behavioral activation (Figure 21D, top and bottom, E). Together with the concomitant evoked bradycardia (Figure 21D, middle, F), this defensive state was comparable to the reaction shown for high intensity optical activation of glutamatergic neurons in the vlPAG that were targeted in a projection-independent manner (Figure 12B). However, contrary to the intensity-dependent dual induced defensive states shown before (Figure 12A, B), here, even low stimulation intensities (0.8 mW, 20 Hz, 20 ms) did not induce freezing behavior (Figure S8A). Instead, incrementally increasing light intensities induced progressively rising motion measure values accompanied by decreasing HRs (Figure S8A-C). Taken together, against hypothesized based on literature (Tovote et al. 2016), expected defensive states (freezing and bradycardia) could not be reproduced upon optogenetic stimulation of vlPAG-to-Mc projecting glutamatergic neurons.

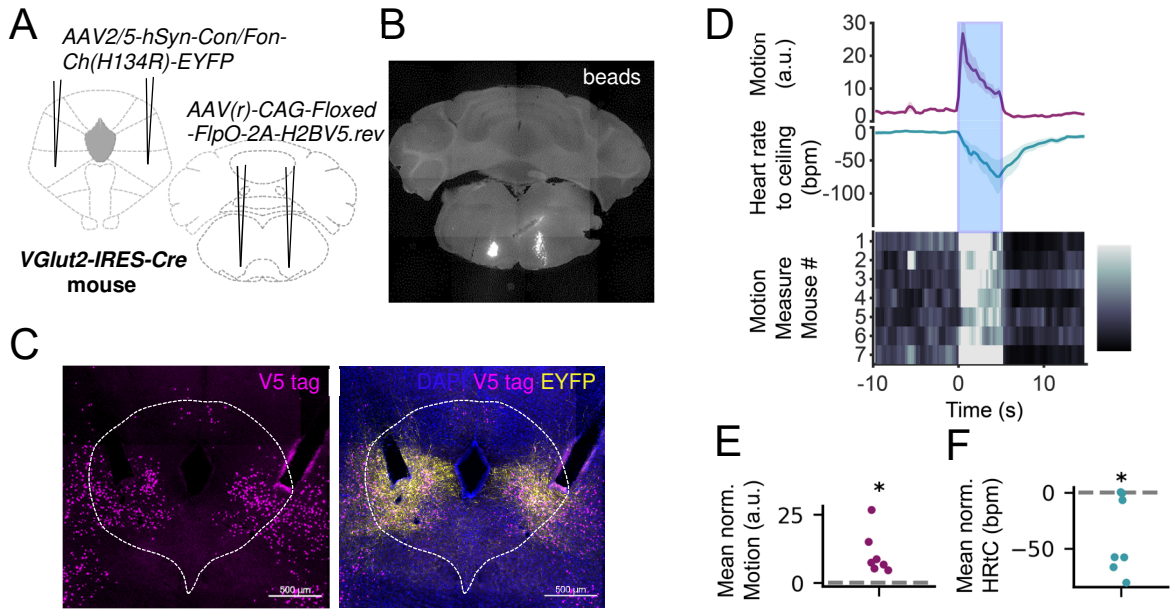

Figure 21 - Projection-specific stimulation of glutamatergic vlPAG-to-Mc neurons.
*(A) Intersectional optogenetic strategy with a retrogradely traveling AAV delivering a Flippase (FlpO) and a V5 tag injected into the magnocellular nucleus (*AAV(retro)-CAG-Floxed-FlpO-2A-H2BV5.rev.WPRE *mixed with fluorescent beads) and a double-conditional (dependent on Cre and FlpO) AAV expressing a Channelrhodopsin-EYFP into the vlPAG (*AAV2/5-hSyn-Con/Fon-hChR2(H134R)-EYFP-WPRE*) of* VGlut2-IRES-Cre *animals. (B) Representative brain section showing placement of fluorescent beads injection mixed with the vector into the Mc. (C) Immunhistologically stained brain sections verifying retrogradely traced V5+ cell bodies (purple) and double infected neurons expressing the Channelrhodopsin (EYFP) in the vlPAG. (D) PSTH showing average behavioral (top ± SEM and bottom, heat plot,) and cardiac (middle, ± SEM) responses during optogenetic stimulation of glutamatergic vlPAG neurons projecting to the Mc (4 stimulations à 5 s, 7 mW, constant). (E, F) Quantifications of motion (E) and HRtC (F) shown in (D) as mean normalized values per animal (stimulation subtracted by baseline). (E) One sample Wilcoxon rank-sum test, W = 0, p < 0.05. (F) One-sample t-test, t(6) = -2.96, p < 0.05, N = 7. Scale bar PAG: 500 µm*

4. Discussion

This thesis characterizes fear and anxiety reactions defined by stereotypic combinations of behavioral and physiological adjustments in mice. By deriving multimodal measurements of mice exposed to a series of fear and anxiety paradigms, the different behavioral and cardiac read-outs and their dynamic interactions were integrated within distinct time ranges. This enabled to characterize integrated defensive states within a novel framework. This reaches beyond the mere equation of behavioral read-outs to a fear state, but takes into account concomitant cardiac adaptations, thereby allowing a more fine-grained description of defensive states. Using optogenetics in the second part of this thesis, different circuit elements of the vlPAG, a region that is known to be involved in mediating defensive responses, were shown to play important state generator roles. While optical activation of glutamatergic PAG neurons revealed rather heterogeneous, light-intensity dependent effects, activation of Chx10+ neurons could evoke robust freezing-bradycardia states, which resembled spontaneous freezing bouts.

4.1 Characterization of cardio-behavioral defensive states

Defensive reactions are accompanied by stereotypical combinations of behavioral and autonomic responses. In fact, cardiac readouts associated with defensive reactions have been described in a multitude of studies (Koba et al. 2016; Swiercz et al. 2018; Walker and Carrive 2003). However, while there is a vast consensus about the behavioral aspect of the defensive reaction (i.e. freezing), cardiac read-outs with their rather complex dynamics have led to heterogeneous, sometimes even seemingly contradictory findings. While many studies report general tachycardia during cue and context retrieval of fear conditioned subjects, some others recurrently find CS and context associated bradycardic responses (Stiedl and Spiess 1997; Tovote et al. 2004; Vianna and Carrive 2005; Walker and Carrive 2003). Furthermore, innately aversive stimuli evoke strong bradycardic responses in both, animals and humans, an aspect coined ‘fear bradycardia’ (Hermans et al. 2013; Yoshimoto et al. 2010). Why did no clear picture on fear associated cardiac responses arose, despite many years of animal and human research?

Firstly, the precise experimental setting as well as the context, the animal is tested in, need to be considered carefully when comparing different studies on defensive cardiac responses. For instance, the handling procedure of the animal that takes place right before the start of the experiment, biases the interpretation of the subsequent cardiovascular changes associated with

a threat, as the handling itself leads to an overall sustained increase in HR (Liu et al. 2014; Walker and Carrive 2003). Furthermore, other external factors like the availability of escape routes or the distance of the threat have a pivotal impact on not only on the defensive behavior, but also on autonomic responses (Blanchard and Blanchard 1989; Roelofs 2017). A second important factor, that need to be considered when analyzing cardio-behavioral changes is there disparate dynamics that lies in the nature of these two different measurements (behavior vs. HR). While behavior is a binary measure (i.e. freezing vs. non-freezing), cardiovascular changes are dynamic on various levels. Crude averaging and thus highly binned data lead to imprecise descriptions of the data by ignoring the much faster dynamics of HR (Resstel et al. 2006; Walker and Carrive 2003). Cardiac responses to threat situations underlie different short-term and long-term dynamics, which are necessary to include into the analysis in order to define defensive states more precisely. Here, an analytical framework has been established, that aims in accommodating the seemingly contradictory findings.

Cardiac interrelated dynamical changes include slow changing HR macrostates, which restrict the theoretical range of the HR and thus limits a momentary microstate defensive response can be manifested in. While the *HR-to-ceiling* macrostate defines the upper limit, the *rigidity* macrostate constraints the HR on the lower limit. The absolute HR of all recordings reflects an overall high tachycardia at the beginning of the sessions. Importantly, the HR-to-ceiling measure affords a detrending of the HR while preventing confounds of comparisons between individuals and different contexts and thus equips with an analytical tool that goes beyond crude averaging of HRs.

While an average HR of a resting mouse is approximately 550 and 620 bpm, HR values measured in the initial phase of all recordings range between 700 and 750 bpm (Kass, Hare, and Georgakopoulos 1998). Connecting the animal to the acquisition system just before the start of the experiment is a highly stressful intervention that presumably leads to stark sympathetic activation and thus a steady increase of HR. Nonetheless, as handling periods in later phases of the session did not have the same sustained effects, the handling can not be the only factor. The transport of the animal into the experimental room and the first confrontation with the unfamiliar, new context could have an additional influence leading to more drastic sympathetic innervation. In line with that, repeated exposure to novel environments has been shown to have a habituation effect, which become apparent by decreasing time periods of highly invariable HRs (Liu et al. 2013).

The overall increase of HR is counteracted by increasing amplitudes of bradycardia in high threat contexts. The observation that cardiac responses as a proxy for autonomic responses are opposed between early and late periods, although behavioral responses appear similar from start

to end of the recording, suggests a marked discrimination between defensive states influenced by the overriding rigidity macrostate, which conceptualizes the lower theoretical boundary of the HR. Moreover, while the ceiling macrostate is thought of as being restricted to a maximal level by purely physiological processes influenced by bodily functions, the rigidity macrostate depends dynamically on behavioral-cardiac interactions. Freezing bouts act differently on the bradycardia amplitude depending on the rigidity macrostate. Conceptually, this can be thought of as a command signal, modulated in an on-or-off fashion, which causes gradually different HR amplitudes depending on the momentary rigidity. As a result, this leads to a time-dependent gain of bradycardia amplitude. Similar to the theory of the baroreflex reset that describes a shift of the baroreflex curve in dependence of the state (i.e. during exercise or stress), the rigidity macrostate could be thought of as being modulated by central command centers in the brain shifting the operating range depending on the (internal) state of the animal (Dampney 2017). At the beginning of the trial, the responsiveness to the same command signal is low and then successively increases throughout the session resulting in gradually increasing bradycardia amplitudes at later time points. Importantly, during CD2, freezing microstates, which can be induced by threatening cues or the context are tightly correlated with bradycardic dips, becoming highly pronounced in later recording phases, when rigidity is low, but are also visible in early phases. Macroscopically this HR development can be described as an increased 'HRV' throughout the recording. Increasing HRV can also be seen in non-threat contexts as for example in animals recorded in their homecage in absence of any threat. Presumably a sudden increase in sympathetic activity triggered by the handling procedure leads to the strong rigidity at the beginning of the recording in both settings. However, the dynamics differ considerably in that rigidity-dependent bradycardia amplitudes in high threat contexts are clearly associated with a tight correlation of freezing bouts and long bradycardic events, while fluctuations of HRV in non-threat contexts are much higher and decreases in the HR are not only associated with freezing bouts. This difference in HR dynamics suggests two different underlying mechanisms. Presumably, a constantly high parasympathetic tone is responsible for the non-threat associated HRV. A critical question here is, what the decreasing rigidity macrostate in fear contexts is driven by then. Cardiac function is antagonistically controlled by sympathetic and parasympathetic activity. While sympathetic activity causes an increase in HR, parasympathetic activity, i.e. by vagus nerve activity slows the heart down. However, the interaction between the two systems is more complex (Silvani et al. 2016). Increased HR during sympathetic stimulation is attenuated the higher the concomitant background vagal tone is and the decrease of HR during vagal stimulation is potentiated the higher the sympathetic tone is, a concept that is described as an 'accentuated antagonism' (Levy 1971). Moreover, freezing-

associated bradycardia has been explained by a 'parasympathetic brake' being active (Roelofs 2017). A parasympathetic activation on the overall highly active sympathetic tone that, importantly, slowly builds up throughout the recording and thus creates progressive increase in the accentuated antagonism, could explain the gradually increasing bradycardia amplitudes. Additionally, rather slow rigidity kinetics suggest the involvement of endocrine processes.

Generally, several other factors seem to contribute to what is perceived as an 'HRV'. Next to the recording time- and threat dependent influences on the rigidity, the varying length of freezing bouts was also shown to have a considerable impact on the bradycardia's amplitude. The longer the freezing bout, the higher the bradycardia was during CD2. The more rigid HR development during the second half of CD2 when compared to CD1 could be thus explained by the variation in the shorter bout duration of freezing episodes during the second half of the recording in CD2. Furthermore, like the temporal dynamics explained above, also the environment can be defined as an overriding macrostate influencing cardio-behavioral microstates. Cardiac responses were shown to be highly dependent on the context the animals are confronted with. A ranking of freezing associated HR-to-ceiling values reflected the threat levels of the respective contexts. This crucially highlights again the fact that freezing is not reflecting a homogenously occurring behavior and that concomitant cardiac activity derived from moment-to-moment HRs can inform about actually distinct threat-dependent states. As mentioned above, handling the animal crucially affects their defensive state. Again, the cardiac aspect of the defensive state diverges in relation to the context, the animal is confronted with. While handling during the session evoked an immediate time-locked increase in HR in the homecage, the same procedure conducted in a new, unfamiliar context, led to a less pronounced tachycardic response that was temporally shifted. The rigidity macrostate differed in the new context and the homecage. The rigidity decreased faster in the homecage than the new context, leading to a more restrained HR in the new context. A similar phenomenon was observed during the retrieval sessions that were compared between the two contexts.

As opposed to the long-term slow changing macrostates, microstates describe second-to-second cardio-behavioral responses (i.e. freezing-bradycardia microstate). The cardiac component of the defensive microstates is influenced by the momentary displayed behavior, but do not simply follow the overall activity of the animal at the same time. Decisively, locomotion associated average cardiac responses were shown to range in between freezing-associated responses and HR changes during other steady behaviors as stretch-attend posture or rearing. It can be concluded that changing HRs during fear states and different behavioral activities depending on the coping style, i.e. freezing or flight, can not simply be explained by the physical need of the animal to adjust the blood flow. Furthermore, freezing can be associated with both, either

bradycardia or tachycardia highly depending on the experimental setting as shown with animals that underwent the retrieveal session of the CFP in their homecage (i.e. freezing-tachycardia microstate). As a consequence, the cardiac response during fear can be considered to be very dynamic and not associated per se with increasing or decreasing HR values. This goes in line with the notion that freezing is associated with a finely balanced co-activation of sympathetic and parasympathetic activation (Roelofs and Dayan 2022). It is well convceivable that when instead of binarizing freezing on a locomotion-based threshold only, defining different types of freezing that can depend on multiple factors (species-specificities, individual trait characteristics, time courses, environmental factors, etc.) will clarify the picture of freezing-associated HR changes further (Hagenaars, Oitzl, and Roelofs 2014).

Having speculated about putative external and internal mechanisms that could contribute to the described macrostates, the question about the biological relevance remains open. What is the evolutionary advantage of a decreased rigidity and thus increased immobility-associated bradycardic responses? Instead of associating fear-evoked immobility with a passive motor output, the concept of 'attentive' or 'active' freezing describes a preparatory state, by which perception is optimized and potential other motor actions are primed (Brandão et al. 2008; Merscher et al. 2022; Roelofs 2017; Rösler and Gamer 2019). It is well conceivable that a decreased HR during those freezing responses reduces internal noise and thus increases the awareness to the environment (Roelofs and Dayan 2022). Connected to that, the impact of interoceptive signaling, by which the brain is informed about the body state, needs to be considered. Rodent and human studies suggest that vagal nerve stimulation, during which an enhanced parasympathetic input form the body to the brain is mimicked, promotes extinction learning (Burger et al. 2016; Peña, Engineer, and McIntyre 2013). From these findings it can be concluded that – among other factors – a decreased HR evokes a reduction in the fear level. Similarly, in the context of this thesis, increasing bradycardia amplitudes could serve as an internal strategy for "emotion regulation" (Klein et al. 2021; Zych and Gogolla 2021). However, while the former deliberations could be a potential explanation for the high bradycardia amplitudes during later recording phases, they do not explain the time-dependent development of rigidity. Another implication of a decreasing rigidity could be simply the physiological need to counteract an extremely high sympathetic state, which can be sustained for a limited period only. By introducing periods of increasingly pronounced HR decelerations, the physiological state is lowered and thus contributes to a balanced homeodynamics.

In neuroscience, the term ‘state’ has been frequently used in the recent years to describe various manifestations of dynamic behavioral readouts (Fustiñana et al. 2021; Gründemann et al. 2019; Lee et al. 2020; Xu et al. 2020). Here, two conceptual approaches are suggested, in order to allow for more fine gradations of defensive states and to enrich the descriptive toolbox to characterize those states. Firstly, including physiological readouts as well as other ‘static’ parameters like context allows for fine distinctions of otherwise seemingly identical behavioral manifestations. Secondly, an integration of dynamical changes on different timescales, i.e. transient micro- and long lasting macrostates is key for the identification of different defensive states. In line with that, instead of binarizing behavior into freezing and non-freezing periods, their dynamic change in bout duration over time should be incorporated into the behavioral analysis. Finally, this approach will proof its applicability by attributing neuronal activity to the identified defensive states and by this potentially refine the characterization of underlying brain circuitries.

4.2 Role of different PAG circuit elements

The PAG, an evolutionary conserved brain structure located in the midbrain, was shown to play an important role in mediating defensive reactions in multiple studies (Hunsperger 1956; Motta, Carobrez, and Canteras 2017b; Tovote et al. 2016). Based on lesion and pharmacological studies, the PAG has been divided into columns with ventral regions associated with passive threat responses and dorsal regions with active coping styles during fear (Bandler et al. 2000; Carrive 1993; Depaulis et al. 1992). Both, in animals and humans, PAG activity was shown to modulate autonomic nervous system activity (Green et al. 2010; Walker and Carrive 2003). Thus, here, next to behavioral changes, also autonomic parameters involved in the defense reaction were used to describe the involvement of the PAG in defensive reactions.

By targeting specific circuit elements instead of manipulating entire brain regions, this thesis aimed in the identification of microstate generators in the PAG. The optical activation experiments on glutamatergic vlPAG neurons conducted in this thesis revealed heterogeneous, light-intensity dependent effects on both the behavioral and the cardiac aspect of the defensive state. While in previous studies in particular glutamatergic neuronal activity in the vlPAG was shown to be associated with marked freezing responses, here, a gradual behavioral switch from freezing to active flight responses depending on the stimulation intensity was observed during optical activation (Tovote et al. 2016). Furthermore, a flight response evoked by stimulation of the vlPAG is in contrast to the behavioral readouts associated with the aforementioned,

proposed columnar organization of the PAG (Bandler et al. 2000). Nonetheless, there are also studies reporting results that deviate from this dichomoty of vl and dlPAG. Assareh et al. have reported that defensive behaviors during nonspecific stimulation of vl and lPAG neurons scaled with light intensity, similarly to the results observed here (Assareh et al. 2016). Furthermore, electrical recordings of identified glutamatergic neurons in the vlPAG were also partly shown to be negatively correlated with freezing (Tovote et al. 2016). Those findings challenge the suggested strict columnar pattern and their associated defensive responses in the PAG. Nonetheless, it should be noted that several other (technical) reasons could account for the observed behavioral effects here. These will be elucidated below (see 4.3).

Cardiac responses during optical vlPAG stimulation of glutamatergic neurons evoked a deceleration of the HR, independent of the behavioral component being a freezing or flight response. While pharmacological activation of dPAG in anesthesized rats was shown to increase respiratory frequency and HR, caudal vlPAG excitation in cats led to decreases in HR and blood pressure (Carrive and Bandler 1991; Huang et al. 2000). Furthermore, vlPAG inhibition suppressed bradycardic responses during innate responses to white noise exposure (Koba et al. 2016). These reports are in line with the effects of vlPAG stimulation observed here. Both, decreases in the sympathetic tone by inhibition of the RVLM as well increases of the parasympathetic tone by monosynaptic projections to the NA has been proposed to explain these effects (Carrive and Bandler 1991; Farkas et al. 1997; Koba et al. 2016). Another aspect of the cardiac response observed during high intensity stimulation of glutamatergic vlPAG neurons was that the amplitudes of the bradycardia did not follow the expected gradual increase throughout the recording, but evaded the influence of the rigidity macrostate. These observations were unexpected and as the concurrent occurrence of flight bouts and bradycardia was not observed in naturally behaving animals, it was concluded that the stimulated neuronal population, even though restricted to excitatory glutamatergic neurons was still too heterogeneous. Decisively, the analysis of the integrated defensive reactions including also cardiac readouts during optical manipulations in the vlPAG allowed conclusions about the artificiality of the evoked response combinations. Implications to this extent would not have been possible, when evaluating only behavioral read-outs, assuring the adequacy of defining defensive reactions as integrated states.

A further restriction based on the neurons projection profile was established by making use of an intersectional viral approach. The vlPAG is known to densely project to the Mc, a brainstem region involved in motor control (Esposito et al. 2014; Tovote et al. 2016). It was expected that activation of those glutamatergic vlPAG neurons projecting to the Mc result in marked freezing responses as reported before (Tovote et al. 2016). Furthermore, this approach was hypothesized

to give more insight into the PAG's role in the mediation of the interacting cardiac and behavioral response by stimulation of presumably only locomotion associated vlPAG projections. However, stimulation of glutamatergic vlPAG-to-Mc neurons likewise evoked drastic flight responses concomitant with a decelerated HR phenotypically not leading to any refinement after stimulation of a more restricted cell population. Potential technical confounds of this experiments will be discussed below (see 4.3).

Another effect observed after specifically high stimulation intensity of glutamatergic vlPAG neurons was a pronounced post-stimulation freezing response. In line with that, vlPAG activity was shown to be associated with a so called 'poststress recovery' period. This describes an extended immobility phase of fear-conditioned animals after returning to a safe environment. Rats that returned to their homecage after context retrieval displayed reduced immobility rates after vlPAG blockade (Walker and Carrive 2003). The post-stimulation freezing could also point towards an aversive effect of the optogenetic stimulation of vlPAG glutamatergic neurons. During the RTPP test, the animals presented decreased latency times to escape the light-paired side after high intensity stimulation. In agreement with this observation, the involvement of the PAG in ascending pain perception has been described (Behbehani 1995; Lovick 2008). However, next to its nociceptive function, the PAG has a well-documented role in descending pain inhibition (Jones and Gebhart 1988; Reynolds 1969). Analgesia poses an important part of the defensive reaction during threat (Tovote et al. 2016). The tail immersion test conducted in this thesis revealed also an analgetic effect after stimulation of glutamatergic, but not other (sub)populations of vlPAG neurons.

Taking together, the heterogeneous results of optogenetic activation of glutamatergic neurons in the vlPAG in this thesis and in particular the evoked flight responses concomitant with drastic bradycardia during high intensity stimulations, a combination that has not been observed in non-perturbed, naturally behaving animals, suggests an overriding of naturally occurring defensive states by the concomitant activation of several glutamatergic subgroups, which are not active together naturally. As a consequence, the targeted neuronal population was restricted further to Chx10+ neurons, a subpopulation of glutamatergic neurons (Bouvier et al. 2015; Vaaga et al. 2020). Activation of Chx10+ neurons in the rostral medulla (Gi) projecting to the spinal cord was associated with an immediate arrest of ongoing locomotion, while inhibiting their synaptic output increased locomotion (Bouvier et al. 2015; Ferreira-Pinto et al. 2018). A study conducted by Vaaga et al. reported recently that optical activation of vlPAG Chx10+ neurons evoked an instant freezing response (Vaaga et al. 2020). In line with that, here, optical activation of Chx10+ neurons in the vlPAG evoked pronounced freezing responses and, importantly, concomitantly derived HRs revealed strong bradycardic responses. In order to

exclude similar light intensity scaling effects as during stimulation of the whole glutamatergic vlPAG stimulation, behavioral and cardiac effects were tested in dependence of different light intensities and frequencies. Even with high intensities of 7 mW (compare to 3.5 mW of high intensity glutamatergic stimulation), flight responses were never observed. Instead, freezing responses were evoked in a binary fashion after the light quantity reached a certain threshold. As the magnitude of light quantity increased with session time in an ascending order, increasing bradycardia amplitudes from the beginning to the end of the recording could not be certainly attributed to either increasing light intensities or the influence of the rigidity macrostate. However, repeated optical stimulation with constant stimulation properties revealed that stimulation-evoked bradycardic responses linearly increased over time from the first to the last stimulation. Similar dynamics of freezing-associated HRs between evoked and spontaneous freezing bouts as well as this subordination to the rigidity macrostate suggests a common underlying mechanism between evoked and spontaneous freezing microstates and proposes that these neurons might be responsible for the mediation of freezing-bradycardia microstates. Additionally, loss-of-function experiments were conducted in order to not only proof sufficiency, but also necessity of this neuronal subgroup of neurons in the vlPAG (Wiegert et al. 2017). As inhibition of Chx10+ vlPAG neurons was hypothesized to inhibit freezing responses, animals underwent two days of conditioning of the conditioned flight paradigm and were then re-exposed to the conditioning context during optical inhibition experiments. While freezing levels significantly decreased during stimulation, cardiac responses showed only a tendency towards increased HR levels during stimulation. However, in this case, effects of a loss-of-function experiment, i.e. reduced freezing and less bradycardic dips are not to be expected as robust as during optoactivation. Effects can be mitigated as only a sufficiently high level of freezing and bradycardia at baseline can reveal reduced levels of such during optic inhibition. Additionally, highest freezing probabilities and thus greatest effect sizes between experimental and control group are expected at the beginning of the recording. However, rigidity is highest during the initial recording phase masking this effect. The results of the RTPP test of Chx10-Cre mice suggests at first glance an appetitive effect of optic stimulation of those neurons. Indeed, animals were observed to repetitively enter the compartment paired with stimulation. Nonetheless, data have to be interpreted carefully, as optical activation of Chx10+ vlPAG neurons evoked strong freezing responses and thus counteracted the potential drive of the mice to leave the compartment. By introducing a light pattern of 1 second on and 3 seconds off, it was aimed to diminish this effect. However, longer off periods could reduce this undesirable side effect even more. As described above, stimulation of Chx10+ neurons did not

evoke any analgetic effects during the tail immersion test, suggesting an exclusive involvement of VGlut+/Chx10- vlPAG neurons in anti-nociception during defensive reactions.

As opposed to the time-locked, robust effects of Chx10+ neurons, optical activation of inhibitory GABAergic neurons in the vlPAG revealed rather diffuse, general behavioral activations. In spite of that, generally effects during optic activation of those neurons were rather weak and should be interpreted only carefully. Possibly, optic activation of inhibitory neurons can not be sufficiently teased apart by conducting experiments in naïve animals. As performed for inhibitory experiments of Chx10+ vlPAG neurons or in previous studies, more robust effects are expected, if experimental animals are brought into a significant fear state beforehand by learned or innate cues to then aim in disrupting defensive states by optical manipulations (Tovote et al. 2016).

In conclusion, presumably during optical activation of all glutamatergic neurons, Chx10+ neurons were included, and thus led to the bradycardic response component during these experiments. However, the concomitant activation of other glutamatergic neurons on top overrode the expected freezing component of the defensive reaction. Decisively, even if artificial, the concurrent flight response and bradycardia during high stimulation of all glutamatergic vlPAG neurons strongly suggests that cardiac responses do not simply follow the behavioral component of the defensive state. However, the critical question of whether the PAG controls behavioral as well as cardiac output in a labelled-line fashion or if integration already happens at that level of the brainstem remains. The schematic includes the Chx10+ vlPAG population as freezing-bradycardia microstate generators into the defensive circuitry in the brainstem (Figure 22). The robust and highly reproducible, intensity-independent effects after optogenetic activation attributes an executive role to these neurons that project in a labeled line fashion to locomotor and cardiac output centers in the brainstem. Chx10+ neurons in the vlPAG projects to the Mc as shown by Vaaga et al. 2020 and putatively synapse again onto Chx10+ neurons in the Mc that were shown to mediate immobility responses via premotor locomotor networks in the spinal cord (Bouvier et al. 2015; Tovote et al. 2016; Vaaga et al. 2020). As the behavioral and cardiac responses were always evoked concomitantly, vlPAG-to-Mc Chx10+ neurons most likely form at the same time collaterals to cardiac centers as the DVC. From there vagal information are passed to the NA which, in turn, forms preganglionic fibers that travel via the vagus nerve to the heart to eventually mediate a deceleration of the heart rate. Alternatively, it is also conceivable that vlPAG Chx10+ neurons target the NA to exert the same effects on cardiac function directly. Vl/lPAG neurons were shown to project directly to the NA previously (Farkas et al. 1997). Furthermore, in this thesis anterograde tracings of glutamatergic vlPAG neurons confirmed the excitatory identity of those cells. In summary, vlPAG Chx10+

neurons mediate the freezing-bradycardia microstate most likely in a labeled line like fashion by innervating locomotor and cardiac output centers through collaterals.

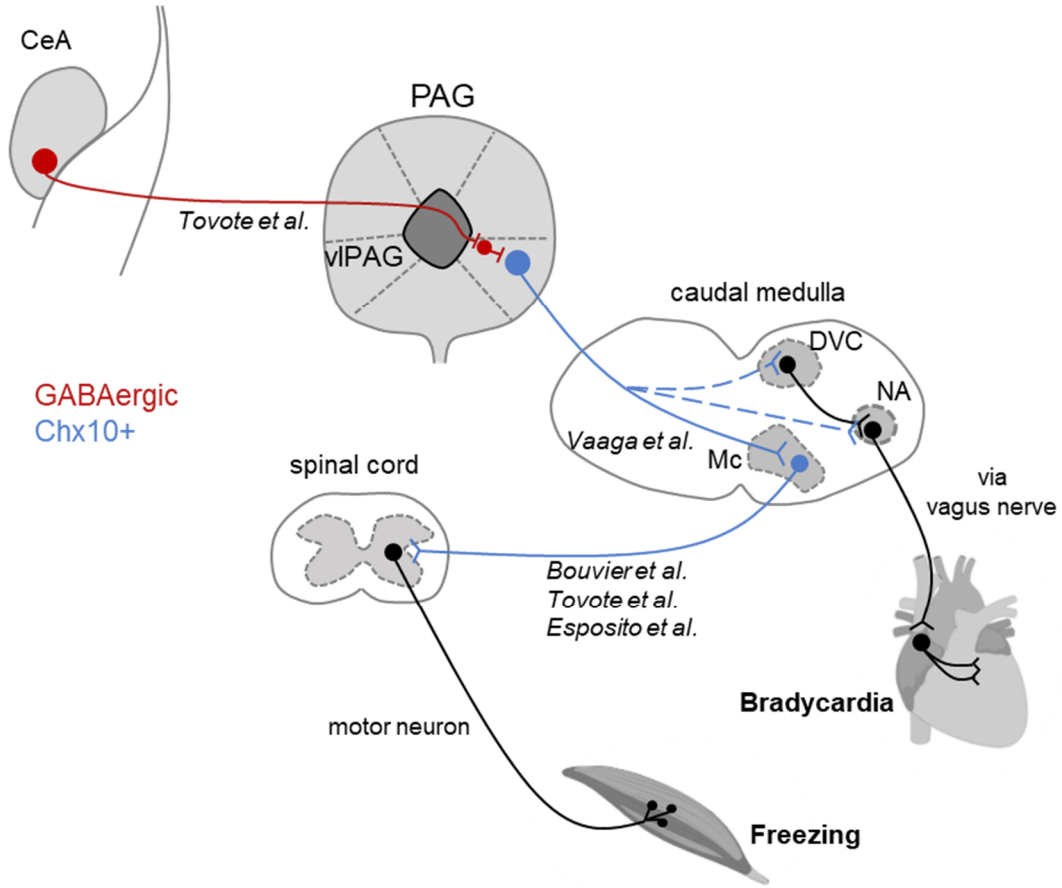

Figure 22 - Chx10+ neurons as freezing-bradycardia microstate generator.
Chx10+ neurons are putatively controlled by the disinhibitory circuitry via a GABAergic long-range projecting neuron for the CeA projecting to a local GABAergic interneuron in the vlPAG. vlPAG Chx10+ neurons project to premotor networks in the Mc, which in turn connect to the spinal cord to eventually mediate a freezing response. vlPAG Chx10+ neurons are suggested to form collaterals to the DVC. From there preganglionic parasympathetic neurons mediate a bradycardic response via the vagus nerve innervating cholinergic, postganglionic neurons. A direct projection of vlPAG Chx10+ neurons to the NA is conceivable, too. Heart and muscle icon adapted from BioRender.

4.3 Limitations of optogenetic experiments

Optogenetics has become an indispensable tool not only in neuroscience, but also in other life sciences, which enables to manipulate activity of molecularly and spatially defined cells upon illumination in a temporally precise manner (Fenno, Yizhar, and Deisseroth 2011; Tye and Deisseroth 2012; Yizhar et al. 2011). Nonetheless, this methodology brings certain limitations and potential confounds with it (Baleisyte, Schneggenburger, and Kochubey 2022; Headley et al. 2019; Owen, Liu, and Kreitzer 2019). A general caveat of perturbational approaches targeting certain elements of brain circuitries is the evocation of imbalanced network function by overriding the natural occurring activity of those elements (Headley et al. 2019).

In the following, technical confounds during optogenetic experiments will be discussed. Importantly, the applied frequency of light pulses should meet the natural firing pattern of the targeted neuronal population as well as the opsins' optimal response. Applied higher frequencies and thus accumulated higher light quantities could led the cells enter a depolarization block and light could lead to an inhibitory effects (Herman et al. 2014). In this thesis, in a screening session it was accounted for this fact by testing different light frequencies and intensities. Indeed, a strong light intensity-dependent effect could be observed in *VGlut2-IRES-Cre* animals. As discussed above, high light intensities evoked an artificial, non-natural response, which suggests that a targeting of a whole neuronal population just restricted by brain area might not be expedient. Another potential confound of optogenetic experiments is the heating of the brain tissue by sustained light exposure. This effect was shown to suppress firing rates and thus leading to incalculable network effects (Owen et al. 2019). However, applied light intensities in high intensity optical activations in *VGlut2-IRES-Cre* mice, were comparably low (3.5 mW), falling by far behind usual applied light intensities and thus can be excluded to affect these experiments. Nevertheless, this issue could likewise affect the loss-of-function experiments of *Chx10-Cre* animals, as high intensities were applied throughout 20 seconds. Importantly, control animals, expressing only a fluorescent protein, did not show any light-associated effects.

A main confound of the optical activation of VGlut2+ neurons was the imprecise vlPAG targeting, as virus leaked to more dorsal regions of the PAG. The activity of dorsal PAG regions are associated with flight response, hypervigilance, and tachycardia (Carrive 1993). Concurrent activation of dorsal PAG regions resulting in active flight responses and ventral regions evoking concomitantly a bradycardic response could explain the response combination observed in those experiments. Additional evidence for a partial dPAG stimulation comes from a study that confirmed an aversion behavior evoked by activation of unidentified dPAG neurons tested in a RTPP assay (Deng et al. 2016). This aversion behavior was comparable to the stimulation effects observed during the RTPP test performed in this thesis. Next to a further molecular restriction of the targeted neurons, a second strategy to overcome this broad, imprecise activation, was to target those glutamatergic neurons, which presumably mediate a behavioral switch by projecting to executing brainstem targets, responsible for locomotion. Thus, the optogenetically targeted neurons were further restricted by introducing an intersectional strategy, which allowed the optical activation of solely those glutamatergic neurons that project to the Mc. The post-experimental histological evaluation confirmed a restricted vlPAG expression pattern, which barely leaked into dorsal portions of the PAG. Regardless, optical activation evoked, similar to activation of all vlPAG glutamatergic neurons to locomotion bouts

and drastic bradycardia. Again, this result stood in contrast to Tovote et al., where freezing behavior during stimulation of glutamatergic vlPAG-to-Mc projecting neurons was shown (Tovote et al. 2016). Another confound next to the choice of the opsin could be the comparability of different constructs that include various promoter sequences as well as different vectors to deliver the plasmids. Different AAV serotypes exhibit various affinities with different neuronal subpopulations, which could result in a distinct preferential targeting of cells and thus could prevent comparability of similar experimental approaches to some extent. Moreover, in Tovote et al., a herpes simplex virus instead of a retrogradely transported AAV was used for the intersectional optogenetic approach, in which glutamatergic vlPAG-to-Mc neurons were targeted. Similarly, this differential use of viral vectors could pose a potential caveat by diverse preferential targeting of molecularly defined subtypes. Another adjacent PAG brain region involved in motor control that could have been unintentionally included in the targeted area, is the mesencephalic locomotor region (MLR). Glutamatergic neurons of both subdivisions of the MLR (cuneiform and pedunculopontine nucleus) project to the Mc and promote locomotion (Caggiano et al. 2018; Capelli et al. 2017). Particularly the cuneiform nucleus was reported to mediate escape locomotion (Caggiano et al. 2018). Importantly, electrical activation of the cuneiform nucleus in anesthesized rats has been shown to evoke bradycardia itself (Korte et al. 1992). Again it is conceivable that the concurrent stimulation of glutamatergic vlPAG and a subset of the MLR could have evoked bradycardia and locomotion, respectively.

In conclusion, using modern optogenetic tools opens a wide range of possibilities to understand brain function. Targeting precise circuit elements instead of manipulating whole brain regions can reveal evermore specific causal relationships between brain activity and fear states. However, manipulating single elements of wide brain circuitries and thus affecting whole brain dynamics could lead to unforeseeable, complex network effects. Moreover, imprecise targeting as well as applying inappropriate frequencies or light powers are potential caveats of perturbational, optogenetic experiments.

4.4 The role of the PAG in the defensive circuitry

The PAG has evolved already in the reptilian brain and is thus an evolutionary conserved brain structure (Silva and McNaughton 2019). It developed after the formation of medullary structures responsible for basic bodily functions and homeodynamics. The PAG thus constitutes an intermediate brain level between higher order cortical regions and lower parts of the brainstem and for the first time took over modulatory tasks. A central question here is, if the PAG still acts as a pure premotor-center by merely executing commands from higher order brain structures or instead as an integration center or threat probability estimator itself. The widely accepted fear circuit involves the amygdala as the main threat probability estimator, which sends information about the size of the threat to the PAG, which in turn commands lower brainstem structures to execute a certain bodily response (Fadok et al. 2018; LeDoux 2000; Tovote et al. 2016). This view identifies the PAG as a network element of fear output. Experiments conducted in this thesis revealed that optical activation of Chx10+ vlPAG neurons during the white noise component of fear conditioned animals during the CFP overrode natural defensive sates consisting of a combination of flight and increased HR and instead evoked a pronounced freezing-bradycardia microstate, which could even diminish shock-associated jumps. This circumvention of any threat-induced responses suggests indeed rather a role as an executing brain region (Figure 22). Chx10+ vlPAG neurons could serve a microstate generator role by triggering stereotypical response patterns evoked by threatening stimuli. However, a different theory about the role of the PAG claims a more integrative function as a threat estimator (Reis et al. 2021; Walker et al. 2020; Wright and McDannald 2019). For example, accumulating evidence attributes a wide range of different defensive responses (escape, freezing, risk-assessment) to the dPAG, instead of confirming the dichotomy of active and passive coping styles evoked by activation of dl and vlPAG, respectively (Deng et al. 2016; Sukikara et al. 2010). Thus, increasing stimulation intensities and frequencies of CaMKII+ neurons in the dPAG evoked increased velocities and freezing probabilities at the same time (Deng et al. 2016). Moreover, recently, by using *in vivo* calcium imaging, the dPAG was reported to dynamically encode approach-avoidance states and to mediate responses related to both freezing and escape (Reis et al. 2021). A growing number of studies confirm that the PAG not only projects to downstream targets in the brainstem to transmit executing commands, but actively participates in fear learning via bottom-up projections to cortical regions (McNally, Johansen, and Blair 2011; Motta et al. 2017a; Yeh, Ozawa, and Johansen 2021). Additional evidence comes from a study that reported feedback information from the PAG to the LA and

thus a modulation of amygdala activity via vlPAG and dRaphe dopaminergic neurons (Groessl et al. 2018). These findings support the conceptual idea of the PAG as an integrator and moves away from defining this brain region serving mere input-output functions. Furthermore, single unit recordings in the vlPAG of rats revealed that neuronal activity onset reflected rather a threat probability, signaled by different tones associated to different probabilities of receiving a foot shock, than a specific fear output (Wright and McDannald 2019). The stimulation intensity-dependent, heterogeneous behavioral responses of glutamatergic vlPAG neurons observed in the results of this thesis argues for a similar threat estimator function of this midbrain structure. However, stimulation of Chx10+ neurons resulted in a very robust stereotypical output, which suggests the PAG's role being closer to an output function already getting integrated information. Nonetheless, the PAG is characterized by its heterogeneity with several topographic and molecular gradients throughout all three axes (Silva and McNaughton 2019). Thus, it is conceivable that the PAG serves both integrator and output functions simultaneously with different subpopulations serving different executive or integrative tasks, respectively. A prerequisite for this would be an extensive intra-PAG connectivity. In fact, except for the dlPAG, all parts of the PAG receive information from the other subdivisions (Silva and McNaughton 2019). Furthermore, pronounced interconnectivity of all PAG columns are hypothesized to build an intrinsic PAG network that reciprocally inhibits output neurons of the respective opposed column to guarantee defensive state switches (Jansen et al. 1998). As described in Tovote et al., due to the local topography in the ventral portion of the PAG (Tovote et al. 2016), Chx10+ neurons could be hypothesized to communicate with an overlying GABA population (disinhibitory circuit). Another network layer could include probability estimator neurons that broadcast through dense intra-PAG connectivity to the output neurons in the PAG. The results presented in this thesis confirmed a pronounced bradycardia during optic vlPAG activation of glutamatergic neurons. As this cardiac response was evident during both, low (freezing response) and high (flight response) intensity activation, an indirect cardiac effect resulting from the momentary presented behavior is unlikely. Rather, a direct functional connectivity from the PAG to central command centers in the brainstem regulating cardiac function is evident. In fact, electrical as well as chemical stimulation of the vlPAG are not only known to provoke bradycardia, but also were shown to facilitate the baroreceptor reflex in anesthesized rats (Inui, Murase, and Nosaka 1994). In line with that, the vlPAG targets the DMV and the NA in the medulla, regions that encompass cardiac parasympathetic preganglionic neurons (Farkas et al. 1997). By adding molecular specificity, results presented in this thesis confirmed that vlPAG neurons projecting to these regions are of glutamatergic identity. Furthermore, glutamatergic projections of the PAG to pre-motor centers in the medulla

have been confirmed in this thesis and has been described as the canonical 'freezing pathway' before (Tovote et al. 2016). Additional intersectional optogenetic experiments, in which only glutamatergic vlPAG neurons that project to the Mc were targeted revealed likewise bradycardic responses. As also here secondary cardiac effects resulting from locomotion are unlikely, these results suggest rather a vlPAG output population that build collaterals sending information concurrently to pre-motor and cardiac centers instead of non-overlapping neuronal PAG clusters target preferentially one or the other brain center (Figure 22). Additional intersectional observational as well as perturbational approaches, in which molecular and projection specificity are established, will elucidate the underlying brain circuitries responsible for the mediation of defensive states. In particular, a characterization of the input/output connectivity of Chx10+ vlPAG population is needed to understand better its role. Similar restrictions of manipulated Chx10+ neurons based on their projection profile as preformed for all glutamatergic neurons will clarify the brain network underlying fear and anxiety.

4.5 Conclusion and Outlook

This thesis aimed in characterizing defensive reactions in response to threat. Next to behavioral read-outs, mainly cardiac measures were used to describe integrated defensive states. Importantly, HR does not simply follow changes in behavioral activity, but cardiac responses in threat situations underlie constantly changing adaptations, which, when incorporated into an integrated analysis together with other readouts, allows a more fine-grained description of defensive states. The novel framework presented incorporated these dynamics of cardio-behavioral adaptations and, by this, dissociates from defining fear based purely on behavioral responses (i.e. freezing). Importantly short- as well as long-lasting cardiovascular changes were conceptualized as interacting micro- and macrostates. Also tail temperatures were measured but only partially included into the description of microstates due to its inherently sluggish dynamics. Nonetheless, on a macrostate level, further analytical efforts of temperature information could potentially refine the description of defensive states. Furthermore, the inclusion of several other physiological read-outs, as for example respiration rate or blood pressure, would unravel further gradations between two seemingly identical defensive states. Hypothetically the more read-outs used, the more precise the characterization of threat-evoked states will be. In order to make sense of the growing amount of data points, an unbiased clustering approach could aid the identification of otherwise hidden states. Furthermore, this

approach will allow an allocation of individuals to subclusters and could identify potentially even pathological states.

In a second step, neuronal correlates associated with previously characterized defensive states were identified by conducting perturbational experiments via optogenetic manipulations. A subpopulation of glutamatergic neurons in the vlPAG, Chx10+ neurons, putatively acting in a labeled-line fashion, have been identified as generators for freezing-bradycardia microstates, which resembles the natural threat-related immobility. However, purely descriptive methods as *in vivo* calcium imaging might be more expedient in attributing neuronal correlates to distinct integrated defensive states. As described above optogenetic methods can generate unwanted artefacts. Observing i.e. the activity of vlPAG Chx10+ neurons in animals that are brought into defensive states via both, innate or learned paradigms and, in a second step, correlate this activity to multifactorial description of displayed output measures will reveal further information about the natural function of this cell population.

Importantly, defensive states do also involve modulation by interoceptive processes, i.e. bodily information that are sent to the central nervous system. Especially feedback of the cardiac state has been shown to play an important role in regulating fear and anxiety states (Garfinkel and Critchley 2016; Klein et al. 2021). Consequently, manipulations of interoceptive signals are expected to alter defensive states. In a first step, effects of those manipulations, i.e. via cardiac optogenetics on defensive states on different timescales would give valuable insight into how cardiac responses can affect emotional processing. The PAG poses a promising brain region to integrate bodily feedback information to modulate ultimately defensive responses. Therefore, observational studies of identified subgroups of neurons in the PAG in combination with manipulations of interoceptive information will elucidate how their integration into fear-related brain circuits is achieved on a neuronal level.

5. References

Anderson, D. J. and R. Adolphs. 2014. “A Framework for Studying Emotions across Species.” *Cell* 157(1):187–200.

Assareh, Neda, Mahsa Sarrami, Pascal Carrive, and Gavan P. McNally. 2016. “The Organization of Defensive Behavior Elicited by Optogenetic Excitation of Rat Lateral or Ventrolateral Periaqueductal Gray.” *Behavioral Neuroscience* 130(4):406–14.

Baleisyte, Aiste, Ralf Schneggenburger, and Olexiy Kochubey. 2022. “Stimulation of Medial Amygdala GABA Neurons with Kinetically Different Channelrhodopsins Yields Opposite Behavioral Outcomes.” *Cell Reports* 39(8):110850.

Bandler, Richard. 1982. “Induction of ‘page’ Following Microinjections of Glutamate into Midbrain but Not Hypothalamus of Cats.” *Neuroscience Letters* 30(2):183–88.

Bandler, Richard and Pascal Carrive. 1988. “Integrated Defence Reaction Elicited by Excitatory Amino Acid Microinjection in the Midbrain Periaqueductal Grey Region of the Unrestrained Cat.” *Brain Research* 439(1–2):95–106.

Bandler, Richard, Pascal Carrive, and Shi Ping Zhang. 1991. “Integration of Somatic and Autonomic Reactions within the Midbrain Periaqueductal Grey: Viscerotopic, Somatotopic and Functional Organization.” *Progress in Brain Research* 87(C):269–305.

Bandler, Richard and Antoine Depaulis. 1988. “Elicitation of Intraspecific Defence Reactions in the Rat from Midbrain Periaqueductal Grey by Microinjection of Kainic Acid, without Neurotoxic Effects.” *Neuroscience Letters* 88(3):291–96.

Bandler, Richard, Kevin A. Keay, Nicole Floyd, and Joseph Price. 2000. “Central Circuits Mediating Patterned Autonomic Activity during Active vs. Passive Emotional Coping.” *Brain Research Bulletin* 53(1):95–104.

Bandler, Richard and Michael T. Shipley. 1994. “Columnar Organization in the Midbrain Periaqueductal Gray: Modules for Emotional Expression?” *Trends in Neurosciences* 17(9):379–89.

Bandler, Richard and Istvan Tork. 1987. “Midbrain Periaqueductal Grey Region in the Cat Has Afferent and Efferent Connections with Solitary Tract Nuclei.” *Neuroscience Letters* 74(1):1–6.

Barbaresi, Paolo. 2006. “GABA-Immunoreactive Neurons and Terminals in the Cat Periaqueductal Gray Matter: A Light and Electron Microscopic Study.” *Journal of Neurocytology* 34(6):471–87.

Behbehani, M. M. 1995. “Functional Characteristics of the Midbrain Periaqueductal Gray.” *Prog Neurobiol* 46(6):575–605.

Behbehani, M. M., M. R. Jiang, S. D. Chandler, and M. Ennis. 1990. “The Effect of GABA and Its Antagonists on Midbrain Periaqueductal Gray Neurons in the Rat.” *Pain* 40(2):195–204.

Benarroch, Eduardo E. 2012. “Periaqueductal Gray: An Interface for Behavioral Control.” *Neurology* 78(3):210–17.

Bittencourt, A. S., E. M. Nakamura-Palacios, H. Mauad, S. Tufik, and L. C. Schenberg. 2005. “Organization of Electrically and Chemically Evoked Defensive Behaviors within the Deeper Collicular Layers as Compared to the Periaqueductal Gray Matter of the Rat.” *Neuroscience* 133(4):873–92.

Blanchard, D. C., G. Griebel, R. Pobbe, and R. J. Blanchard. 2011. “Risk Assessment as an Evolved Threat Detection and Analysis Process.” *Neurosci Biobehav Rev* 35(4):991–98.

Blanchard, R. J., K. J. Flannelly, and D. C. Blanchard. 1986. “Defensive Behavior of Laboratory and Wild Rattus Norvegicus.” *Journal of Comparative Psychology (Washington, D.C. : 1983)* 100(2):101–7.

Blanchard, Robert J. and D. Caroline Blanchard. 1989. “Attack and Defense in Rodents as Ethoexperimental Models for the Study of Emotion.” *Progress in Neuropsychopharmacology and Biological Psychiatry* 13(SUPPL. 1).

Blanchard, Robert J. and D. Caroline Blanchard. 1990. “Anti-Predator Defense as Models of Animal Fear and Anxiety.” Pp. 89–108 in *Fear and defence.*, *Ettore Majorana international life sciences series, Vol. 8.* Amsterdam, Netherlands: Harwood Academic Publishers.

Blanchard, Robert J., D. Caroline Blanchard, and Kevin Hori. 1989. “An Ethoexperimental Approach to the Study of Defense.” Pp. 114–36 in *Ethoexperimental approaches to the study of behavior.*, *NATO Advanced Science*

Institutes series. Series D: Behavioural and social sciences, Vol. 48. New York, NY, US: Kluwer Academic/Plenum Publishers.

Blanchard, Robert J., D. Caroline Blanchard, Scott M. Weiss, and Scott Meyer. 1990. "The Effects of Ethanol and Diazepam on Reactions to Predatory Odors." *Pharmacology, Biochemistry and Behavior* 35(4):775–80.

Blomqvist, A. and A. D. Craig. 1991. "Organization of Spinal and Trigeminal Input to the PAG." Pp. 345–63 in *The Midbrain Periaqueductal Gray Matter: Functional, Anatomical, and Neurochemical Organization*, edited by A. Depaulis and R. Bandler. Boston, MA: Springer US.

Bouvier, Julien, Vittorio Caggiano, Roberto Leiras, Vanessa Caldeira, Carmelo Bellardita, Kira Balueva, Andrea Fuchs, and Ole Kiehn. 2015. "Descending Command Neurons in the Brainstem That Halt Locomotion." *Cell* 163(5):1191–1203.

Brandão, Marcus L., Janaína M. Zanoveli, Raquel C. Ruiz-Martinez, Luciana C. Oliveira, and Jesus Landeira-Fernandez. 2008. "Different Patterns of Freezing Behavior Organized in the Periaqueductal Gray of Rats: Association with Different Types of Anxiety." *Behavioural Brain Research* 188(1):1–13.

Burger, Andreas M., Bart Verkuil, Ilse Van Diest, Willem Van der Does, Julian F. Thayer, and Jos F. Brosschot. 2016. "The Effects of Transcutaneous Vagus Nerve Stimulation on Conditioned Fear Extinction in Humans." *Neurobiology of Learning and Memory* 132:49–56.

Caggiano, V., R. Leiras, H. Goñi-Erro, D. Masini, C. Bellardita, J. Bouvier, V. Caldeira, G. Fisone, and O. Kiehn. 2018. "Midbrain Circuits That Set Locomotor Speed and Gait Selection." *Nature*.

Canteras, Newton S. 2002. "The Medial Hypothalamic Defensive System: Hodological Organization and Functional Implications." *Pharmacology Biochemistry and Behavior* 71(3):481–91.

Capelli, Paolo, Chiara Pivetta, Maria Soledad Esposito, and Silvia Arber. 2017. "Locomotor Speed Control Circuits in the Caudal Brainstem." *Nature* 551(7680):373–77.

Carrive, P. 1993. "The Periaqueductal Gray and Defensive Behavior: Functional Representation and Neuronal Organization." *Behavioural Brain Research* 58(1–2):27–47.

Carrive, Pascal. 1991. "Functional Organization of PAG Neurons Controlling Regional Vascular Beds." *The Midbrain Periaqueductal Gray Matter* 67–100.

Carrive, Pascal and Richard Bandler. 1991. "Viscerotopic Organization of Neurons Subserving Hypotensive Reactions within the Midbrain Periaqueductal Grey: A Correlative Functional and Anatomical Study." *Brain Research* 541(2):206–15.

Chen, S. and G. Aston-Jones. 1996. "Extensive Projections from the Midbrain Periaqueductal Gray to the Caudal Ventrolateral Medulla: A Retrograde and Anterograde Tracing Study in the Rat." *Neuroscience* 71(2):443–59.

Chow, Brian Y., Xue Han, Allison S. Dobry, Xiaofeng Qian, Amy S. Chuong, Mingjie Li, Michael A. Henninger, Gabriel M. Belfort, Yingxi Lin, Patrick E. Monahan, and Edward S. Boyden. 2010. "High-Performance Genetically Targetable Optical Neural Silencing by Light-Driven Proton Pumps." *Nature* 463(7277):98–102.

Ciocchi, S., C. Herry, F. Grenier, S. B. Wolff, J. J. Letzkus, I. Vlachos, I. Ehrlich, R. Sprengel, K. Deisseroth, M. B. Stadler, C. Muller, and A. Luthi. 2010. "Encoding of Conditioned Fear in Central Amygdala Inhibitory Circuits." *Nature* 468(7321):277–82.

Clements, J. R., J. E. Madl, R. L. Johnson, A. A. Larson, and A. J. Beitz. 1987. "Localization of Glutamate, Glutaminase, Aspartate and Aspartate Aminotransferase in the Rat Midbrain Periaqueductal Gray." *Experimental Brain Research* 67(3):594–602.

Clovis, Yoanne M., So Yeon Seo, Ji sun Kwon, Jennifer C. Rhee, Sujeong Yeo, Jae W. Lee, Seunghee Lee, and Soo Kyung Lee. 2016. "Chx10 Consolidates V2a Interneuron Identity through Two Distinct Gene Repression Modes." *Cell Reports* 16(6):1642–52.

Crawley, Jacqueline and Frederick K. Goodwin. 1980. "Preliminary Report of a Simple Animal Behavior Model for the Anxiolytic Effects of Benzodiazepines." *Pharmacology Biochemistry and Behavior* 13(2):167–70.

Cregg, Jared M., Roberto Leiras, Alexia Montalant, Paulina Wanken, Ian R. Wickersham, and Ole Kiehn. 2020. "Brainstem Neurons That Command Mammalian Locomotor Asymmetries." *Nature Neuroscience* 23(6):730–40.

Critchley, H. D. and N. A. Harrison. 2013. "Visceral Influences on Brain and Behavior." *Neuron* 77(4):624–38.

Dampney, Roger A. L. 2016. "Central Neural Control of the Cardiovascular System: Current Perspectives."

Advances in Physiology Education 40(3):283–96.

Dampney, Roger A. L. 2017. "Resetting of the Baroreflex Control of Sympathetic Vasomotor Activity during Natural Behaviors: Description and Conceptual Model of Central Mechanisms." *Frontiers in Neuroscience* 11(AUG).

Denenberg, Victor H. 1969. "Open-Field Behavior in the Rat: What Does It Mean?" *Annals of the New York Academy of Sciences* 159(3 Experimental):852–59.

Deng, H., X. Xiao, and Z. Wang. 2016. "Periaqueductal Gray Neuronal Activities Underlie Different Aspects of Defensive Behaviors." *Journal of Neuroscience* 36(29).

Depaulis, Antoine, Kevin A. Keay, and Richard Bandler. 1992. "Longitudinal Neuronal Organization of Defensive Reactions in the Midbrain Periaqueductal Gray Region of the Rat." *Experimental Brain Research* 90(2):307–18.

Depaulis, Antoine, Kevin A. Keay, and Richard Bandler. 1994. "Quiescence and Hyporeactivity Evoked by Activation of Cell Bodies in the Ventrolateral Midbrain Periaqueductal Gray of the Rat." *Exp Brain Res* (1994):75–83.

Dielenberg, R. A., P. Carrive, and I. S. McGregor. 2001. "The Cardiovascular and Behavioral Response to Cat Odor in Rats: Unconditioned and Conditioned Effects." *Brain Research* 897(1–2):228–37.

Esposito, M. S., P. Capelli, and S. Arber. 2014. "Brainstem Nucleus MdV Mediates Skilled Forelimb Motor Tasks." *Nature* 508(7496):351–56.

Esteban Masferrer, Maria, Bianca A. Silva, Kensaku Nomoto, Susana Q. Lima, and Cornelius T. Gross. 2020. "Differential Encoding of Predator Fear in the Ventromedial Hypothalamus and Periaqueductal Grey." *The Journal of Neuroscience* 40(48):9283–92.

Evans, Dominic A., A. Vanessa Stempel, Ruben Vale, Sabine Ruehle, Yaara Lefler, and Tiago Branco. 2018. "A Synaptic Threshold Mechanism for Computing Escape Decisions." *Nature* 558(7711):590–94.

Fadok, Jonathan P., Sabine Krabbe, Milica Markovic, Julien Courtin, Chun Xu, Lema Massi, Paolo Botta, Kristine Bylund, Christian Müller, Aleksandar Kovacevic, Philip Tovote, and Andreas Lüthi. 2017. "A Competitive Inhibitory Circuit for Selection of Active and Passive Fear Responses." *Nature* 542(7639):96–100.

Fadok, Jonathan P., Milica Markovic, Philip Tovote, and Andreas Lüthi. 2018. "New Perspectives on Central Amygdala Function." *Current Opinion in Neurobiology* 49:141–47.

Fanselow, Michael S. 1991. "The Midbrain Periaqueductal Gray as a Coordinator of Action in Response to Fear and Anxiety" edited by A. Depaulis and R. Bandler. *The Midbrain Periaqueductal Gray Matter* 151–73.

Fanselow, Michael S. and Laurie S. Lester. 1988. "A Functional Behavioristic Approach to Aversively Motivated Behavior: Predatory Imminence as a Determinant of the Topography of Defensive Behavior." Pp. 185–212 in *Evolution and learning*. Hillsdale, NJ, US: Lawrence Erlbaum Associates, Inc.

Fanselow, Michael S. and Andrew M. Poulos. 2005. "The Neuroscience of Mammalian Associative Learning." *Annual Review of Psychology* 56:207–34.

Fardin, Véronique, Jean Louis Oliveras, and Jean Marie Besson. 1984. "A Reinvestigation of the Analgesic Effects Induced by Stimulation of the Periaqueductal Gray Matter in the Rat. I. The Production of Behavioral Side Effects Together with Analgesia." *Brain Research* 306(1–2):105–23.

Farkas, E., A. S. Jansen, and A. D. Loewy. 1997. "Periaqueductal Gray Matter Projection to Vagal Preganglionic Neurons and the Nucleus Tractus Solitarius." *Brain Res* 764(1–2):257–61.

Fenno, Lief, Ofer Yizhar, and Karl Deisseroth. 2011. "The Development and Application of Optogenetics." *Annual Review of Neuroscience* 34(1):389–412.

Ferreira-Pinto, Manuel J., Ludwig Ruder, Paolo Capelli, and Silvia Arber. 2018. "Connecting Circuits for Supraspinal Control of Locomotion." *Neuron* 100(2):361–74.

Floyd, Nicole S., Joseph L. Price, Amon T. Ferry, Kevin A. Keay, and Richard Bandler. 2000. "Orbitomedial Prefrontal Cortical Projections to Distinct Longitudinal Columns of the Periaqueductal Gray in the Rat." *Journal of Comparative Neurology* 422(4):556–78.

Fustiñana, Maria Sol, Tobias Eichlisberger, Tewis Bouwmeester, Yael Bitterman, and Andreas Lüthi. 2021. "State-Dependent Encoding of Exploratory Behaviour in the Amygdala." *Nature* 592(7853):267–71.

Garfinkel, S. N. and H. D. Critchley. 2016. "Threat and the Body: How the Heart Supports Fear Processing." *Trends Cogn Sci* 20(1):34–46.

Gentile, Christopher G., Theodore W. Jarrell, Alan Teich, Philip M. McCabe, and Neil Schneiderman. 1986. "The

Role of Amygdaloid Central Nucleus in the Retention of Differential Pavlovian Conditioning of Bradycardia in Rabbits." *Behavioural Brain Research* 20(3):263–73.

Gladwin, Thomas E., Mahur M. Hashemi, Vanessa van Ast, and Karin Roelofs. 2016. "Ready and Waiting: Freezing as Active Action Preparation under Threat." *Neuroscience Letters* 619:182–88.

Gomes, Felipe V., Alessandra M. Kakihata, Ana Carolina G. Semedo, Sara C. Hott, Daniela L. Uliana, Francisco S. Guimarães, and Leonardo B. M. Resstel. 2014. "D-Cycloserine Injected into the Dorsolateral Periaqueductal Gray Induces Anxiolytic-like Effects in Rats." *Behavioural Brain Research* 271:374–79.

Green, A. L., J. A. Hyam, C. Williams, S. Wang, D. Shlugman, J. F. Stein, D. J. Paterson, and T. Z. Aziz. 2010. "Intra-Operative Deep Brain Stimulation of the Periaqueductal Grey Matter Modulates Blood Pressure and Heart Rate Variability in Humans." *Neuromodulation* 13(3):174–81.

Groessl, Florian, Thomas Munsch, Susanne Meis, Johannes Griessner, Joanna Kaczanowska, Pinelopi Pliota, Dominic Kargl, Sylvia Badurek, Klaus Kraitsy, Arash Rassoulpour, Johannes Zuber, Volkmar Lessmann, and Wulf Haubensak. 2018. "Dorsal Tegmental Dopamine Neurons Gate Associative Learning of Fear." *Nature Neuroscience* 21(July).

Gross, C. T. and N. S. Canteras. 2012. "The Many Paths to Fear." *Nat Rev Neurosci* 13(9):651–58.

Gründemann, Jan, Yael Bitterman, Tingjia Lu, Sabine Krabbe, Benjamin F. Grewe, Mark J. Schnitzer, and Andreas Lüthi. 2019. "Amygdala Ensembles Encode Behavioral States." *Science* 364(6437).

Haery, Leila, Benjamin E. Deverman, Katherine S. Matho, Ali Cetin, Kenton Woodard, Connie Cepko, Karen I. Guerin, Meghan A. Rego, Ina Ersing, Susanna M. Bachle, Joanne Kamens, and Melina Fan. 2019. "Adeno-Associated Virus Technologies and Methods for Targeted Neuronal Manipulation." *Frontiers in Neuroanatomy* 13(November):1–16.

Hagenaars, Muriel A., Melly Oitzl, and Karin Roelofs. 2014. "Updating Freeze: Aligning Animal and Human Research." *Neuroscience and Biobehavioral Reviews* 47:165–76.

Han, Xue, Brian Y. Chow, Huihui Zhou, Nathan C. Klapoetke, Amy Chuong, Reza Rajimehr, Aimei Yang, Michael V. Baratta, Jonathan Winkle, Robert Desimone, and Edward S. Boyden. 2011. "A High-Light Sensitivity Optical Neural Silencer: Development and Application to Optogenetic Control of Non-Human Primate Cortex." *Frontiers in Systems Neuroscience* 5(APRIL 2011):1–8.

Hayashi, Marito, Christopher A. Hinckley, Shawn P. Driscoll, Niall J. Moore, Ariel J. Levine, Kathryn L. Hilde, Kamal Sharma, and Samuel L. Pfaff. 2018. "Graded Arrays of Spinal and Supraspinal V2a Interneuron Subtypes Underlie Forelimb and Hindlimb Motor Control." *Neuron* 97(4):869-884.e5.

Headley, Drew B., Vasiliki Kanta, Pinelopi Kyriazi, and Denis Paré. 2019. "Embracing Complexity in Defensive Networks." *Neuron*.

Henderson, L. .., K. .. Keay, and R. Bandler. 1998. "The Ventrolateral Periaqueductal Gray Projects to Caudal Brainstem Depressor Regions: A Functional-Anatomical and Physiological Study." *Neuroscience* 82(1):201–21.

Herbert, Horst and Clifford B. Saper. 1992. "Organization of Medullary Adrenergic and Noradrenergic Projections to the Periaqueductal Gray Matter in the Rat." *Journal of Comparative Neurology* 315(1):34–52.

Herman, Alexander M., Longwen Huang, Dona K. Murphey, Isabella Garcia, and Benjamin R. Arenkiel. 2014. "Cell Type-Specific and Time-Dependent Light Exposure Contribute to Silencing in Neurons Expressing Channelrhodopsin-2." *ELife* 3:1–18.

Hermans, Erno J., Marloes J. A. G. Henckens, Karin Roelofs, and Guillén Fernández. 2013. "Fear Bradycardia and Activation of the Human Periaqueductal Grey." *NeuroImage* 66:278–87.

Herry, C. and J. P. Johansen. 2014. "Encoding of Fear Learning and Memory in Distributed Neuronal Circuits." *Nat Neurosci* 17(12):1644–54.

Hersman, Sarah, David Allen, Mariko Hashimoto, Salvador Brito, and Todd E. Anthony. 2020. "Stimulus Salience Determines Defensive Behaviors Elicited by Aversively Conditioned Serial Compound Auditory Stimuli." *ELife* 9:1–26.

Huang, Zheng Gui, S. Hari Subramanian, Ron J. Balnave, A. Bulent Turman, and Chin Moi Chow. 2000. "Roles of Periaqueductal Gray and Nucleus Tractus Solitarius in Cardiorespiratory Function in the Rat Brainstem." *Respiration Physiology* 120(3):185–95.

Hunsperger, Robert W. 1956. "Affective reaction from electric stimulation of brain stem in cats." *Helvetica physiologica et pharmacologica acta* 14(1):70–92.

Inui, K., Sumio Murase, and Shoichiro Nosaka. 1994. “Facilitation of the Arterial Baroreflex by the Ventrolateral Part of the Midbrain Periaqueductal Grey Matter in Rats.” *The Journal of Physiology* 477(1):89–101.

Iwata, Jiro, Koichi Chida, and Joseph E. LeDoux. 1987. “Cardiovascular Responses Elicited by Stimulation of Neurons in the Central Amygdaloid Nucleus in Awake but Not Anesthetized Rats Resemble Conditioned Emotional Responses.” *Brain Research* 418(1):183–88.

Janak, Patricia H. and Kay M. Tye. 2015. “From Circuits to Behaviour in the Amygdala.” *Nature* 517(7534):284–92.

Jansen, Arthur S. P., Eszter Farkas, J. Mac Sams, and Arthur D. Loewy. 1998. “Local Connections between the Columns of the Periaqueductal Gray Matter: A Case for Intrinsic Neuromodulation.” *Brain Research* 784(1–2):329–36.

Jimenez, Stephanie A. and Stephen Maren. 2009. “Nuclear Disconnection within the Amygdala Reveals a Direct Pathway to Fear.” *Learning and Memory* 16(12):766–68.

Jones, S. L. and G. F. Gebhart. 1988. “Inhibition of Spinal Nociceptive Transmission from the Midbrain, Pons and Medulla in the Rat: Activation of Descending Inhibition by Morphine, Glutamate and Electrical Stimulation.” *Brain Research* 460(2):281–96.

Jürgens, U. 1994. “The Role of the Periaqueductal Grey in Vocal Behaviour.” *Behavioural Brain Research* 62(2):107–17.

Kass, D. A., J. M. Hare, and D. Georgakopoulos. 1998. “Murine Cardiac Function: A Cautionary Tail.” *Circulation Research* 82(4):519–22.

Kennedy, Ann, Prabhat S. Kunwar, Ling-yun Li, Stefanos Stagkourakis, Daniel A. Wagenaar, and David J. Anderson. 2020. “Stimulus-Specific Hypothalamic Encoding of a Persistent Defensive State.” *Nature* (October 2019).

Kincheski, G. C., S. R. Mota-Ortiz, E. Pavesi, N. S. Canteras, and A. P. Carobrez. 2012. “The Dorsolateral Periaqueductal Gray and Its Role in Mediating Fear Learning to Life Threatening Events.” *PLoS ONE* 7(11):50361.

Kingsbury, Marcy A., Aubrey M. Kelly, Sara E. Schrock, and James L. Goodson. 2011. “Mammal-like Organization of the Avian Midbrain Central Gray and a Reappraisal of the Intercollicular Nucleus.” *PLoS ONE* 6(6).

Klein, Alexandra S., Nate Dolensek, Caroline Weiand, and Nadine Gogolla. 2021. “Fear Balance Is Maintained by Bodily Feedback to the Insular Cortex in Mice.” *Science* 374(6570):1010–15.

Koba, Satoshi, Ichiro Hisatome, and Tatsuo Watanabe. 2019. “Augmented Fear Bradycardia in Rats with Heart Failure.” *Journal of Physiological Sciences* 69(6):875–83.

Koba, Satoshi, Ryo Inoue, and Tatsuo Watanabe. 2016. “Role Played by Periaqueductal Gray Neurons in Parasympathetically Mediated Fear Bradycardia in Conscious Rats.” *Physiological Reports* 4(12):1–13.

Korte, S. M., D. Jaarsma, P. G. M. Luiten, and B. Bohus. 1992. “Mesencephalic Cuneiform Nucleus and Its Ascending and Descending Projections Serve Stress-Related Cardiovascular Responses in the Rat.” *Journal of the Autonomic Nervous System* 41(1–2):157–76.

Krabbe, Sabine, Jan Gründemann, and Andreas Lüthi. 2018. “Amygdala Inhibitory Circuits Regulate Associative Fear Conditioning.” *Biological Psychiatry*.

Krause, Elischa, Christoph Benke, Julian Koenig, Julian F. Thayer, Alfons O. Hamm, and Christiane A. Pané-Farré. 2018. “Dynamics of Defensive Response Mobilization to Approaching External Versus Interoceptive Threat.” *Biological Psychiatry: Cognitive Neuroscience and Neuroimaging* 3(6):525–38.

Kunwar, Prabhat S., Moriel Zelikowsky, Ryan Remedios, Haijiang Cai, Melis Yilmaz, Markus Meister, and David J. Anderson. 2015. “Ventromedial Hypothalamic Neurons Control a Defensive Emotion State.” *ELife* 4.

La-Vu, Mimi Q., Ekayana Sethi, Sandra Maesta-Pereira, Peter J. Schuette, Brooke C. Tobias, Fernando MCV Reis, Weisheng Wang, Anita Torossian, Amy Bishop, Saskia J. Leonard, Lilly Lin, Catherine M. Cahill, and Avishek Adhikari. 2022. “Sparse Genetically Defined Neurons Refine the Canonical Role of Periaqueductal Gray Columnar Organization.” *ELife* 11:1–26.

La-vu, Mimi, Ekayana Sethi, Sandra Maesta-pereira, Peter J. Schuette, Brooke C. Tobias, Fernando M. C. V Reis, Weisheng Wang, Saskia J. Leonard, Lilly Lin, and Avishek Adhikari. 2022. “A Genetically-Defined Population in the Lateral and Ventrolateral Periaqueductal Gray Selectively Promotes Flight to Safety.”

Lammers, J. H. C. M., M. R. Kruk, W. Meelis, and A. M. van der Poel. 1988. “Hypothalamic Substrates for Brain

Stimulation-Induced Patterns of Locomotion and Escape Jumps in the Rat." *Brain Research* 449(1):294–310.

LeDoux, J. E. 2000. "Emotion Circuits in the Brain." *Annu Rev Neurosci* 23:155–84.

LeDoux, J. E., J. Iwata, P. Cicchetti, and D. J. Reis. 1988. "Different Projections of the Central Amygdaloid Nucleus Mediate Autonomic and Behavioral Correlates of Conditioned Fear." *J Neurosci* 8(7):2517–29.

LeDoux, Joseph. 2012. "Rethinking the Emotional Brain." *Neuron* 73(4):653–76.

Lee, Conrad C. Y., Ehsan Kheradpezhouh, Mathew E. Diamond, and Ehsan Arabzadeh. 2020. "State-Dependent Changes in Perception and Coding in the Mouse Somatosensory Cortex." *Cell Reports* 32(13):108197.

Levy, Matthew N. 1971. "Sympathetic-Parasympathetic Interactions in the Heart." *Circulation Research* 29(5):437–45.

Li, Yi, Jiawei Zeng, Juen Zhang, Chenyu Yue, Weixin Zhong, Zhixiang Liu, Qiru Feng, and Minmin Luo. 2018. "Hypothalamic Circuits for Predation and Evasion." *Neuron* 97(4):911-924.e5.

Lin, John Y., Per Magne Knutsen, Arnaud Muller, David Kleinfeld, and Roger Y. Tsien. 2013. "ReaChR: A Red-Shifted Variant of Channelrhodopsin Enables Deep Transcranial Optogenetic Excitation." *Nature Neuroscience* 16(10):1499–1508.

Liu, Jun, Wei Wei, Hui Kuang, Joe Z. Tsien, and Fang Zhao. 2014. "Heart Rate and Heart Rate Variability Assessment Identifies Individual Differences in Fear Response Magnitudes to Earthquake, Free Fall, and Air Puff in Mice." *PLoS ONE* 9(3).

Liu, Jun, Wei Wei, Hui Kuang, Fang Zhao, and Joe Z. Tsien. 2013. "Changes in Heart Rate Variability Are Associated with Expression of Short-Term and Long-Term Contextual and Cued Fear Memories." *PLoS ONE* 8(5):1–14.

Lonstein, Joseph S. and Judith M. Stern. 1997. "Role of the Midbrain Periaqueductal Gray in Maternal Nurturance and Aggression: C-Fos and Electrolytic Lesion Studies in Lactating Rats." *Journal of Neuroscience* 17(9):3364–78.

Lovick, T. A. 1992. "Inhibitory Modulation of the Cardiovascular Defence Response by the Ventrolateral Periaqueductal Grey Matter in Rats." *Experimental Brain Research* 89(1):133–39.

Lovick, T. A. 2008. "Pro-Nociceptive Action of Cholecystokinin in the Periaqueductal Grey: A Role in Neuropathic and Anxiety-Induced Hyperalgesic States." *Neuroscience and Biobehavioral Reviews* 32(4):852–62.

Löw, Andreas, Mathias Weymar, and Alfons O. Hamm. 2015. "When Threat Is Near, Get Out of Here: Dynamics of Defensive Behavior During Freezing and Active Avoidance." *Psychological Science* 26(11):1706–16.

Martinez, Raquel C. R., Eduardo F. Carvalho-Netto, Vanessa C. S. Amaral, Ricardo L. Nunes-de-Souza, and Newton S. Canteras. 2008. "Investigation of the Hypothalamic Defensive System in the Mouse." *Behavioural Brain Research* 192(2):185–90.

Mathis, Alexander, Pranav Mamidanna, Kevin M. Cury, Taiga Abe, Venkatesh N. Murthy, Mackenzie Weygandt Mathis, and Matthias Bethge. 2018. "DeepLabCut: Markerless Pose Estimation of User-Defined Body Parts with Deep Learning." *Nature Neuroscience* 21(9):1281–89.

McDougall, Alan, Roger Dampney, and Richard Bandler. 1985. "Cardiovascular Components of the Defence Reaction Evoked by Excitation of Neuronal Cell Bodies in the Midbrain Periaqueductal Grey of the Cat." *Neuroscience Letters* 60(1):69–75.

McGarry, Laura M. and Adam G. Carter. 2017. "Prefrontal Cortex Drives Distinct Projection Neurons in the Basolateral Amygdala." *Cell Reports* 21(6):1426–33.

McNally, G. P., J. P. Johansen, and H. T. Blair. 2011. "Placing Prediction into the Fear Circuit." *Trends Neurosci* 34(6):283–92.

Meller, S. T. and B. J. Dennis. 1991. "Efferent Projections of the Periaqueductal Gray in the Rabbit." *Neuroscience* 40(1):191–216.

Merscher, Alma Sophia, Philip Tovote, Paul Pauli, and Matthias Gamer. 2022. "Centralized Gaze as an Adaptive Component of Defensive States in Humans." *Proceedings of the Royal Society B: Biological Sciences* 289(1975).

Mobbs, Dean, Ralph Adolphs, Michael S. Fanselow, Lisa Feldman Barrett, Joseph E. LeDoux, Kerry Ressler, and Kay M. Tye. 2019. "Viewpoints: Approaches to Defining and Investigating Fear." *Nature Neuroscience* 22(8):1205–16.

Mobbs, Dean, Drew B. Headley, Weilun Ding, and Peter Dayan. 2020. “Space, Time, and Fear: Survival Computations along Defensive Circuits.” *Trends in Cognitive Sciences* 24(3):228–41.

Mobbs, Dean, Predrag Petrovic, Jennifer L. Marchant, Demis Hassabis, and Nikolaus Weiskopf. 2007. “When Fear Is Near :” *Science* 1119(August):1079–83.

Motta, Simone C., Antônio P. Carobrez, and Newton S. Canteras. 2017a. “The Periaqueductal Gray and Primal Emotional Processing Critical to Influence Complex Defensive Responses, Fear Learning and Reward Seeking.” *Neuroscience and Biobehavioral Reviews* 76:39–47.

Motta, Simone C., Antônio P. Carobrez, and Newton S. Canteras. 2017b. “The Periaqueductal Gray and Primal Emotional Processing Critical to Influence Complex Defensive Responses, Fear Learning and Reward Seeking.” *Neuroscience & Biobehavioral Reviews* 76:39–47.

Nath, Tanmay, Alexander Mathis, An Chi Chen, Amir Patel, Matthias Bethge, and Mackenzie Weygandt Mathis. 2019. “Using DeepLabCut for 3D Markerless Pose Estimation across Species and Behaviors.” *Nature Protocols* 14(7):2152–76.

Orlovsky, G. N., T. G. Deliagina, and S. Grillner. 1999. *Neuronal Control of Locomotion: From Mollusc to Man*. Oxford University Press.

Owen, Scott F., Max H. Liu, and Anatol C. Kreitzer. 2019. “Thermal Constraints on in Vivo Optogenetic Manipulations.” *Nature Neuroscience* 22(7):1061–65.

Pellow, Sharon, Philippe Chopin, Sandra E. File, and Mike Briley. 1985. “Validation of Open : Closed Arm Entries in an Elevated plus-Maze as a Measure of Anxiety in the Rat.” *Journal of Neuroscience Methods* 14(3):149–67.

Peña, David F., Navzer D. Engineer, and Christa K. McIntyre. 2013. “Rapid Remission of Conditioned Fear Expression with Extinction Training Paired with Vagus Nerve Stimulation.” *Biological Psychiatry* 73(11):1071–77.

Pereira, Talmo D., Joshua W. Shaevitz, and Mala Murthy. 2020. “Quantifying Behavior to Understand the Brain.” *Nature Neuroscience* 23(December):1–13.

Ramabadran, Krishnaswami, Mylarrao Bansinath, Herman Turndorf, and Margarita M. Puig. 1989. “Tail Immersion Test for the Evaluation of a Nociceptive Reaction in Mice. Methodological Considerations.” *Journal of Pharmacological Methods* 21(1):21–31.

Reichling, D. B. and A. I. Basbaum. 1991. “Collateralization of Periaqueductal Gray Neurons to Forebrain or Diencephalon and to the Medullary Nucleus Raphe Magnus in the Rat.” *Neuroscience* 42(1):183–200.

Reis, Fernando MCV, Johannes Y. Lee, Sandra Maesta-Pereira, Peter J. Schuette, Meghmik Chakerian, Jinhan Liu, Mimi Q. La-Vu, Brooke C. Tobias, Juliane M. Ikebara, Alexandre Hiroaki Kihara, Newton S. Canteras, Jonathan C. Kao, and Avishek Adhikari. 2021. “Dorsal Periaqueductal Gray Ensembles Represent Approach and Avoidance States.” *ELife* 10:1–22.

Resstel, L. B. M., S. R. L. Joca, F. G. Guimarães, and F. M. A. Corrêa. 2006. “Involvement of Medial Prefrontal Cortex Neurons in Behavioral and Cardiovascular Responses to Contextual Fear Conditioning.” *Neuroscience* 143(2):377–85.

Reynolds, David V. 1969. “Surgery in the Rat during Electrical Analgesia Induced by Focal Brain Stimulation.” *Science* 164(3878):444–45.

Rizvi, Tilat A., Matthew Ennis, Michael M. Behbehani, and Michael T. Shipley. 1991. “Connections between the Central Nucleus of the Amygdala and the Midbrain Periaqueductal Gray: Topography and Reciprocity.” *Journal of Comparative Neurology* 303(1):121–31.

Roeling, T. A. P., J. G. Veening, M. R. Kruk, J. P. W. Peters, M. E. J. Vermelis, and R. Nieuwenhuys. 1994. “Efferent Connections of the Hypothalamic ‘Aggression Area’ in the Rat.” *Neuroscience* 59(4):1001–24.

Roelofs, Karin. 2017. “Freeze for Action: Neurobiological Mechanisms in Animal and Human Freezing.” *Philosophical Transactions of the Royal Society B: Biological Sciences* 372(1718).

Roelofs, Karin and Peter Dayan. 2022. “Freezing Revisited: Coordinated Autonomic and Central Optimization of Threat Coping.” *Nature Reviews Neuroscience*.

Roelofs, Karin, Muriel A. Hagenaars, and John Stins. 2010. “Facing Freeze: Social Threat Induces Bodily Freeze in Humans.” *Psychological Science* 21(11):1575–81.

Rogan, Michael T., Ursula V. Stäubli, and Joseph E. LeDoux. 1997. “Fear Conditioning Induces Associative Long-Term Potentiation in the Amygdala.” *Nature* 390(6660):604–7.

Rösler, Lara and Matthias Gamer. 2019. “Freezing of Gaze during Action Preparation under Threat Imminence.” *Scientific Reports* 9(1):1–9.

Rozeske, Robert R., Daniel Jercog, Nikolaos Karalis, Delphine Girard, and Cyril Herry. 2018. “Prefrontal-Periaqueductal Gray-Projecting Neurons Mediate Context Fear Discrimination.” 1–13.

Samulski, R. Jude and Nicholas Muzyczka. 2014. “AAV-Mediated Gene Therapy for Research and Therapeutic Purposes.” *Annual Review of Virology* 1(1):427–51.

Saper, Clifford B. and Bradford B. Lowell. 2014. “The Hypothalamus.” *Current Biology* 24(23):R1111–16.

Schneider, Franziska, Christiane Grimm, and Peter Hegemann. 2015. “Biophysics of Channelrhodopsin.” *Annual Review of Biophysics* 44:167–86.

Schwerdtfeger, Andreas R., Gerhard Schwarz, Klaus Pfurtscheller, Julian F. Thayer, Marc N. Jarczok, and Gert Pfurtscheller. 2020. “Heart Rate Variability (HRV): From Brain Death to Resonance Breathing at 6 Breaths per Minute.” *Clinical Neurophysiology* 131(3):676–93.

Shaffer, Fred, Rollin McCraty, and Christopher L. Zerr. 2014. “A Healthy Heart Is Not a Metronome: An Integrative Review of the Heart’s Anatomy and Heart Rate Variability.” *Frontiers in Psychology* 5(September):1–19.

Shaffer, Fred and John Venner. 2013. “Heart Rate Variability Anatomy and Physiology.” *Biofeedback* 41(1):13–25.

Shimogawa, Yuji, Yasuo Sakuma, and Korehito Yamanouchi. 2015. “Efferent and Afferent Connections of the Ventromedial Hypothalamic Nucleus Determined by Neural Tracer Analysis: Implications for Lordosis Regulation in Female Rats.” *Neuroscience Research* 91:19–33.

Silva, B. A., C. Mattucci, P. Krzywkowski, E. Murana, A. Illarionova, V. Grinevich, N. S. Canteras, D. Ragozzino, and C. T. Gross. 2013. “Independent Hypothalamic Circuits for Social and Predator Fear.” *Nat Neurosci* 16(12):1731–33.

Silva, Bianca A., Cornelius T. Gross, and Johannes Gräff. 2016. “The Neural Circuits of Innate Fear: Detection, Integration, Action, and Memorization.” *Learning & Memory* 23(10):544–55.

Silva, Carlos and Neil McNaughton. 2019. “Are Periaqueductal Gray and Dorsal Raphe the Foundation of Appetitive and Aversive Control? A Comprehensive Review.” *Progress in Neurobiology* 177(January):33–72.

Silvani, Alessandro, Giovanna Calandra-buonaura, Roger A. L. Dampney, and Pietro Cortelli. 2016. “Brain – Heart Interactions : Physiology and Clinical Implications.” *Philosophical Transactions of the Royal Society A* 374(2067).

Silveira, Maria Cristina L. and Frederico G. Graeff. 1992. “Defense Reaction Elicited by Microinjection of Kainic Acid into the Medial Hypothalamus of the Rat: Antagonism by a GABAA Receptor Agonist.” *Behavioral and Neural Biology* 57(3):226–32.

Stiedl, O. and J. Spiess. 1997. “Effect of Tone-Dependent Fear Conditioning on Heart Rate and Behavior of C57BL/6N Mice.” *Behav Neurosci* 111(4):703–11.

Storchi, Riccardo, Nina Milosavljevic, Annette E. Allen, Antonio G. Zippo, Aayushi Agnihotri, Timothy F. Cootes, and Robert J. Lucas. 2020. “A High-Dimensional Quantification of Mouse Defensive Behaviors Reveals Enhanced Diversity and Stimulus Specificity.” *Current Biology* 1–12.

Sukikara, Marcia Harumi, Sandra Regina Mota-Ortiz, Marcus Vinícius Baldo, Luciano Freitas Felicio, and Newton Sabino Canteras. 2010. “The Periaqueductal Gray and Its Potential Role in Maternal Behavior Inhibition in Response to Predatory Threats.” *Behavioural Brain Research* 209(2):226–33.

Swiercz, Adam P., Antonia V. Seligowski, Jeanie Park, and Paul J. Marvar. 2018. “Extinction of Fear Memory Attenuates Conditioned Cardiovascular Fear Reactivity.” *Frontiers in Behavioral Neuroscience* 12(November).

Szeska, Christoph, Jan Richter, Julia Wendt, Mathias Weymar, and Alfons O. Hamm. 2021. “Attentive Immobility in the Face of Inevitable Distal Threat—Startle Potentiation and Fear Bradycardia as an Index of Emotion and Attention.” *Psychophysiology* 58(6):1–17.

Thireau, J., B. L. Zhang, D. Poisson, and D. Babuty. 2008. “Heart Rate Variability in Mice: A Theoretical and Practical Guide.” *Experimental Physiology* 93(1):83–94.

De Toledo, Leyla and A. H. Black. 1966. “Heart Rate: Changes during Conditioned Suppression in Rats.” *Science* 152(3727):1404–6.

Totty, Michael S., Naomi Warren, Isabella Huddleston, Karthik R. Ramanathan, Reed L. Ressler, Cecily R. Oleksiak, and Stephen Maren. 2021. "Behavioral and Brain Mechanisms Mediating Conditioned Flight Behavior in Rats." *Scientific Reports* 11(1):1–15.

Tovote, P., M. S. Esposito, P. Botta, F. Chaudun, J. P. Fadok, M. Markovic, S. B. Wolff, C. Ramakrishnan, L. Fenno, K. Deisseroth, C. Herry, S. Arber, and A. Luthi. 2016. "Midbrain Circuits for Defensive Behaviour." *Nature* 534(7606):206–12.

Tovote, P., J. P. Fadok, and A. Luthi. 2015. "Neuronal Circuits for Fear and Anxiety." *Nat Rev Neurosci* 16(6):317–31.

Tovote, Philip, Michael Meyer, Annette G. Beck-Sickinger, Stephan Von Hörsten, Sven Ove Ögren, Joachim Spiess, and Oliver Stiedl. 2004. "Central NPY Receptor-Mediated Alteration of Heart Rate Dynamics in Mice during Expression of Fear Conditioned to an Auditory Cue." *Regulatory Peptides* 120(1–3):205–14.

Tye, K. M. and K. Deisseroth. 2012. "Optogenetic Investigation of Neural Circuits Underlying Brain Disease in Animal Models." *Nat Rev Neurosci* 13(4):251–66.

Tye, K. M., R. Prakash, S. Y. Kim, L. E. Fenno, L. Grosenick, H. Zarabi, K. R. Thompson, V. Gradinaru, C. Ramakrishnan, and K. Deisseroth. 2011. "Amygdala Circuitry Mediating Reversible and Bidirectional Control of Anxiety." *Nature* 471(7338):358–62.

Vaaga, Christopher E., Spencer T. Brown, and Indira M. Raman. 2020. "Cerebellar Modulation of Synaptic Input to Freezing-Related Neurons in the Periaqueductal Gray." *ELife* 9.

Vianna, D. M., J. Landeira-Fernandez, and M. L. Brandao. 2001. "Dorsolateral and Ventral Regions of the Periaqueductal Gray Matter Are Involved in Distinct Types of Fear." *Neurosci Biobehav Rev* 25(7–8):711–19.

Vianna, Daniel M. L. and Pascal Carrive. 2005. "Changes in Cutaneous and Body Temperature during and after Conditioned Fear to Context in the Rat." *European Journal of Neuroscience* 21(9):2505–12.

Walker, P. and P. Carrive. 2003. "Role of Ventrolateral Periaqueductal Gray Neurons in the Behavioral and Cardiovascular Responses to Contextual Conditioned Fear and Poststress Recovery." *Neuroscience* 116(3):897–912.

Walker, Rachel A., Kristina M. Wright, Thomas C. Jhou, and Michael A. McDannald. 2020. "The Ventrolateral Periaqueductal Grey Updates Fear via Positive Prediction Error." *European Journal of Neuroscience* 51(3):866–80.

Wang, L., I. Z. Chen, and D. Lin. 2015. "Collateral Pathways from the Ventromedial Hypothalamus Mediate Defensive Behaviors." *Neuron* 85(6):1344–58.

Watson, Thomas C., Nadia L. Cerminara, Bridget M. Lumb, and Richard Apps. 2016. "Neural Correlates of Fear in the Periaqueductal Gray." *Journal of Neuroscience* 36(50):12707–19.

Wehrwein, Erica A. and Michael J. Joyner. 2013. *Regulation of Blood Pressure by the Arterial Baroreflex and Autonomic Nervous System*. Vol. 117. 1st ed. Elsevier B.V.

Weingarten, Harvey and Norman White. 1978. "Exploration Evoked by Electrical Stimulation of the Amygdala of Rats." *Physiological Psychology* 6(2):229–35.

Wiegert, J. Simon, Mathias Mahn, Matthias Prigge, Yoav Printz, and Ofer Yizhar. 2017. "Silencing Neurons: Tools, Applications, and Experimental Constraints." *Neuron* 95(3):504–29.

Wolff, S. B., J. Grundemann, P. Tovote, S. Krabbe, G. A. Jacobson, C. Muller, C. Herry, I. Ehrlich, R. W. Friedrich, J. J. Letzkus, and A. Luthi. 2014. "Amygdala Interneuron Subtypes Control Fear Learning through Disinhibition." *Nature* 509(7501):453–58.

Wright, Kristina M., Thomas C. Jhou, Daniel Pimpinelli, and Michael A. McDannald. 2019. "Cue-Inhibited Ventrolateral Periaqueductal Gray Neurons Signal Fear Output and Threat Probability in Male Rats." *ELife* 8:1–16.

Wright, Kristina M. and Michael A. McDannald. 2019. "Ventrolateral Periaqueductal Gray Neurons Prioritize Threat Probability over Fear Output." *ELife* 8.

Xu, Shengjin, Hui Yang, Vilas Menon, Andrew L. Lemire, Lihua Wang, Fredrick E. Henry, Srinivas C. Turaga, and Scott M. Sternson. 2020. "Behavioral State Coding by Molecularly Defined Paraventricular Hypothalamic Cell Type Ensembles." *Science* 370(6514).

Yeh, Li Feng, Takaaki Ozawa, and Joshua P. Johansen. 2021. "Functional Organization of the Midbrain Periaqueductal Gray for Regulating Aversive Memory Formation." *Molecular Brain* 14(1):1–9.

Yizhar, Ofer, Lief E. Fenno, Thomas J. Davidson, Murtaza Mogri, and Karl Deisseroth. 2011. "Optogenetics in Neural Systems." *Neuron* 71(1):9–34.

Yoshimoto, Misa, Keiko Nagata, and Kenju Miki. 2010. "Differential Control of Renal and Lumbar Sympathetic Nerve Activity during Freezing Behavior in Conscious Rats." *American Journal of Physiology - Regulatory Integrative and Comparative Physiology* 299(4):1114–20.

Zhang, Yujie, Kunfu Ouyang, Tatiana V. Lipina, Hong Wang, and Qiang Zhou. 2019. "Conditioned Stimulus Presentations Alter Anxiety Level in Fear-Conditioned Mice." *Molecular Brain* 12(1):1–12.

Zych, Anna D. and Nadine Gogolla. 2021. "Expressions of Emotions across Species." *Current Opinion in Neurobiology* 68:57–66.

6. Appendix

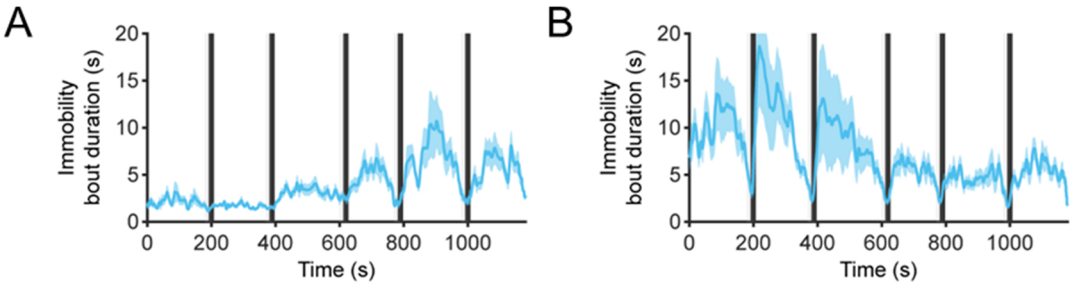

Figure S1 - Length of immobility bouts varies throughout the session during the conditioning days of the conditioned flight paradigm.
Average immobility bout durations (± SEM) of 29 animals during CD1 (A) and CD2 (B) are depicted.

Figure S2 - Histology of optogenetic experiments in VGlut2-IRES-Cre *mice.*
Placement of optical fiber (left panel) and expression pattern as overlay (right panel) of ReaChR (A) and mCherry (B) sorted according to bregma level.

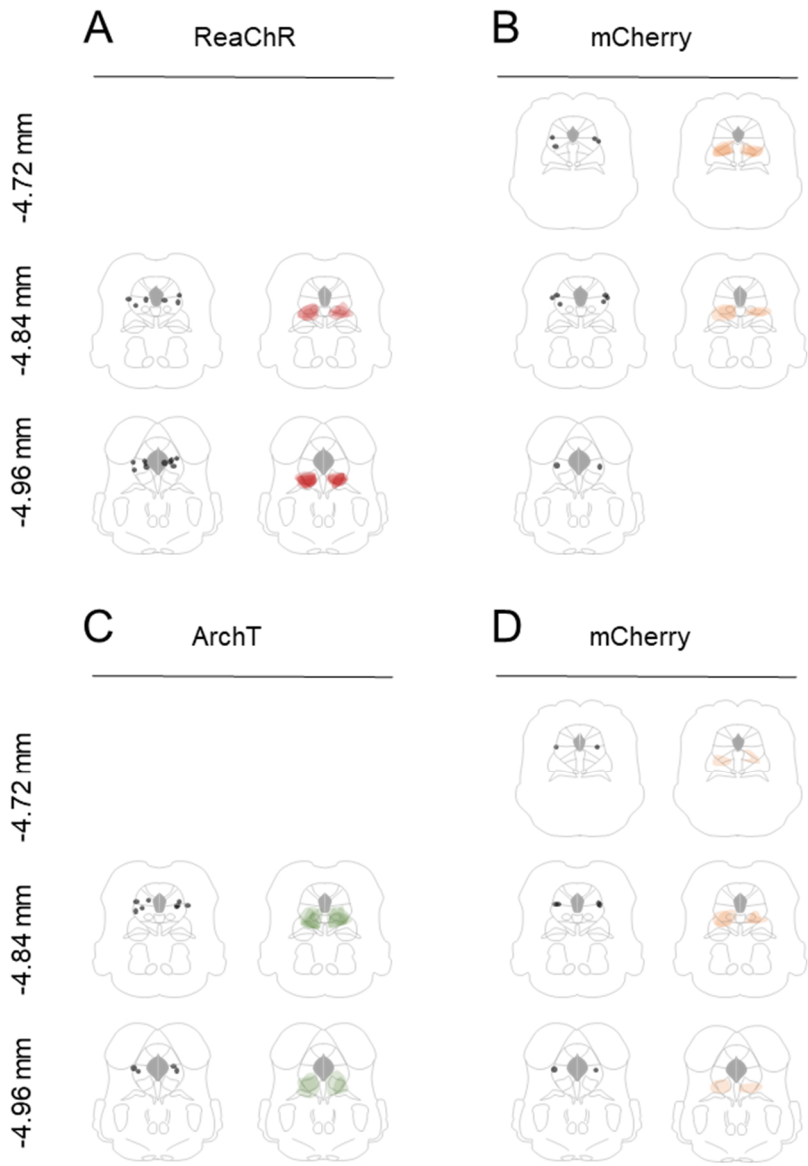

Figure S3 - Histology of optogenetic experiments in Chx10-Cre *mice.*
Placement of optical fiber (left panel) and expression pattern as overlay (right panel) of optical activation experiments (ReaChR, A and mCherry, B), and optical inhibition experiments (ArchT, C and mCherry, D) sorted according to bregma level.

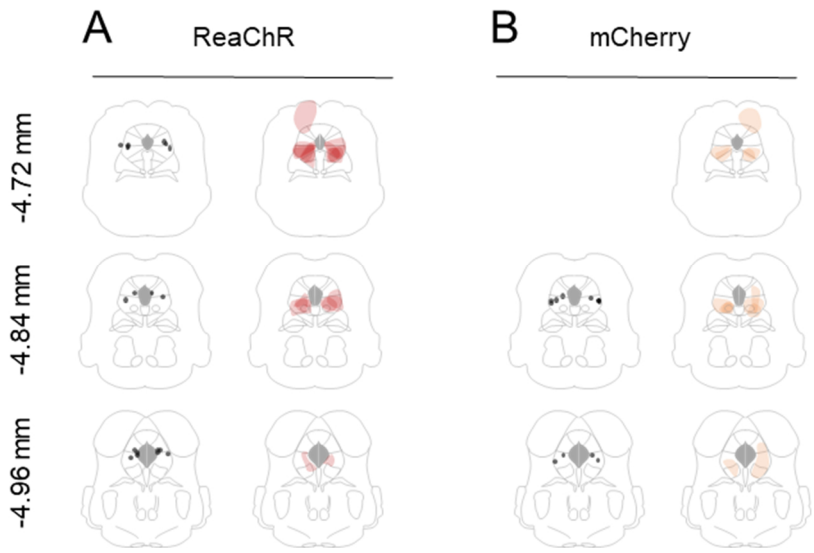

Figure S4 - Histology of optogenetic experiments in Gad2-IRES-Cre *mice.*
Placement of optical fiber (left panel) and expression pattern as overlay (right panel) of ReaChR (A) and mCherry (B) sorted according to bregma level.

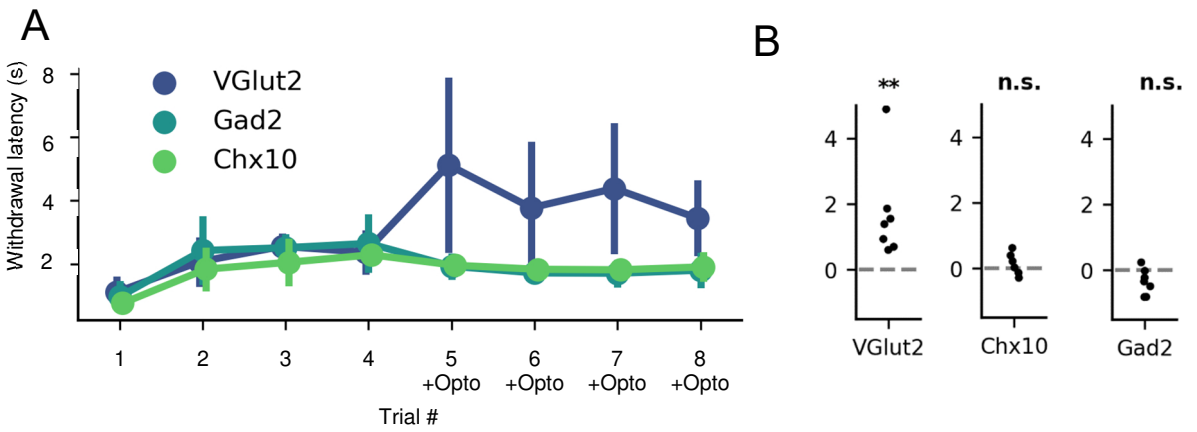

Figure S5 - Tail immersion test paired with optical stimulation of different vlPAG subpopulations.
(A) Tail withdrawal latencies during baseline (first 4 trials) and after 5 seconds optogenetic stimulation of vlPAG VGlut2-, Chx10- *and* Gad2*-positive neuronal populations. (B) Boxplots showing shift of withdrawal latencies from baseline. Average withdrawal latency per animal after optogenetic stimulation substracted by baseline compared against 0 (no change). VGlut2: One sample Wilcoxon rank-sum test, W = 0, p < 0.01; Chx10: One sample t-test, t(5) = 1.05, p = 0.34; Gad2: One sample t-test, t(6) = -2.36, p = 0.06.* $N_{VGlut2} = 8$, $N_{Chx10} = 6$, $N_{Gad2} = 7$

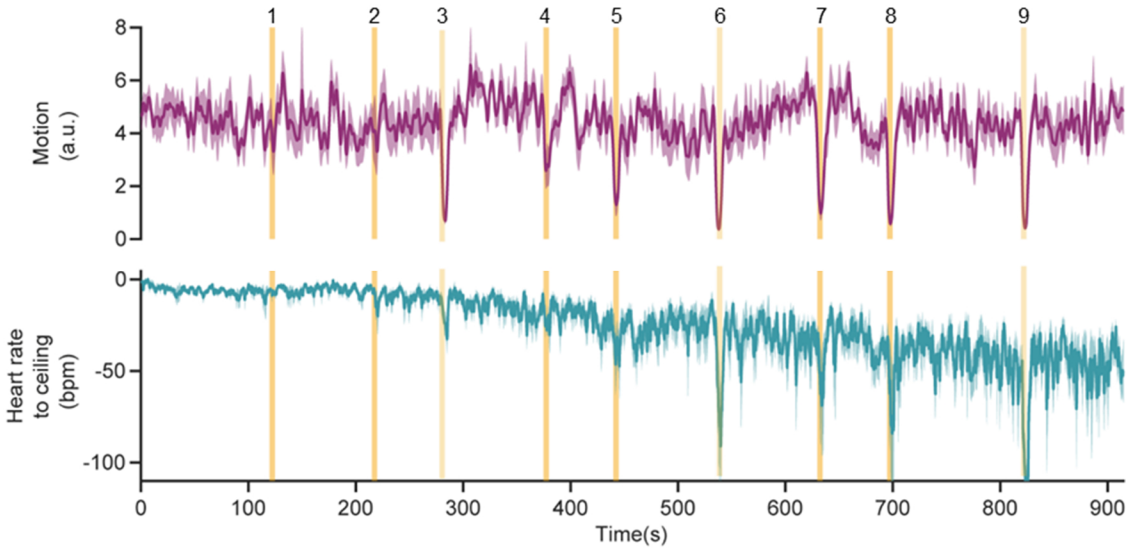

Figure S6- Optogenetic screening session of Chx10-Cre animals expressing ReaChR in the vlPAG.
Average motion (top, ± SEM) and HR-to-ceiling (bottom, ± SEM) responses during a screening session in which different stimulation patterns were tested for 5 seconds each. 1: 1 mW, 10 Hz, 10 ms; 2: 1 mW, 20 Hz, 10 ms; 3: 1 mW, constant; 4: 3.4 mW, 10 Hz, 10 ms; 5: 3.4 mW, 20 Hz, 10 ms; 6: 3.4 mW, constant; 7: 9 mW, 10 Hz, 10 ms; 8: 9 mW, 20 Hz, 10 ms; 9: 9 mW, constant.

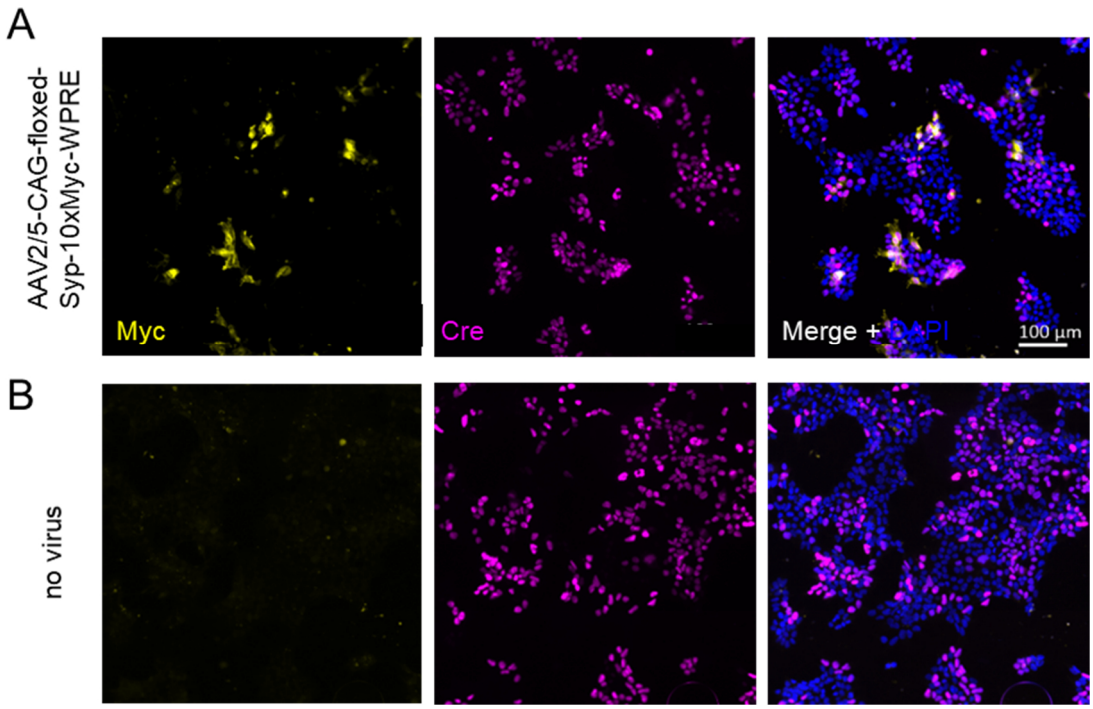

Figure S7 - Illustration of a qualitative in vitro *virus testing.*
Stable HEK293-Cre line infected with an AAV2/5-CAG-floxed-Syp-10xMyc-WPRE *construct (A) and non-infected control cells (B) visualized by immunhistochemical stainings of the Myc-tag (yellow) and the Cre enzyme (magenta). Scale bar: 100 µm*

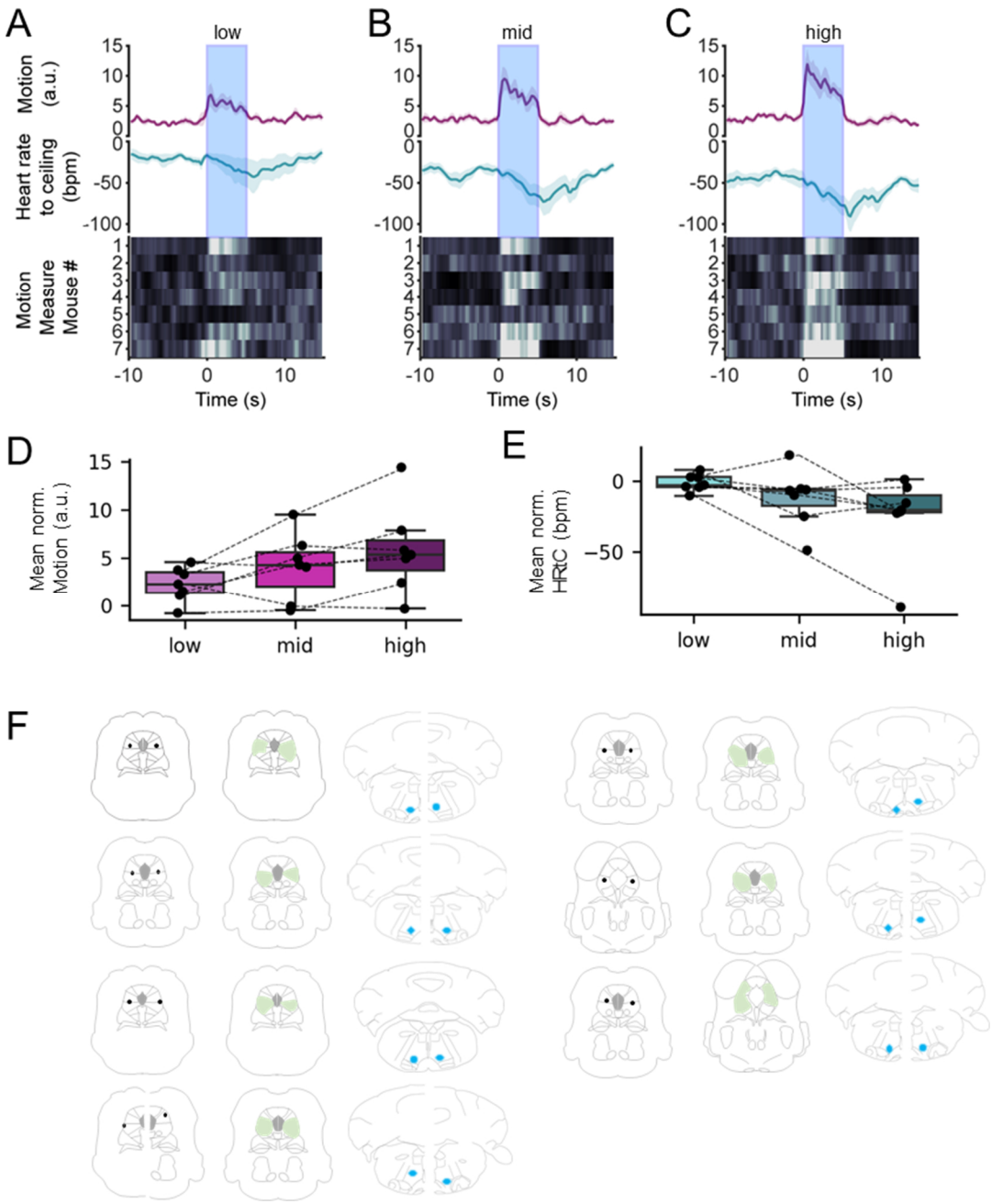

Figure S8 - Intensity-dependent behavioral and cardiac responses and histology of animals used for optogenetic experiments targeting glutamatergic vlPAG-to-Mc neurons.
(A, B, C) Increasing light intensities ((A) low: 0.8 mW, (B) mid: 1.8 mW, and (C) high: 4.6 mW; all 20 Hz, 20 ms) induced increasing locomotion as well as bradycardia, but no freezing. PSTHs centered around optical stimulation of VGlut2-IRES-Cre *animals injected with a projection-specifically expressed ChR in the vlPAG. Each PSTH shows the average of 3 repetitions of each stimulation intensity with motion (top and bottom, heat plot with average motion measure per mouse) and HR-to-ceiling (middle). (D, E) Quantifications of Motion (D) and HR-to-ceiling (E) shown in (A-C) as mean normalized values per animal (stimulation subtracted by baseline). (D) One-way repeated measurements ANOVA, $F_{(2,12)} = 4.41$, $p < 0.05$ followed by pairwise comparisons with two-sided t-tests, high vs. low: p = 0.07, high vs. mid: p = 0.06, low vs. mid: p = 0.14. (E) Friedman-ANOVA, $\chi^2(2) = 5.43$, p = 0.07 followed by pairwise comparisons with two-sided t-tests, high vs. low: p = 0.09, high vs. mid: p = 0.22, low vs. mid: p = 0.16. (F) Optical fiber placement (left column),* Con/Fon-ChR-EYFP *expression pattern (middle column), and location of* AAV(retro)-CAG-Floxed-FlpO-2A-H2BV5.rev.WPRE *injection verified by mixed fluorescent beads (right column).*

I. Abbrevations

AAV	Adeno-associated virus
ANS	autonomous nervous system
AP	Anterior-posterior
ArchT	Archaerhodopsin-T
BA	basal amygdala
BLA	basolateral amygdala
BMA	basal medial amygdala
bpm	beats per minute
CD	conditioning day
CeA	central amygdala
CFP	conditioned flight paradigm
ChR2	Channelrhodopsin
CS	conditioned stimulus
d	dorsal
DAPI	4′,6-diamidino-2-phenylindole
dl	dorsolateral
DLC	DeepLabCut
dm	dorsomedial
Dv	dorsoventral
DMV	dorsal motor nucleus of the vagus
dR	dorsal Raphe
dv	dorsoventral
DVC	Dorsal vagal complex
ECG	electrocardiogram
EPM	elevated plus maze
EYFP	enhanced yellow fluorescent protein
GABA	gamma-aminobutyric acid
Gad2	glutamic acid decarboxylase 2

gc	Gene copy
GFP	green fluorescent protein
GiA	gigantocellular nucleus, alpha part
GiV	gigantocellular nucleus, ventral part
HC	homecage
HEK	human embryonic kidney
HR	Heart rate
HRV	Heart rate variability
ISI	inter-stimulus interval
ITR	internal terminal repeats
IQR	interquartile range
l	lateral
L.F.	low frequency
LA	lateral amygdala
LDB	light-dark box
LPGi	lateral paragigantocellular nucleus
Mc	magnocellular nucleus
ml	medio-lateral
MLR	Mesencephalic locomotor region
mPFC	medial prefrontal cortex
N	number of analyzed animals
NA	Nucleus ambiguus
NTS	nucleus of the solitary tract
OF	open field
PAG	periaqueductal grey
PBS	phosphate buffered saline
PFA	paraformaldehyde
PNS	parasympathetic nervous system
PSTH	peristimulus time histogram

ReaChR	red-activatable Channelrhodopsin
RFP	Red fluorescent protein
RTPP	real-time place preference
RVLM	rostral ventrolateral medulla
SCS	serial compound stimulus
SEM	Standard error of mean
SNS	sympathetic nervous system
US	unconditioned stimulus
VGlut2	vesicular glutamate transporter 2
vl	ventrolateral

II. List of Figures

III. List of Tables

IV. Acknowledgements

First and foremost, I would like to thank my primary supervisor Prof. Philip Tovote. Your visions on our next scientific goals and incredible motivation to understand the brain better is an example for me. It was your fierce conviction that we can play in the top league with our science, that made our publication possible. You have taught me to approach things without hesitation, go through with them and get them done. From teaching how to solder through lessons of conflict management to the basics of scientific writing and an appealing composition of a talk, I have learned from you not only skills for the lab but also things for life.

Furthermore, I would like to thank Prof. Matthias Gamer and Prof. Charlotte Förster for their willingness to be party of my thesis committee. Moreover, I would like to thank Prof. Michael Sendtner, the head of the Institute of Clinical Neurobiology.

I am infinitely grateful for the close cooperation with you, Jérémy. You are an essential part of this lab and your computational work raise our scientific work to a higher level. Your genius contributed more than a crucial part to our success with the recent publication. Thanks for your tireless efforts to bail me out even with the 1000th MATLAB error and to answer me day and night to desperate messages about analysis or technical problems during experiments.

Dear Sara, your energy and dedication are unparalleled. Thank you so much for your amazing support during my maternity leave, help with the revision experiments and beyond. Instead of setting boundaries and say “Enough!”, you always just asked where you could support me more and what other experiments to take on. Thank you so much for that!

Dennis, you always have a sympathetic ear for me. In countless lunch breaks you let me unload my frustration about failed experiments and I could always count on your constructive input, mental support and encouraging cheering. Thank you very much! Your way of working scientifically as well as your ambition to reach set goals are an example for me. Moreover, I would like to thank you for providing the Stats-n-Plots Tool as well as for proofreading this thesis.

Many thanks to the whole lab, which in the last 6 years has grown from a small team of 5 members to a widely networked team with numerous collaborations. Thanks to Orlando, Alexia and César for your support and great understanding. A huge thanks also goes to you, Katrin. You are one of the mainstays of this lab and without you, chaos would ensue. Thank you for always getting things done with a verve that is second to none. Elisabete, we miss you. With your organizational talent and your incredible warmth you were an enrichment for this lab. Many thanks for that! A big thank you also to Hilde and Regine with her team for virus production and animal husbandry, respectively. Thank you Christian for your support with the lab infrastructure.

Zum Schluss möchte ich mich natürlich bei meiner Familie bedanken. Zu allererst bei Dir, Marc. Danke für Dein aberwitzig großes Verständnis… nicht nur dann, wenn es doch mal wieder länger im Labor gedauert hat und Du trotzdem mit dem Essen auf mich gewartet hast. Danke, dass Du so oft mein verbarler Punching Ball bist, indem ich einfach immer all meinen Stress und Frust bei Dir abladen kann. Du gibst mir Halt und unterstützt mich bedingungslos. Es fühlt sich an, als könne mir mit Dir an meiner Seite einfach nichts passieren. Danke auch an Papa, auf Dich ist wirklich in jeder Lebenssituation Verlass und Kai, mit Deiner Neugierde, was ich denn eigentlich ganz genau erforsche, forderst Du mich immer wieder heraus, auch einem Nicht-Wissenschaftler unsere Forschung mit all ihren Details und Facetten zu erklären.